Lévy walks

V. Zaburdaev,[1, *] S. Denisov,[2, 3, 4, †] and J. Klafter[5, ‡]

[1]*Max Planck Institute for the Physics of Complex Systems, Nöthnitzer Str. 38, D-01187 Dresden, Germany*

[2]*Institute of Physics, University of Augsburg, Universitätstr. 1, D-86159 Augsburg, Germany*

[3]*Lobachevsky State University, Gagarin Avenue 23, 603950 Nizhny Novgorod, Russia*

[4]*Sumy State University, Rimsky-Korsakov Street 2, 40007 Sumy, Ukraine*

[5]*School of Chemistry, Tel Aviv University, 69978 Tel Aviv, Israel*

Random walk is a fundamental concept with applications ranging from quantum physics to econometrics. Remarkably, one specific model of random walks appears to be ubiquitous across many fields as a tool to analyze transport phenomena in which the dispersal process is faster than dictated by Brownian diffusion. The Lévy walk model combines two key features, the ability to generate anomalously fast diffusion and a finite velocity of a random walker. Recent results in optics, Hamiltonian chaos, cold atom dynamics, bio-physics, and behavioral science demonstrate that this particular type of random walks provides significant insight into complex transport phenomena. This review provides a self-consistent introduction to Lévy walks, surveys their existing applications, including latest advances, and outlines further perspectives.

Contents

*Electronic address: vzaburd@pks.mpg.de

†Electronic address: sergey.denisov@physik.uni-augsburg.de

‡Electronic address: klafter@post.tau.ac.il

I. INTRODUCTION

In this review we want to demonstrate how a simple idea of the giving a finite velocity to a diffusing particle increases flexibility and diversity of diffusion models in describing complex transport phenomena. We consider processes resulting from a motion of many identical non-interacting particles. There are two key complimentary approaches to statistical description of such motion. The first approach is based on the concept of random walks (Weiss, 1994) while the second is based on stochastic differential equations. Among the latter are the Langevin equation (Coffey and Kalmykov, 2012) and the concept of Brownian motion (Mörters and Peres, 2010). Although having different terminologies and mathematical apparatus, the two approaches are closely related and their exact equivalence can be demonstrated in some cases. The framework of our review is random walks and we would like to start with a historical overview of the development of the concept, with a special focus on how the idea of the finite velocity of walking particles was born and matured over the years.

As if to predict its interdisciplinary future, the theory of random walks was developed independently in the context of biology (Brown, 1828), probability theory (Bernoulli, 1713), finance (Bachelier, 1900), and physics (Pearson, 1905; Rayleigh, 1880). The seminal works of Einstein (1905) and von Smoluchowski (1906) marked the start of rigorous and quantitative approach connecting microscopic dynamics of particles to the macroscopic

process of diffusion [see, for example, (Nelson, 1967) for more historical background on Brownian motion]. The diffusion equation was already known for nearly a century as it was derived to describe the heat conduction by Fourier (1822). Despite the success of this equation in various applications, it had one particular drawback that did not escape the attention of contemporary scientists. According to the diffusion equation, when starting with a localized initial condition, even after an infinitesimally short elapsed time there will be a nonzero density of diffusing particles at any arbitrary distance from the staring point. This implies an infinite propagation speed of some particles and thus contradicts our understanding of how physical objects move [see an interesting discussion on this issue in the context of relativistic statistical physics in Dunkel and Hänggi (2009); Dunkel *et al.* (2009)]. The infinite speed is also inconsistent with the original schematization of a random walk process by Karl Pearson (Pearson, 1905): "*A man starts from a point* 0 *and walks l yards in a straight line; he then turns through any angle whatever and walks another l yards in a second straight line. He repeats this process n times. I require the probability that after these n stretches he is at a distance between r and r + dr from his starting point,* 0." After this drawback was noted, two approaches to resolve the issue have been proposed. In 1920, G. I. Taylor, concerned with the problem of turbulent transport, formulated a random walk model in which the motion of a particle between two turning events was characterized by a finite velocity (Taylor, 1922). The same year the finiteness of the velocity was mentioned by Fürth (1920) in the context of the so-called persistent Brownian motion. Both these models assume that there should be no particles outside the ballistic cone defined by the maximal velocity of the particles. In 1935 Davydov proposed to use the telegraph equation, which contains additional second order time derivative, to address the existence of the ballistic cone (Bakunin, 2003; Davydov, 1934). As with the diffusion equation, the telegraph equation was discovered much earlier by Kirchhoff and Heaviside in the context of electric current transmission through a conducting line. Around 1950 it was demonstrated that the telegraph equation could be derived from the random walk model proposed by Taylor (Goldstein, 1951). The next milestone in the development of the modern random walk theory was due to Montroll and Weiss who introduced the continuous time random walks model (CTRW)(Montroll and Weiss, 1965; Scher and Montroll, 1975). The main innovation of that model is that a particle has to wait for a random time before moving to another point. This model provided the framework necessary for describing anomalous diffusion with the spreading of particles *slower* than in the Brownian diffusion, a process that was named "subdiffusion".

Richardson (1926b) pointed out the possibility of the anomalous diffusion in turbulent flows, where particles spread *faster* than in normal diffusion, and referred to as "superdiffusion". To accommodate for superdiffusive

transport, the random walk model was modified to allow particles to perform very long excursions. To step beyond the premises of the central limit theorem (CLT), slow decaying functions with power law tails and diverging second moment were used as the distributions of the excursion lengths. The scaling properties of the corresponding particle distributions were found to be different from those of the standard Brownian diffusion and thus required a new mathematical apparatus. At this point, a link between the superdiffusion and Lévy stable distributions (Gnedenko and Kolmogorov, 1954; Lévy, 1937) was established. The random walk model with walkers covering long distances instantaneously received the name of *Lévy flight* (Mandelbrot, 1982). In its simplest schematization, this stochastic process could drive a particle over very long distance in a single motion event, that is called "flight" (although, in fact, it is a *jump*), so that the mean squared flight length is infinite (Shlesinger and Klafter, 1986). Similar to the concept of Brownian diffusion, Lévy flights served well to describe different transport phenomena. However, Lévy flights have the same trait of infinite propagation speed as the diffusion equation. In addition, the distribution of the particles performing Lévy flight has a divergent second and all higher moments[1]. This poses a significant difficulty in relating Lévy flight models to experimental data, especially when analyzing the scaling of the measured moments in time. Akin to the Taylor model, the Lévy flight model was then equipped with a finite velocity of moving particles and therefore produced distributions which are confined to ballistic cones and thus have finite moments. As a contrast to the flight process with instantaneous jumps, the name *Lévy walk* was coined by Shlesinger *et al.* (1982). The aim of this review is to show how versatile and powerful the concept of Lévy walks is in describing a wide spectrum of physical and biological processes involving stochastic transport.

In order to orient the reader in the existing literature on random walks in the context of anomalous diffusion, we would like to mention several monographs which can serve as a good introductory material to continuous time random walks (Klafter and Sokolov, 2011), anomalous diffusion, Lévy flights and subdiffusion (Bouchaud and Georges, 1990; Havlin and Ben-Avraham, 1987; Isichenko, 1992; Metzler and Klafter, 2000, 2004; Mon-

---

[1] It is not correct, however, to think of the Lévy flight as an abstract mathematical formalism. The mechanisms leading to the dispersion of the observable of interest may not be related to a physical motion of an entity in Euclidean space. For example, it may be caused by long-range interactions (Barkai *et al.*, 2003), or by a nontrivial "crumpled" topology of a phase (or configuration) space of polymer systems (Brockmann and Geisel, 2003; Sokolov *et al.*, 1997) and small-world networks (Kozma *et al.*, 2005), or by spectral characteristics of disordered media, amorphous materials, and glasses (Klauder and Anderson, 1962; Zumofen and Klafter, 1994b); see review by Bouchaud and Georges (1990) for more information and other examples where the Lévy flights are of relevance.

troll and Shlesinger, 1984), and some reviews on particular applications of these formalisms (Balescu, 2005; Bardou *et al.*, 2001).

A. Lévy stable laws

One of the fundamental theorems in probability theory is the central limit theorem. It states that the sum of independent identically distributed random variables with a finite second moment is a random variable with the distribution tending to a normal distribution as the number of summands increases. It has a history of development spanning several hundred years, from initial considerations by Laplace and Poisson at the end of the 18th century to the stage of rigorous analysis by Markov, Chebyshev, Lyapunov, Feller, Lévy and others in the beginning of the 20th century, see Fischer (2010) for historical overview. Remarkably, the CLT can be cast into the dynamical problem of a particle hopping at random distances. The sum of all displacements (independent random variables) will then determine the final position of a particle (their sum). As a result, the distribution of particle's position is normal (or Gaussian) if the second moment of the displacement length distribution is finite. Normal distributions are also known to be stable distributions meaning that the sum (or, more generally, a linear combination with positive weights) of two independent random variables has the same distribution (up to a scaling factor and shift). Around 1920, Paul Lévy showed that there are other stable distributions which now bare the name of Lévy alpha-stable distributions. In particular, they have power law tails and diverging second moments. The generalized central limit theorem (gCLT) was then formulated to state that the sum of identically distributed random variables with distributions having power law tails converges to one of the Lévy distributions. We can now look at the total displacement of a particle whose individual hops are distributed as a power law. The position of the particle after many hops will be described, according to the gCLT, by a Lévy distribution, see e.g. (Uchaikin, 2003). That is why such random walks are also known as Lévy flights. It has been found that a big variety of natural and man-made phenomena exhibit power law statistics (Bouchaud, 1995; Clauset *et al.*, 2009; Uchaikin and Zolotarev, 1999). While relating the empirical data to the theoretical models with Lévy distributions, it became clear that the model solutions could not be characterized by the second moment: Like every individual jump in a sequence, the distribution of particle's final positions has an infinite variance.

One of the most straightforward ways to resolve this inconsistency is to regularize the power-law distributions by truncating them at large values (Mantegna and Stanley, 1994). That would make the moments of the distribution finite while still retaining some properties of the power-law distributions for intermediate values. However, the truncation introduces a certain arbitrariness

and, as a phenomenological procedure, it can not be always justified in a particular physical (or economical, biological, etc.) context.

Importantly, there is an alternative way to remedy the problem of divergent moments. A fundamental property of having a finite velocity while moving couples the displacement of a walker and time it takes to cover the corresponding distance and puts a larger time-cost to a longer displacement. In the simple picture of a hopping particle, that would mean that at any moment of time the position of the particle after many hops is bounded by the ballistic cone with the fronts matching the maximal particle velocity multiplied by the observation time. In between these fronts, the long displacements of the particle would still exist, as necessary for the Lévy-like statistics, but all moments of the distribution of particle's position will be finite for any given time (Shlesinger *et al.*, 1986).

We hope that at this point we already convinced the reader that random walks is an appropriate language to describe the stochastic transport phenomena. We now proceed to introduce the theoretical framework of continuous-time random walks (Klafter and Sokolov, 2011) and describe how it changes when the finite velocity of walkers is taken into account. Below, we mainly focus on one-dimensional systems (some open problems concerning the generalization to higher dimensions are mentioned in the Outlook section).

B. Continuous time random walks

Consider a random motion of passive particles in homogeneous media. We are interested in the macroscopic behavior of the density of particles $P(x,t)$ as a function of space and time. Each particle can make instantaneous jumps to the left or to the right with equal probabilities. The probability density function (PDF) of the jump lengths x, $g(x)$, is chosen to be symmetric $g(x) = g(-x)$ and independent of the starting point. Before making a jump, a particle waits for a time τ defined by another PDF $\psi(\tau)$, see Fig. 1(a). Both distributions are normalized: $\int_{-\infty}^{\infty} g(x)dx = 1$ and $\int_0^{\infty} \psi(\tau)d\tau = 1$. These two functions determine the macroscopic properties of the transport process. In the standard continuous time random walk model, random variables x and τ are independent from each other. We can define the survival probability $\Psi(t)$, that is the probability for a particle not to jump away until time t, as

$$\Psi(t) = 1 - \int\limits_0^t \psi(\tau)d\tau. \qquad (1)$$

The first transport equation governs the outgoing flow of particles $Q(x,t)$, which defines how many particles leave the point x per unit of time. The equation connects the flux at the current point in space and time to the flux from all neighboring points in the past (Klafter and

Silbey, 1980):

$$Q(x,t) = \int\limits_{-\infty}^{+\infty} g(y) \int\limits_{0}^{t} \psi(\tau)Q(x-y,t-\tau)dyd\tau + P_0(x)\psi(t).$$
(2)

It is time for a particle to leave from the point x if its waiting time τ has elapsed, which is taken care of via the multiplication by $\psi(\tau)d\tau$. The particle could arrive to the point x time τ ago from some other point $x - y$ by making a jump of length y with probability density $g(y)$. We next integrate over all possible waiting times and jump distances. The last term on the right hand side assumes that at the moment of time $t = 0$ particles had an initial distribution $P_0(x) = P(x, t = 0)$. Particles gradually leave their initial spots according to the waiting time distribution. We also assume that all particles were introduced to the system at $t = 0$ and the probability density of making the first jump is given by $\psi(\tau)$. The situation is different if the particles have some prehistory. In that case, the probability distribution of the first waiting time is in general different from $\psi(\tau)$ (Haus and Kehr, 1987), see Section IV.D for more detailed discussion.

The next step is to connect the outgoing flux in the past to the current density of particles at a given point in space and time,

$$P(x,t) = \int\limits_{-\infty}^{+\infty} g(y) \int\limits_{0}^{t} \Psi(\tau)Q(x-y,t-\tau)dyd\tau + P_0(x)\Psi(t).$$
(3)

The density is a sum of outgoing particles from all other points at different times, weighted by the jump length probability, provided the particles survived for a time τ after their arrival to x at $t-\tau$. The last term on the right hand side of Eq. (3) accounts for the particles which stay in their starting points until the observation time t.

The above set of equations specifies the standard continuous-time random walk (CTRW) process with an arbitrary initial condition. These integral equations can be solved by using the combination of Fourier (with respect to space) and Laplace (with respect to time) integral transforms (Erdélyi, 1954). We exploit the fundamental property of these transforms which turns convolution integrals into products in the Fourier-Laplace space. We use k and s to denote coordinates in Fourier and Laplace space, respectively. By explicitly providing the argument of a function, we will distinguish between the normal or transformed space, for example $\psi(\tau) \rightarrow \psi(s)$ and $g(x) \rightarrow g(k)$. As a result, the solution for the density of particles is given by the Montroll-Weiss equation (Klafter et $al.$, 1987; Montroll and Weiss, 1965):

$$P(k,s) = \frac{\Psi(s)P_0(k)}{1 - \psi(s)g(k)},$$
(4)

where $\Psi(s) = [1 - \psi(s)]/s$. This solution allows us to reduce the pair of original equations (2)-(3) to a single equation for the density $P(x,t)$:

$$P(x,t) = \int\limits_{-\infty}^{+\infty} g(y) \int\limits_{0}^{t} \psi(\tau)P(x-y,t-\tau)dyd\tau + \Psi(t)P_0(x).$$
(5)

In our derivation, we intentionally used an intermediate step of introducing the flow of particles $Q(x,t)$. For a more general initial condition with a non-trivial distribution of particles over their lifetimes, it provides the proper way to obtain the corresponding transport equation for the density of particles (Zaburdaev, 2008). In addition, a very similar set of equations will be used for the models that incorporate velocity of particles.

Below we will frequently use the notion of the $propagator$ (and sometimes, depending on the context, Green's function). It is the solution of the transport equation for the delta-like initial distribution[2] $P_0(x) = \delta(x)$. From Eq. (4) the propagator can be identified as

$$G(k,s) = \frac{\Psi(s)}{1 - \psi(s)g(k)}.$$
(6)

Then, for any arbitrary initial distribution, the solution will be given by the convolution of an initial profile with the propagator,

$$P(x,t) = \int\limits_{-\infty}^{\infty} G(x-y)P_0(y)dy.$$
(7)

The above Eqs. (4) and (6) give a formal solution of the transport equation. When given functions $g(y)$, $\psi(\tau)$, and $P_0(x)$, one should find their Fourier and Laplace transforms, insert them into Eq. (4), and calculate their inverse transform. Unfortunately, in general it is almost impossible to find this inverse transform analytically. Instead an asymptotic analysis for large time and space scales can be employed. To proceed, we must specify the probability densities $g(y)$ and $\psi(\tau)$. Motivated by applications and also mathematical convenience, we choose a power law form of these PDFs. By varying the exponent of their power law tails, different regimes of diffusion can be accessed. Assume the following particular forms:

$$\psi(\tau) = \frac{1}{\tau_0}\frac{\gamma}{(1 + \tau/\tau_0)^{1+\gamma}}, \quad \gamma > 0;$$
(8)

$$g(x) = \frac{\Gamma[\beta + 1/2]}{x_0\sqrt{\pi}\Gamma[\beta](1 + (x/x_0)^2)^{\beta+1/2}}, \quad \beta > 0.$$
(9)

---

[2] A biology-oriented definition of the propagator was nicely put by Ronald Ross, the Nobel laureate for medicine in 1902 (Ross, 1905): "...$suppose$ a box $containing$ a $million$ $gnats$ $were$ to be $opened$ in the $centre$ of a $large$ $plain,$ and $that$ the $insects$ $were$ $allowed$ to $wander$ $freely$ in all $directions,$ how $many$ of $them$ $would$ be $found$ $after$ $death$ at a $given$ $distance$ $from$ the $place$ $where$ the box was $opened?$"

The exact details of these distributions are not qualitatively important in the asymptotic limit. Crucial are their power law tails which determine the behavior of their moments. All other details will be absorbed into constant pre-factors; yet we will keep track of those for the sake of completeness.

There are two important moments of these PDFs, the mean squared jump length,

$$\langle x^2 \rangle = \int_{-\infty}^{\infty} x^2 g(x) dx, \tag{10}$$

and the mean waiting time,

$$\langle \tau \rangle = \int_{0}^{\infty} \tau \psi(\tau) d\tau. \tag{11}$$

If these moments exist, for the chosen functions in Eqs.(8)-(9), they are given by simple expressions:

$$\langle \tau \rangle = \frac{\tau_0}{\gamma - 1}, \gamma > 1; \quad \langle x^2 \rangle = \frac{x_0^2}{2(\beta - 1)}, \beta > 1. \tag{12}$$

When both quantities are finite, the resulting transport equation reduces to the standard diffusion equation with a diffusion coefficient $D = \langle x^2 \rangle / (2 \langle \tau \rangle)$,

$$\frac{\partial P}{\partial t} = D \triangle P(x,t). \tag{13}$$

It is easy to demonstrate by assuming that the typical spatial and temporal scales of interest are significantly larger then $\langle x^2 \rangle$ and $\langle \tau \rangle$ respectively. It is then possible to expand the expression under the integral in Eq. (5) in a Taylor series with respect to y and τ yielding the diffusion equation above; its propagator is the well known Gaussian distribution:

$$P(x,t) = \frac{1}{\sqrt{4\pi Dt}} e^{-\frac{x^2}{4Dt}}. \tag{14}$$

The second moment of this distribution is the mean squared displacement (MSD) which scales linearly with time:

$$\langle x^2(t) \rangle = \int_{-\infty}^{\infty} x^2 P(x,t) dx = 2Dt. \tag{15}$$

Another important property of the diffusion process is the scaling of the density profile. As we will see for different models and regimes of random walks, in the limit of large times, the propagator may be represented as

$$G(x,t) = t^{-\alpha} F\left(\frac{x}{t^\alpha}\right), \tag{16}$$

where $F(\xi)$ is a scaling function (for example, Gaussian, in the case of normal diffusion) and α is a model specific scaling exponent (with $\alpha = 1/2$ in the case of normal diffusion). Such a functional form suggests a scaling variable $\xi = x/t^\alpha$, meaning that a characteristic spatial

scale on which the density changes, $\bar{x}$, scales with time as $\bar{x} \propto t^\alpha$. From the solution given by Eq. (14), we see that the width of the cloud of particles grows as $\overline{x} \propto t^{1/2}$.

The asymptotic limit $x, t \to \infty$ corresponds to the dual transition $k, s \to 0$ in the Fourier-Laplace domain. That is why, instead of the full Fourier and Laplace transforms of g and ψ in Eq. (4), their expansion in Taylor series with respect to small k and s can be used[3]. In the Fourier-Laplace coordinates, the leading terms of the expansion for the chosen power-law functions are (Prudnikov *et al.*, 1986):

$$g(k) = 1 - \frac{x_0^2}{\beta - 1} \frac{k^2}{4} - \frac{x_0^{2\beta} \Gamma[1-\beta]}{2^{2\beta} \Gamma[1+\beta]} |k|^{2\beta} + O(k^{2+2\beta}) \tag{17}$$

$$\psi(s) = 1 - \frac{\tau_0}{\gamma - 1} s - \tau_0^\gamma \Gamma[1-\gamma] s^\gamma + O(s^{1+\gamma}) \tag{18}$$

In the marginal cases, when γ or β have values where one of the moments starts to diverge (for example, $\gamma, \beta = 1$), there are logarithmic correction terms appearing in this expansion. We will not consider these cases here (see for example Chukbar (1995); Zumofen and Klafter (1993) for more information). The finite waiting time and the mean squared jump distance correspond to $\gamma, \beta > 1$. In this case, the first two terms in the above expansions are dominant for small k and s. The pre-factors in front of k^2 and s can be recognized as the mean squared jump distance and the mean waiting time from Eq.(12) respectively. By substituting them into the formal solution, Eq. (4), we can rewrite it as the diffusion equation in the Fourier-Laplace space, or simply compute the inverse transforms and obtain the Gaussian distribution Eq. (14). For $\gamma < 1$ and $\beta < 1$, terms with fractional powers dominate over linear and quadratic terms in Eqs. (18) and (17), respectively. By substituting them in Eq. (4) we obtain the following equation in the Fourier-Laplace space

$$s^\gamma \Gamma[1-\gamma] P(k,s) = -|k|^{2\beta} K' P(k,s) + s^{\gamma-1} \Gamma[1-\gamma] P_0(k), \tag{19}$$

where $K' = (x_0/2)^{2\beta} \Gamma[1-\beta] / (\tau_0^\gamma \Gamma[1+\beta])$. After returning to the original space-time domain, we obtain an equation with integral nonlocal operators:

$$\frac{\partial}{\partial t} \int_0^t \frac{P(x,\tau)}{(t-\tau)^\gamma} d\tau = K \int_{-\infty}^{\infty} \frac{P(y,t)}{|x-y|^{2\beta+1}} dy + \frac{P_0(x)}{t^\gamma}, \tag{20}$$

where $K = (x_0)^{2\beta} \Gamma[\beta + 1/2] / (\tau_0^\gamma \sqrt{\pi} \Gamma[\beta])$. The integral nonlocal operators in the above equation are the *fractional derivatives* (the integral on the right hand side is understood as the principle value) (Kilbas *et al.*, 2006;

---

[3] Taylor series are normally understood as an expansion in integer powers of the argument. In our case the leading terms of expansion with respect to the small k and s may involve fractional powers. Below we use the notion of Taylor series in this extended sense.

Podlubny, 1999; Samko *et al.*, 1993; West, 2014). The notion of fractional derivative allows us to rewrite the asymptotic balance equation in a compact form of the fractional diffusion equation (Barkai, 2002; Metzler and Klafter, 2000; Saichev and Zaslavsky, 1997):

$$\frac{\partial^\gamma P}{\partial t^\gamma} = K_{\beta,\gamma}\triangle^\beta P + \frac{P_0(x)}{t^\gamma}. \tag{21}$$

This equation describes the stochastic spreading of a cloud of particles and besides the case of normal diffusion has several interesting regimes. If the mean squared jump length is finite but the waiting times are anomalously long, $\langle\tau\rangle = \infty$, the resulting dispersal is anomalously slow or subdiffusive. The typical width of the cloud scales as $\overline{x} \propto t^{\gamma/2}$, with $\gamma < 1$. In the opposite case, when the average waiting time is finite but jumps are very long, $\langle x^2\rangle = \infty$, the equation describes superdiffusion. The typical width of the distribution of particles scales as $\overline{x} \propto t^{1/2\beta}$. Finally, when long waiting times compete with long jumps, the scaling is defined by both distributions of waiting times and jump lengths, $\overline{x} \propto t^{\gamma/2\beta}$. The stochasticity of the transport process reveals itself in the "forgetting" of the initial distribution and the tendency of the particles' density to the universal self-similar profile of the corresponding propagator, Eq. (16), with $\alpha = \gamma/2\beta$.

Before closing this section, let us have a closer look at the superdiffusion regime. The jump length distribution has a diverging second moment ($\beta < 1$) whereas the mean waiting time is finite. Therefore the leading terms in the expansion of $\psi(s)$ in Eq. (18) could be written as: $\psi(s) \simeq 1 + s\langle\tau\rangle$. The propagator in the Fourier-Laplace space is then given by

$$G(k,s) = \frac{1}{s + K_\beta |k|^{2\beta}} \tag{22}$$

with $K_\beta = (x_0/2)^{2\beta}\Gamma[1-\beta]/(\langle\tau\rangle\,\Gamma[1+\beta])$. By performing the inverse Laplace transform we obtain:

$$G(k,t) = \exp\left(-K_\beta |k|^{2\beta}t\right). \tag{23}$$

This expression is the Fourier transform (a characteristic function) of the symmetric Lévy distribution $L_\kappa[x,\sigma(t)]$, which describes the distribution of the sum of independent and identically distributed variables with power law PDFs (Uchaikin, 2003). Here $\kappa = 2\beta$ is the Lévy index and $\sigma^\kappa = K_\beta t$ is the scaling parameter. For some particular values of κ, the Lévy distribution has an analytical expression in coordinates space, such as Cauchy distribution ($\kappa = 1$), Lévy-Smirnov ($\kappa = 1/2$) or Holtsmark distribution ($\kappa = 3/2$) (Klafter and Sokolov, 2011; Uchaikin, 2003). The key feature of all of these distributions is the asymptotic power law tail $G(x,t) \sim t/|x|^{\kappa+1}$ (Chukbar, 1995; Klafter and Sokolov, 2011). In the scaling relation given by Eq.(16), the scaling function Φ is also given by the Lévy distribution with $\alpha = 1/\kappa$. Because of this intimate relation of the particles density to the Lévy distribution, the model of random walks with

instantaneous jumps received the name of Lévy flight (Mandelbrot, 1982)[4]. We can now ask about the behavior of the second moment of the density profile given by the Lévy distribution. This and higher moments in the Fourier (or the Fourier-Laplace) space are:

$$\langle x^n\rangle = \int\limits_{-\infty}^{\infty} x^n P(x,t)dx = (-i)^n \frac{d^n}{dk^n}\,P(k,t)|_{k=0}. \tag{24}$$

By substituting Eq. (23) into this formula, we immediately see that all moments with $n \geqslant 2$ diverge. It is thus impossible to compute the MSD as a function of time for a particle performing Lévy flights for a simple reason: it does not exist. Already after the first jump all particles will be distributed as $g(x)$ and this distribution has an infinite second moment. This feature of Lévy flights is often referred to as a shortcoming of the model when applied to physical processes, in which one expects regular behavior of moments (Mantegna and Stanley, 1994). However, as we have already mentioned, physical intuition points to the possibility to modify the Lévy flight model assuming that longer jumps must have a higher cost; there has to be a certain coupling between the length of the flight and its duration. The simplest coupling is the finite velocity of particles, when the time to accomplish a flight is linearly proportional to its length. As we show below, the introduction of the finite velocity of particles into the Lévy flight model retains the anomalous character of the transport process while regularizing the behavior of moments of the particle density. We believe that the compliance of the new model with physical intuition and ability to account for the velocity of particles explains its success in applications.

II. LÉVY WALKS

We will discuss several ways to introduce a coupling between jump length and time in the upcoming sections. Here we start with the conventional dynamical coupling of the particle position and current time via a constant velocity of the particle.

There are two closely related models which incorporate finite velocity of random walkers. The first one is a direct modification of the CTRW model: After spending its waiting time, a random walker does not jump instantaneously but instead moves with a constant speed to its destination (Klafter and Zumofen, 1994; Zaburdaev and Chukbar, 2002), see Fig. 1(c). Long excursions are still responsible for the anomalously fast diffusion, but now there are well-defined ballistic fronts and behavior

---

[4] Shlesinger and Klafter (1986) proposed an alternative schematization of Lévy flights: The are no waiting pauses and the duration of each step is constant so that the velocity of a flight is proportional to the step length drawn from a Lévy distribution.
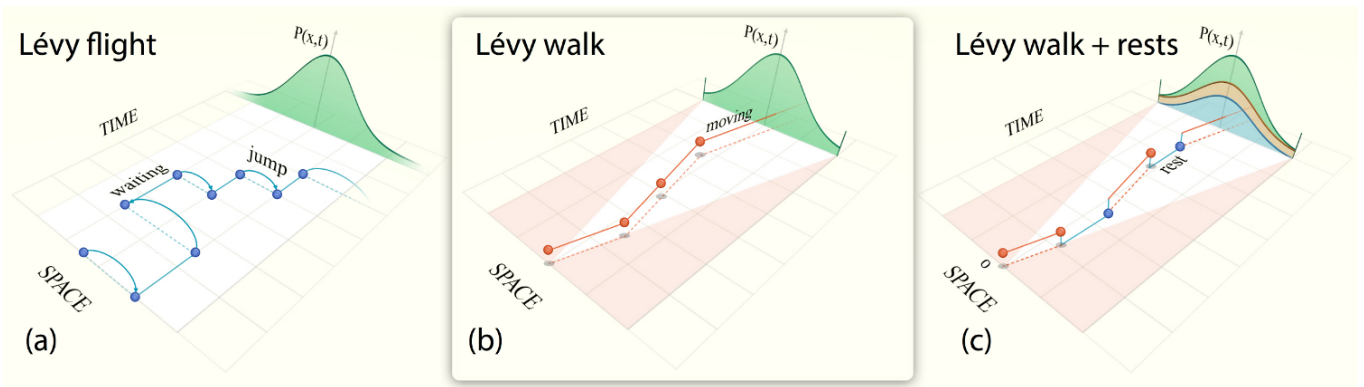
FIG. 1 (Color online) Random walk models of superdiffusion. (a) Lévy flight: A particle performs instantaneous jumps alternated with waiting pauses. The length of jumps and durations of waiting events are independent random variables. The resulting PDF $P(x,t)$ is not local in space at any moment of time. (b) Lévy walk: A particle moves with a constant velocity for a random time and then, at a turning point, instantaneously chooses a new direction and moves again. In this basic model particle's velocity can assume two values $\pm v$ only. As a result the length and duration of each event of ballistic motion are coupled. There is a ballistic cone $x_{\mathrm{f}} = \pm vt$ beyond which no particle can go (shaded area). As a result the PDF is bounded in space and its fronts are marked by two delta peaks. (c) Lévy walk with rests: Ballistic flights of a particle are alternated with pauses during which the particle does not move. At any instant of time the statistical ensemble consists of two fractions of particles, flying and resting. The total PDF is the sum of the two.

of all moments is regularized. In the second model, waiting periods are eliminated and the particle is always on the move (Klafter and Zumofen, 1994; Shlesinger *et al.*, 1986; Zumofen and Klafter, 1993), see Fig. 1(b). The distance of ballistic flights is distributed randomly and each flight is performed with a finite speed. At the end of the flight, the particle randomly changes direction. The latter model is what historically received the name of Lévy walks. Note that the Lévy walk model has only one distribution function to parametrize the motion of the particles as it discards waiting. This minimalistic setup remains the most popular model in modern applications.

A. Lévy walk model

The formulation of the microscopic model is very similar to that by Pearson cited in the introduction. A particle moves on a straight line with a fixed speed for some random time. At the end of the excursion, the particle randomly chooses a new direction of motion and moves for another random time with the same speed, see Fig. 1(b). There are only two characteristics of this model, that are the PDF of the duration of movements, which we will denote by $\psi(\tau)$, and the speed v of the particles. Despite its simplicity, this model is able to describe various regimes of stochastic transport, from classical to ballistic superdiffusion.

We now derive the transport equations of the Lévy walk model. First we introduce the frequency of velocity changes at a given point (analogue of the flux of particles

from a given point in the CTRW model),

$$
\begin{aligned}
\nu(x,t) \;=\; & \int_{-\infty}^{\infty} dy \int_{0}^{t} \phi(y,\tau)\nu(x-y,t-\tau)d\tau \\
& +\; \delta(t)P_0(x).
\end{aligned}
\tag{25}
$$

Here we incorporated a *coupled* transition probability density $\phi(y,t)$ which takes care of the fact that only particles flying from $x - v\tau$ and $x + v\tau$ can reach x in time τ and change the direction of their velocities after the flight time of τ:

$$
\phi(y,\tau) = \frac{1}{2}\delta(|y| - v\tau)\psi(\tau)
\tag{26}
$$

Therefore, a particle changes its velocity if it is at the end of the flight of duration τ which originated from $x \pm v\tau$. We assume that at $t = 0$ all particles at once choose new velocities and hence the second term on the right hand side of Eq.(25) contains a delta-function (note a difference to a gradual leaving of particles from their waiting positions for the CTRW model, Eq.(2)).

To calculate the actual amount of particles at a given point, we write

$$
P(x,t) = \int_{-\infty}^{\infty} dy \int_{0}^{t} \Phi(y,\tau)\nu(x-y,t-\tau)d\tau,
\tag{27}
$$

where

$$
\Phi(y,\tau) = \frac{1}{2}\delta(|y| - v\tau)\Psi(\tau).
\tag{28}
$$

is the probability density to travel a distance y and remain in the state of flight (note that with respect to τ Eq.

(26) has the meaning of the probability density whereas Eq. (28) is probability). Therefore, a particle is at the point (x, t) if it has started some time τ ago at $x \pm v\tau$ and is still in the state of the flight, taken care of by multiplication with $\Psi(\tau)$, Eq.(1). Note that in Eq.(27), the influence of the initial condition appears only indirectly, through the frequency of velocity changes $\nu(x, t)$ (cf. Eq.(3) for the CTRW model with an extra term for immobile particles survived from the start). By taking the limit $t \to 0+$ we can substitute $\nu(x, t)$ by $P_0(x)\delta(t)$ and recover $P(x, t) \to P_0(x)$.

The equations can be solved by using the combined Fourier-Laplace transform, but an additional technical complexity due to the coupling of space and time variables occurs (Klafter *et al.*, 1987; Zumofen and Klafter, 1993). We resolve it by using the shift property of the Laplace and Fourier transforms; as a result the corresponding Laplace transformed functions hold a linear combination of Fourier/Laplace coordinates $s \pm ikv$ as its argument:

$$P(k, s) = \frac{[\Psi(s + ikv) + \Psi(s - ikv)] P_0(k)}{2 - [\psi(s + ikv) + \psi(s - ikv)]} \qquad (29)$$

This is a formal solution of the problem and, as in the case of Lévy flights, the next step is to perform the asymptotic analysis. Due to the simple ballistic coupling $x = v\tau$, the possible scaling regimes of diffusion are governed by the power law tail of the flight time distribution, which we again take in the form given by Eq. (8).

1. Telegraph equation

If the mean squared flight distance is finite, $\gamma > 2$, the classical diffusion takes place in the asymptotic limit. However, the effects of finite velocity can be seen in this regime too. Consider for a moment an exponentially distributed flight time $\psi(\tau) = (1/\tau_0) \exp(-\tau/\tau_0)$. By taking its Laplace transform and substituting it into Eq. (29), we can invert the Fourier and Laplace transforms to obtain the telegraph equation (Goldstein, 1951):

$$\frac{\partial P}{\partial t} + \tau_0 \frac{\partial^2 P}{\partial t^2} = D \triangle P(x, t), \qquad (30)$$

where $D = v^2 \tau_0$. On very short times, it describes almost ballistic spreading of particles. As time goes, ballistic fronts run away much faster than spreading of the diffusive evolution ($\overline{x} \propto t$ vs. $\overline{x} \propto t^{1/2}$, for $t \gg \tau_0$) which starts to dominate the central part of the density profile. Finite velocity ensures, however, that there are no particles beyond the ballistic fronts.

2. Superdiffusion

As the flights get longer, $1 < \gamma < 2$, the mean squared flight length diverges (but the average flight time is still

finite) and we turn to the regime of superdiffusion. By using the expansion from Eq. (18) for small s and substituting its leading terms in Eq. (29) we arrive at the similar answer as Eq. (22) for the propagator

$$G(k, s) \simeq \frac{1}{s + K_v |k|^\gamma} \qquad (31)$$

with $K_v = \tau_0^{\gamma-1} v_0^\gamma (\gamma - 1)\Gamma[1 - \gamma] \sin(\pi\gamma/2)$. Several things to be noted here. After the inverse Fourier-Laplace transform we get the stable time-parametrized Lévy distribution with a scaling given by Eq. (16) and $\Phi(\xi) = L_\gamma(\xi)$, $\alpha = 1/\gamma$. For $1 < \gamma < 2$ the cloud of particles spreads faster than classical diffusion but still slower than the running ballistic fronts. Therefore ballistic fronts do not appear in this analysis and affect (like in previous subsection) only the far tails of the particle density distribution. Nevertheless, the existence of fronts is crucial for the calculation of moments, as we show below. Now we take a closer look at what is happening at the ballistic fronts. Assume that at the moment of time $t = 0$ we start with all particles initiating their flights at $x = 0$. Ballistic fronts are formed mostly by the particles which are still in their very first flights. The probability to remain in the flight is $\Psi(t)$ and therefore we can write down the density of particles in the ballistic peaks or "chubchiks" (Klafter and Sokolov, 2011)

$$G_{\text{front}}(x, t) = \frac{1}{2}\Psi(t) [\delta(x - vt) + \delta(x + vt)] \qquad (32)$$

This gives the first approximation of the whole density of particles as a Lévy distribution sandwiched between two running ballistic delta-like peaks (see Fig.2). A more detailed understanding of the density can be achieved by using the so-called infinite density measure (Rebenshtok *et al.*, 2014a,b), as we discuss in Section IV.C.

3. Ballistic diffusion

In case of even longer flights $0 < \gamma < 1$, when the mean flight time diverges, the diffusion process changes dramatically. In the case of Lévy flight, the scaling $\overline{x} \propto t^{1/\gamma}$ for small γ results in spreading which is faster than ballistic, leading to an obvious conflict with the light front limitation in the Lévy walk setup. Clearly, the ballistic front is playing a crucial role here. An asymptotic expansion of the propagator [obtained from Eq. (29) with $P_0(x) = \delta(x)$] has the following form:

$$G(k, s) \simeq \frac{(s + ikv)^{\gamma-1} + (s - ikv)^{\gamma-1}}{(s + ikv)^\gamma + (s - ikv)^\gamma}. \qquad (33)$$

Now Fourier and Laplace variables appear in the same scaling $s \sim k$ and indicate the ballistic behavior. It was suggested to call the inverse Fourier-Laplace transform of $(s + ikv)^\gamma + (s - ikv)^\gamma$ as a fractional generalization of the substantial or material derivative operator, $(v^{-1}\partial/\partial t \pm \partial/\partial x)^{1/\gamma}$ (Sokolov and Metzler, 2003). In the ballistic
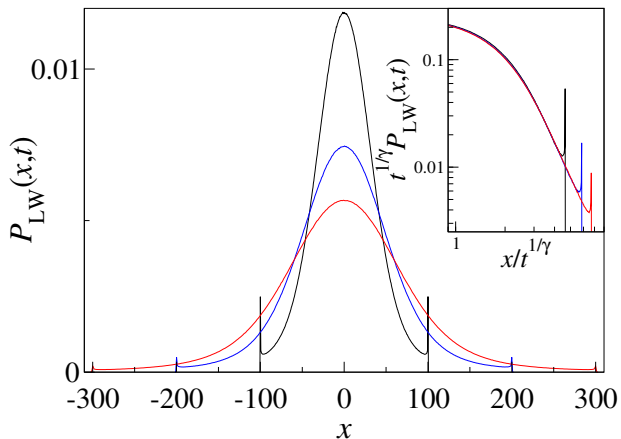
FIG. 2 (Color online) Propagators of the superdiffusive Lévy walk for different times. The propagators have a central part of the profile approximated by the Lévy distribution sandwiched between two ballistic peaks. In the inset, the same curves are shown in double logarithmic scale after the rescaling as given on the axis labels. A characteristic linear slope on the log-log plot illustrates the power-law tails of the density. The propagators were obtained by numerical simulations with $\gamma = 3/2$, $\tau_0 = 1$, and all particles starting their flights at $t = 0, x = 0$ with velocities $v = \pm 1$. The PDFs was sampled at $t = 100, 200$, and 300 (the width increases with time).
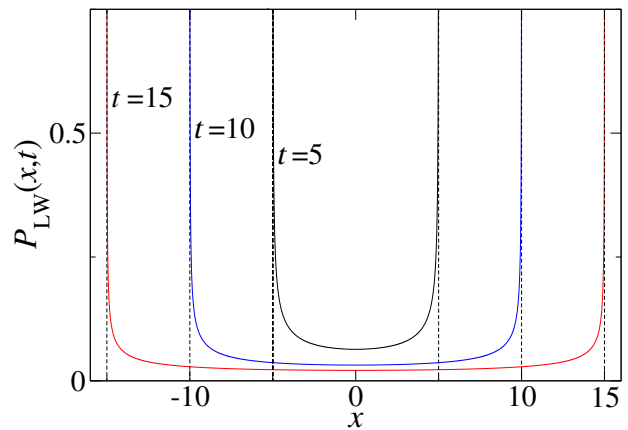

FIG. 3 (Color online) PDF of the Lévy walk model in the ballistic regime. This plot shows the density of particles, Eq.(34), at different moments of time. The parameters are $\gamma = 1/2$, $v = \pm 1$, $\tau_0 = 1$, and $P_0(x) = \delta(x)$. The densities have integrable divergences at the ballistic fronts due to the conservation of the total amount of particles.

regime there is again a technical difficulty to find the inverse Fourier-Laplace transform. The ballistic case is special in that its analytical solution can be found by the method discussed in Section IV.B. Here we just illustrate the shape of the propagator on a particular example $\gamma = 1/2$ [for arbitrary γ the answer is given by the Lamperti distribution (Bel and Barkai, 2005; Lamperti, 1958), see also below, Eqs. (61) and (83)]:

$$G(x,t) = \frac{1}{\pi(v_0^2 t^2 - x^2)^{1/2}}. \tag{34}$$

Figure 3 shows a U-shaped profile (for $\gamma \gtrsim 0.6$ the shape is W-like, see Fig. 6 b) with a divergent density at the ballistic fronts (Zumofen and Klafter, 1993). This divergence is, however, integrable and the total number of particles is conserved. Although the density profile is very different from the Gaussian profile of the classical diffusion, the ballistic diffusion remains a stochastic transport phenomena where the initial condition is gradually forgotten with time and the solution approaches the universal self-similar profile of the corresponding Green's function.

4. Mean squared displacement and other moments

The PDFs of the Lévy walk in general do not possess a global scaling where the whole propagator can be represented in the form of Eq. (16), unlike the case of the Gaussian profile and normal diffusion. A clear example is the superdiffusive regime ($1 < \gamma < 2$), where the mid-

dle part of the profile scales as $\overline{x} \propto t^{1/\gamma}$, but, at the same time, the fronts exhibit the ballistic scaling. As a consequence, in Lévy walks the scaling exponents of the propagator and MSD are not the same; for a summary of these issues we refer to Rebenshtok et $al.$ (2014a,b); Schmiedeberg et $al.$ (2009).

As we have discussed, the asymptotic dynamics of propagators can be analyzed by considering the limits $k \to 0$ and $s \to 0$. Remarkably, in coupled models these two limits do not commute (Schmiedeberg et $al.$, 2009). In general, by changing the order of these limits we imply which effect is dominating: larger distance or longer time, or maybe the interplay of both. The MSD can be calculated by using Eq. (24) via the second derivative with respect to k and taking the limit $k \to 0$. To compute the asymptotic time dependence of the MSD we can take the second limit $s \to 0$ and then calculate the inverse Laplace transform. By inverting the order of limits and first taking $s \to 0$, we can follow the behavior of the density of particles closer to the origin, from where the the scaling exponent of the propagator α [see Eq. (16)] could be obtained. Finally, in order to find the shape of the propagator, both limits have to be taken simultaneously. We first provide the results for the scaling of the MSD (Zumofen and Klafter, 1993). To compute the MSD for superdiffusive sub-ballistic regime, (the LW processes with the finite mean flight time $\langle\tau\rangle$, corresponding to $1 < \gamma < 2$), one more term in the expansion of the nominator has to be included, in order to capture the effect of the ballistic fronts. This leads to

$$\langle x^2(t) \rangle \propto \begin{cases} t^2 & 0 < \gamma < 1 \\ t^2/\ln t & \gamma = 1 \\ t^{3-\gamma} & 1 < \gamma < 2 \\ t\ln t & \gamma = 2 \\ t & \gamma > 2 \end{cases} \tag{35}$$
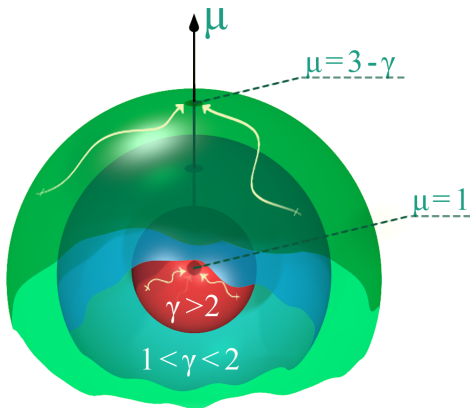
FIG. 4 (Color online) Scaling exponent of the mean squared displacement for Lévy walks, Eq. (35). When the second moment of the PDF $\psi(\tau) \sim t^{-\gamma-1}$ exists, $\gamma > 2$, the scaling $\langle x^2(t) \rangle \propto t^\mu$ is universal with the exponent $\mu = 1$. When $1 < \gamma < 2$ and the variance $\langle \tau^2 \rangle$ diverges, the mean squared displacement scales with the exponent $\mu = 3 - \gamma$. Finally, for very heavy tails $0 < \gamma < 1$, the scaling is ballistic $\mu = 2$. Inspired by a sketch in Bouchaud and Georges (1990).

Figure 4 gives a pictorial view of the MSD scaling regimes. The scaling exponent α is given by Zumofen and Klafter (1993):

$$\alpha = \begin{cases} 1 & 0 < \gamma < 1 \\ 1/\gamma & 1 < \gamma < 2 \\ 1/2 & \gamma > 2 \end{cases} \qquad (36)$$

It is important to note that in the sub-ballistic regimes the scaling exponent α refers to the central part of the density profile.

There is an interesting concept to characterize the stochastic transport phenomena by using a spectrum of fractional moments (de Anna *et al.*, 2013; Artuso and Cristadoro, 2003; Castiglione *et al.*, 1999; Metzler and Klafter, 2000; Rebenshtok *et al.*, 2014b; Sanders and Larralde, 2006; Seuront and Stanley, 2014):

$$\langle |x|^q \rangle = \int_{-\infty}^{\infty} |x|^q P(x,t) dx \simeq M_q \cdot t^{q\nu(q)}. \qquad (37)$$

For normal diffusion, because of its self-similar shape and the unique scaling $\overline{x} \propto t^{1/2}$, Eq.(37) leads to a constant value of $\nu(q) = 1/2$. If $\nu(q)$ is not constant, this kind of diffusion process is referred to as *strongly anomalous* (Castiglione *et al.*, 1999). Because of its multi-scaling property, sub-ballistic Lévy walks belong to this class. Figure 5 shows characteristic be-linear shape of $q\nu(q)$ as a function of the moment order q. The linear dependencies are q/γ for small q is replaced by the dependence $q - \gamma + 1$ for higher moments. For small values of q, the
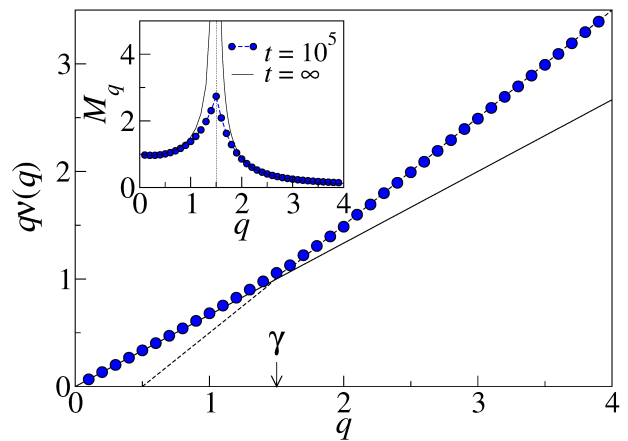

FIG. 5 (Color online) Scaling of the fractional moments of the Lévy walk process. Scaling exponent $q\nu(q)$ for the $q - $th moment of the PDF, see Eq. (37) as a function of q for the sub-ballistic Lévy walk model, $\gamma = 3/2$. It has a characteristic bi-linear behavior: $q\nu(q) = q/\gamma$ for $q < \gamma$ (solid line) and $q\nu(q) = q+1-\gamma$ (dashed line) otherwise. The inset shows the pre-factors of fractional moments M_q. Dots correspond to the numerical data sampled for $t = 10^5$, whereas lines diverging at $q = \gamma$ are analytical predictions in the limit $t \to \infty$. Adapted from Rebenshtok *et al.* (2014a).

dominating contribution to the averaging integral comes from the central part of the propagator, where it can be approximated by the self-similar Lévy distribution. For $1 < \gamma < 2$ the fractional moments of Lévy distribution exist for $q < 2$ and $q\nu(q) = q/\gamma$. For higher moments, the far tails of the propagator are important and this is where the ballistic cut-off by the running peaks plays a crucial role. The scaling of the fractional moments for large q can be obtained by assuming that the PDF has an asymptotic shape $P(x,t) \sim t/|x|^{1+\gamma}$ and has to be integrated with $|x|^q$ till the cut-off distance $|x| = v_0 t$. That would lead to the $q - \gamma + 1$ result or $\nu(q) \sim 1$. Exact results on the behavior of fractional moments could be obtained by using the concept of infinite densities (Rebenshtok *et al.*, 2014b), which is discussed in Section IV.C.

For $q \to 0$, the $\nu(q) \to \alpha$ gives a possible way of estimating the scaling from the experimental data. Recently Gal and Weihs (2010) measured the spectrum of exponents $q\nu(q)$ for the dispersion of polystyrene bead particles internalized by live human metastatic breast cancer epithelial cells and found for large q a linear behavior $q\nu(q) \sim cq$ with $c \simeq 0.8 - 0.6$. That means that the observed spreading is of the sub-ballistic superdiffusion type. This is probably related to the active transport of the beads within a cell.

B. Lévy walks with rests

When performing Lévy walks, a particle always moves, see Fig. 1(b), whereas during CTRW evolution its makes instantaneous jumps alternated with waiting events, see

Fig. 1(a). By combining both of them, we arrive at the model where waiting periods alternate with periods of ballistic motion, see Fig. 1(c). One can describe this model as Lévy walk interrupted by rests (Klafter and Sokolov, 2011; Klafter and Zumofen, 1994; Zaburdaev and Chukbar, 2002). As in the standard Lévy walk model, there can not be particles beyond the fronts $|x| > vt$. Interestingly, there is a natural separation of particles into two groups: sitting in a given point and moving somewhere else. The total density of particles at a given point x is the sum of two fractions (Uchaikin, 2003; Zaburdaev and Chukbar, 2002). The PDF of resting times we denote $\psi_r(\tau)$ (Klafter and Sokolov, 2011) and the PDF $\psi(\tau)$, as before for Lévy walks, is used to describe the durations of ballistic phases. Both functions are of the same power-law form but may have different exponents. By $\tilde{\nu}(x,t)$ we denote the flux of particles which finished their rest and start moving out of a given point x (analogy to the velocity re-orientation points in the standard Lévy walk model). It satisfies the following balance equation:

$$
\begin{aligned}
\tilde{\nu}(x,t) &= \int_0^t \psi_r(\tau) \int_0^{t-\tau} \phi(y,\tau_1)\tilde{\nu}(x-y,t-\tau-\tau_1)d\tau_1 d\tau \\
&+ \psi_r(t)P_0(x),
\end{aligned}
\tag{38}
$$

where $\phi(y,\tau)$ is the coupled transition probability of the Lévy walk model. The densities of sitting and flying particles are then given by

$$
\begin{aligned}
P_r(x,t) &= \int_0^t \Psi_r(\tau) \int_0^{t-\tau} \phi(y,\tau_1)\tilde{\nu}(x-y,t-\tau-\tau_1)d\tau_1 d\tau \\
&+ \Psi_r(t)P_0(x),
\end{aligned}
\tag{39}
$$

$$
P_{fly}(x,t) = \int_0^t \Phi(y,\tau)\tilde{\nu}(x-y,t-\tau)d\tau,
\tag{40}
$$

where $\Phi(x,t)$ is the coupled survival probability of Lévy walks (28). The total density of particles is the sum of flying and sitting PDFs, $P_\Sigma = P_{fly} + P_r$. In the Fourier-Laplace space it can be expressed as (Klafter and Sokolov, 2011)

$$
P_\Sigma(k,s) = \frac{[\Phi(k,s)\psi_r(s) + \Psi_r(s)]P_0(k)}{1 - \psi_r(s)\phi(k,s)}
\tag{41}
$$

The first and second terms in the brackets of the nominator correspond to the contributions from the flying and sitting particles, respectively. As in the case of the CTRW, the long trapping times can compete with long excursions. If, however, the mean trapping time is finite, the scaling of the propagator and of the corresponding MSD is the same as in the Lévy walk model. It is also easy to see from Eq. (41) that if both mean resting time and the mean moving time are finite, the density of the flying particles is locally proportional to
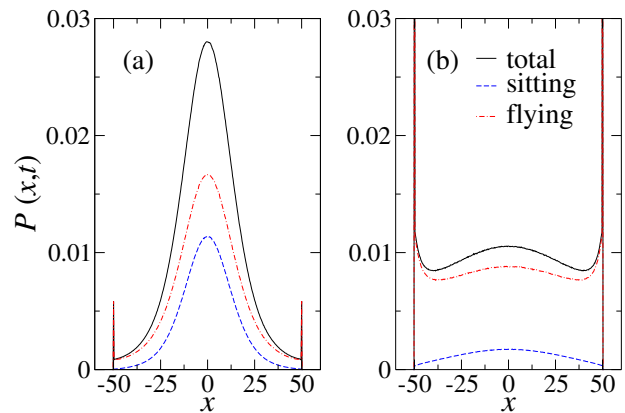

FIG. 6 (Color online) Lévy walks with rests. Panel (a) shows the PDF of the Lévy walk model with exponentially distributed resting times and power-law distribution of flight times with $\gamma = 3/2$. Both average resting, $\langle \tau_r \rangle$, and flying times are finite. The total density of particles (solid line) is the sum of sitting (dashed line) and flying (dash-dotted line) particles. Panel (b) shows the PDF for the ballistic regime with $\gamma = 0.8$. Here the number of sitting particles is greatly reduced. In the asymptotic limit $t \to \infty$ the total PDF and the PDF of flying particles will coincide. The parameters are $v = \tau_0 = \langle \tau_r \rangle = 1$ and $t = 50$.

that of the resting particles. The coefficient of proportionality is the ratio of times a particle spends on average in each phase (Zaburdaev and Chukbar, 2002), $P_{fly}(x,t) = (\langle \tau \rangle_{fly} / \langle \tau \rangle_r)P_r(x,t)$. In the regime when the mean flight time diverges, there is an irreversible transition of resting particles into flying ones, see Fig. 6, and therefore a convergence to the standard Lévy walk process. If at $t = 0$ all particles are resting, their total population will decrease in time as $\int_{-\infty}^{\infty} P_r(x,t)dx \propto t^{\gamma-1}$.

With that we close the discussion of the relatives of the standard Lévy walk model. We will meet them again in Sections V and VI, when discussing their applications both in physics and biology. We now proceed to the generalizations of the Lévy walk model.

III. GENERALIZATIONS OF THE LÉVY WALK MODEL

A. Random walks with random velocities

A natural generalization of the Lévy walk model is the process in which the velocity of a particle is not fixed but is a random variable itself (Barkai and Klafter, 1998; Zaburdaev et al., 2008). A number of examples where a random walker has a changing velocity is discussed in (Zaburdaev et al., 2008). When the velocity of particles is characterized by a heavy tailed distribution, the palette of possible diffusion regimes is defined by the interplay of flight time and velocity distributions. We denote the velocity PDF by $h(v)$ and write down the corresponding transport equations of random walks with random
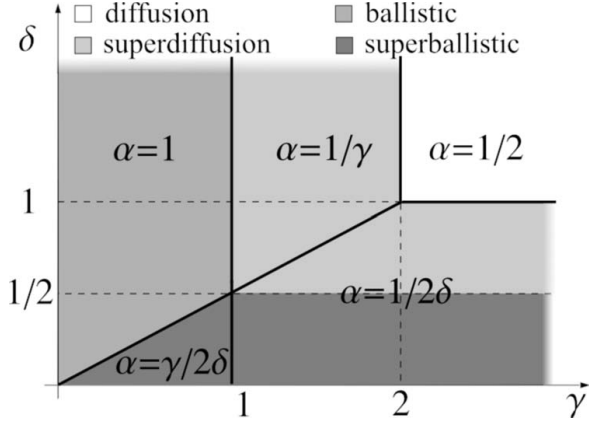
FIG. 7 Scaling regimes of the random walks with random velocities. By varying the exponents of the power-law tails of the velocity distribution δ and of the flight time distribution γ, the model can be tuned into different diffusion regimes, from classical diffusion to super-ballistic superdiffusion. From Zaburdaev et al. (2008).

velocities (RWRV) (Zaburdaev et al., 2008):

$$
\nu(x,t) = \int_{-\infty}^{\infty} dv \int_{0}^{t} \nu(x - v\tau, t - \tau)h(v)\psi(\tau)d\tau
$$
$$
+ \ \delta(t)P_0(x). \tag{42}
$$

$$
P(x,t) = \int_{-\infty}^{\infty} dv \int_{0}^{t} \nu(x - v\tau, t - \tau)\Psi(\tau)h(v)d\tau. \tag{43}
$$

Despite the fact that equations now are more complicated they can still be resolved by using the integral transforms

$$
P(k,s) = \frac{\int_{-\infty}^{+\infty} \Psi(s + ikv)h(v)dv}{1 - \int_{-\infty}^{+\infty} \psi(s + ikv)h(v)dv}. \tag{44}
$$

It is easy too see that for $h(v) = [\delta(v - u_0) + \delta(v + u_0)]/2$ we recover the standard Lévy walk model result Eq. (29). Because of the additional complexity added through velocity distribution it is even harder to find an example where an exact analytical solution can be obtained. However, one very remarkable example is the case of the Lorentzian or Cauchy velocity distribution:

$$
h(v) = \frac{1}{u_0\pi} \frac{1}{1 + v^2/u_0^2}. \tag{45}
$$

It appears in physical problems of two-dimensional turbulence (Chukbar, 1999; Min et al., 1996; Tong and Goldburg, 1988), as a model distribution of kinetic theory (Ben-Naim et al., 2005; Trizac et al., 2007), and also as a particular case of the generalized kappa-distributions

of plasma physics applications (Hasegawa et al., 1985; Meng et al., 1992) and statistics (Tsallis, 1988, 1999). It was also reported for the distribution of velocities of starving amoeba cells (Takagi et al., 2008). In this case the density of particles does not depend on the flight time distribution at all and also has a shape of the Lorentzian:

$$
P(x,t) = \frac{u_0 t}{\pi(x^2 + u_0^2 t^2)}. \tag{46}
$$

To understand the scaling behavior of the RWRV model, we use the scaling regimes of the CTRW model as a guideline. For that we calculate the effective jump length distribution, which, due to a simple coupling $x = vt$, can be obtained by the following integration:

$$
g_{\text{eff}}(x) = \int_{-\infty}^{+\infty} dv \int_{0}^{+\infty} \delta(x - v\tau)h(v)\psi(\tau)d\tau. \tag{47}
$$

For the velocity distribution we assume a generic power-law form, $h(v) \propto |v|^{-1-2\delta}$. We can now integrate Eq. (47) and find the exponent of the tail of the effective jump length distribution $\beta(\gamma, \delta)$. The waiting time distribution of CTRW model represents the time cost of the flight, therefore we can use the flight time distribution exponent. By substituting γ and $\beta(\gamma, \delta)$ into the scaling relation for the CTRW, we find the scaling exponent $\alpha = \gamma/2\beta$ of the RWRV model, see Fig. 7.

Besides the classical diffusive, superdiffusive, and ballistic transport, superballistic scaling is possible. In the latter case, the mean absolute velocity has to be infinite ($\delta < 1/2$). As in the Lévy walk model, the regime of sub-diffusion is inaccessible; with non-zero velocities there is no possibility to trap a particle for a long time. As we see, the introduction of the velocity distribution significantly increases the flexibility of the model while still keeping it amenable to the analytical approach.

B. Random walks with velocity fluctuations

In all previous models we neglected interactions of the walker with its environment or assumed that it had no effect on the particle as it moved. In this section we discuss a model of random walks in active media. We assume that a particle can interact with its surrounding which results in the weak fluctuations of particle's velocity. The term "active" emphasizes the fact that particles not simply lose velocity as a result of passive friction but can gain positive and negative velocity increments such that on average their velocity remains constant during a single flight event, see Fig. 8. This model was applied to reproduce the perturbation spreading in Hamiltonian many particle systems by Denisov et al. (2012); Zaburdaev et al. (2011a), see Section V.B. To setup the model accounting for velocity fluctuations, we modify the Lévy walk model (Zaburdaev et al., 2011a).

During each flight of a particle, its position is described by a simple Langevin equation: $\dot{x} = v_0 + \zeta(t)$
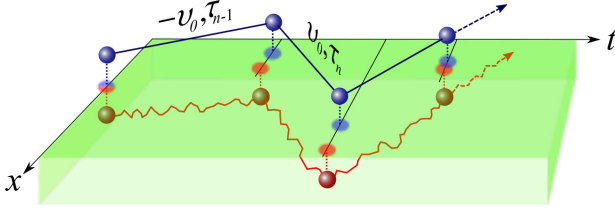
FIG. 8 (Color online) Sketch of the random walk in active media. Velocity during flights fluctuates around a fixed averaged value. As a result the fluctuations accumulate with time and the final position of the particle, passing through the active medium, will differ from that produced by an ideal Lévy walk process. From Zaburdaev *et al.* (2011a).

(Van Kampen, 2011), where $\zeta(t)$ is a delta-correlated Gaussian noise of zero mean and finite intensity D_v, i.e., $\langle \zeta(t)\zeta(s) \rangle = D_v \delta(t-s)$. This equation describes the well known biased Wiener process with drift v_0 (Karatsas and Shreve, 1997). After an integration over a time interval τ, we obtain:

$$x(t + \tau) = x(t) + v_0\tau + w(\tau), \qquad (48)$$

where $w(\tau) = \int_t^{t+\tau} \zeta(s)ds$ is characterized by a Gaussian PDF $p(w,\tau)$ with the dispersion $\sigma_\tau^2 = \langle (x(\tau) - v_0\tau)^2 \rangle = D_v\tau$. Transport equations for this model can also be written and solved in the Fourier-Laplace space. When velocity fluctuations are small, $(D_v\langle\tau\rangle)^{1/2} \ll v_0\langle\tau\rangle$, the central part of the density profile of particles is given by the same Lévy distribution as in the case of the standard model. New phenomena appear in the ballistic regions, where fronts, due to fluctuations, now look like humps (see Fig. 9):

$$P_{\text{hump}}(x,t) = \Psi(t) \left[p(x + v_0t, t) + p(x - v_0t, t) \right]/2 \quad (49)$$

As before, $\Psi(t)$ is the probability of not changing the direction of flight during time t, Eq. (1), and has a power-law asymptotic $\Psi(t) \propto (t/\tau_0)^{-\gamma}$. Consequently, the area under the ballistic humps, Eq. (49), also scales as $t^{-\gamma}$. During ballistic flights, the particles undergo random fluctuations caused by velocity variations. All particles in the hump are in the state of their first flight of duration t, thus the dispersion of the Gaussian-like humps grows as $t^{1/2}$, and we arrive at the following scaling for the particles density in the humps:

$$P_{\text{hump}}(\bar{x},t') \simeq u^{-\gamma-1/2} P_{\text{hump}}(\bar{x}/u^{-1/2}, t), \qquad (50)$$

where $u = t'/t$ and $\bar{x} = x - v_0t$, see inset in Fig. 9. From this result we learn that ballistic humps may carry some additional information about the interactions between the random walking particles and their environment.

The two models we discussed are the most frequently used modifications of the original Lévy walk setup. In the next subsection, we are going to mention two more
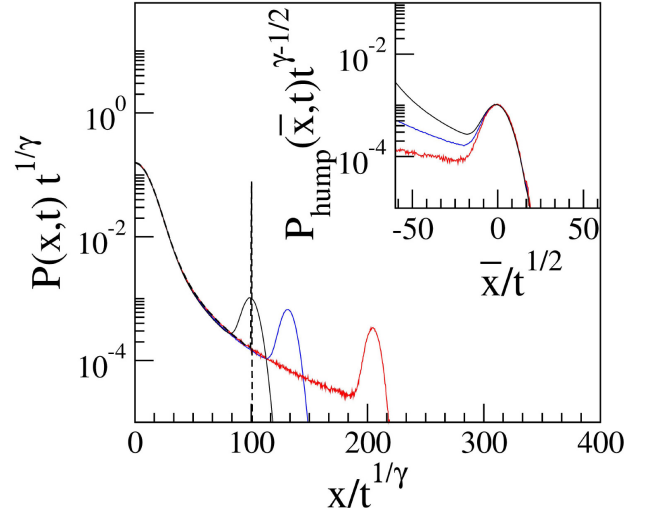

FIG. 9 (Color online) Profile of the Lévy walk model with velocity fluctuations. The inset shows the scaling of humps. Please note that the figure is adapted from Zaburdaev *et al.* (2011a); Zaburdaev *et al.* (2012) where a so-called equilibrated initial condition was used (see Sec. IV.D for details), as a result the height of the hump decays slower than discussed in the text, Eq. (50). Independent of the type of the initial condition, the shape of humps is Gaussian, with their width growing as $t^{1/2}$.

models of coupled random walks which introduce higher time cost for longer jumps, but still have instantaneous jumps as the standard CTRW model.

C. Other coupled models

There are two modifications of the CTRW model which are very similar to the Lévy walk model, but still do not have a well defined velocity of particles (Becker-Kern *et al.*, 2004; Jurlewicz *et al.*, 2012; Kotulski, 1995; Meerschaert and Scalas, 2006; Straka and Henry, 2011). In both models the waiting time and jump distance are coupled but jumps are instantaneous. There are two possibilities: In the "jump first" model, a random walker first jumps to a random distance y and then waits at the arrival point for a time $\tau = a|y|$, where a is a positive coupling constant (Zaburdaev, 2006). In the "wait first" model, a particle first waits for a random time τ and then makes a jump of the length $|y| = \tau a^{-1}$ (Barkai, 2002; Shlesinger *et al.*, 1982). Figure 10 shows trajectories of these two models compared to the one of the standard Lévy walk model. We see that in (x,t) plane the turning points of all three random walks are identical, and it is the paths which are different. At time t the models differ only by their last step. However, this difference is crucial. The transport equations for jump first and wait first models can be written down and solved in the Fourier-Laplace space, see Schmiedeberg *et al.* (2009). The MSD of the jump first model for the anomalous diffusion regime (long jumps) is diverging, which is clear if one looks at the dis-
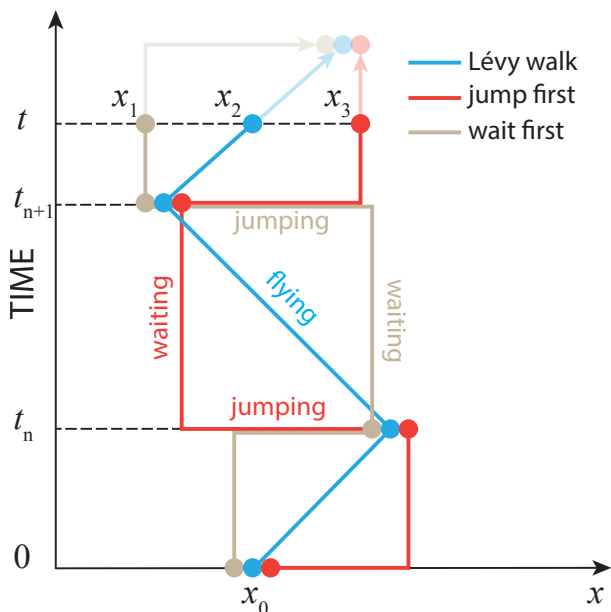
FIG. 10 (Color online) Comparison of trajectories of the Lévy walk model and two coupled models, "wait first" and "jump first". Trajectories of all three models are passing through the same points on the (x, t) diagram, but taking different paths. The positions of particles at time t are determined by their last steps.
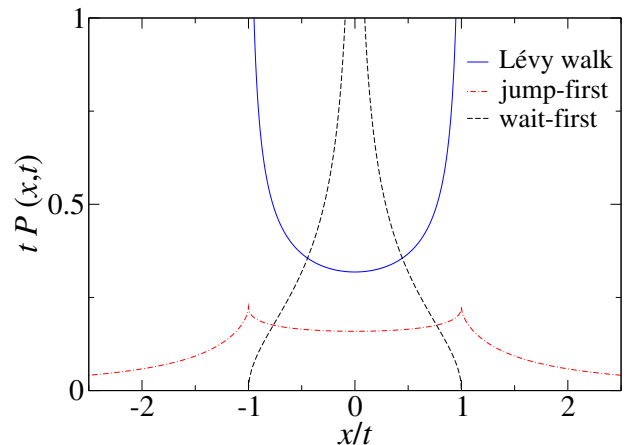

FIG. 11 (Color online) Propagators of coupled models. Analytical solutions for the propagators of the wait first (dashed line) and jump first (dash-dotted line) models are compared with a Lévy walk propagator (solid line) in the ballistic regime with $\gamma = 1/2$. The results are obtained by the method discussed in Section IV.B, see Froemberg *et al.* (2014).

tribution after the first jump. The wait first model resembles a Lévy walk model in that it also has a defined light front and therefore finite moments (Schmiedeberg *et al.*, 2009). All three models have the same scaling properties of their propagators, but the shapes of propagators are model specific. Figure 11 shows the density profiles for the three models with similar (leading to the same scaling) jump, waiting, and flight time distributions, and with all remaining proportionality constants set to one, $a = v = 1$.

These two simple coupled models can serve as a starting point for further generalizations. Here we looked only at linear couplings but it can be extended to the case when the flight distance is some power law function of the flight time (Metzler and Klafter, 2004); it will then effect the scaling of the propagator and its moments. One interesting example of the wait first model assumes that the jump length is distributed as a Gaussian function with a variance which linearly depends on the waiting time. In this case, for the power-law distributed waiting times, the resulting equation contains the diffusion operator but in a fractional power (Becker-Kern *et al.*, 2004; Shlesinger *et al.*, 1982). In the spirit of the Lévy walk model with rests, one can also add velocity to the above two coupled models. It is interesting to see how a new effective velocity arises as a combination of the coupling, a^{-1} and actual velocity of the particles v, $v_{\text{eff}} = v/(1 + av)$ (Zaburdaev, 2006). In this direction, one could consider more general models. For example, variation of the Lévy walk, in which the waiting times are power law distributed

but jump lengths scale non-linearly with waiting times $\psi(x|\tau) = \psi(\tau)\delta(|x| - u\tau^\beta)$, with $\beta > 0$ and $\beta \neq 1$. A nonlinear coupling provides a way to step beyond ballistic scaling regime of Lévy walks. It appears in the description of anomalous Richardson diffusion (Klafter *et al.*, 1987; Shlesinger *et al.*, 1986, 1987) with $\beta = 3/2$ or, in a slightly more involved form, in the context of cold atom dynamics with the same $\beta = 3/2$, which we discuss in Section V.E.

With this subsection we finalize the review of the existing random walk models which embrace the concept of finite velocity of particles and the coupled nature of the spatiotemporal transport process. The following sections are dedicated to more sophisticated properties of Lévy walks and more advanced tools for their analysis.

IV. PROPERTIES OF LÉVY WALKS

While the results of the previous sections can be rated as basic tools needed for applications of Lévy walks in practice, the following material goes in more details and as a result is more involved. However, it touches upon fundamental concepts of physics, such as aging, ergodicity, and space-time correlations. Most of these results are very recent thus indicating that the properties of Lévy walks are still being explored.

A. Space-time velocity auto-correlation function

Finite velocity of walking particles brings a random walk model closer to the basic physical principles and makes its more suitable for the description of real-life phenomena. However, the presence of the well defined velocity in random walks brings additional properties to

these stochastic process. In the realm of the continuous mechanics, the space-time velocity auto-correlation function is a fundamental quantity characterizing the dynamics of a fluid or other media. It reveals the relation between the velocities at two distant points and two different instants of time. Remarkably, the notion of continuous theory can be adapted to the single particle process of random walks. We can ask how the velocity of a random walker is correlated to its own velocity at some later moment of time but also at a certain distance from the starting point. A naive expectation for a random walk, where each next step is independent from the previous one, is that the correlations will be zero at a distances larger than a single flight. It was shown, however, that even for the regime of classical diffusion, but with finite velocity, the space-time velocity correlation function is different from zero and has a non-trivial space-time dependence (Zaburdaev *et al.*, 2013).

The space-time velocity auto-correlation function for a single-particle process can be redefined from the conventional expression (Monin *et al.*, 2007)

$$\mathcal{C}_{vv}(x,t) = \langle v(0,0)v(x,t) \rangle . \quad (51)$$

We assume that the particle starts its walk with an initial velocity $v(x=0,t=0)=v_0$. After a time t the particle is found at the point x with some velocity $v(x,t)$. To estimate $\mathcal{C}_{vv}(x,t)$, an observer at time t averages the product of the actual and the initial velocities of all particles that are located within a bin $[x, x+dx]$. It can be formalized in the following way:

$$\mathcal{C}_{vv}(x,t) = \int\limits_{-\infty}^{\infty} \int\limits_{-\infty}^{\infty} vv_0 \frac{P(v,x,v_0,t)}{P(x,t)} dv_0 dv, \quad (52)$$

where $P(v,x,v_0,t)$ is the joint PDF for a particle to start with velocity v_0 and to be in the point x at time t with velocity v. The particle has first to arrive at the point x for the measurement to occur, therefore we use Bayes' rule (Grinstead and Snell, 1997) for the conditional probability to obtain the integral above. The spatial density $P(x,t)$ is usually a known quantity for a given random walk model. In contrast, a challenging quantity to tackle is the joint probability of particles' positions and velocities. To focus on its role, the spatial density of the velocity correlation function can be introduced:

$$C(x,t) = \int\limits_{-\infty}^{\infty} \int\limits_{-\infty}^{\infty} vv_0 P(v,x,t|v_0)h(v_0)dv_0 dv. \quad (53)$$

Here $h(v_0)$ is the distribution of the initial velocities, which also signals that we are using the formulation of the random walk with random velocities. The integration over x, Eq. (53) yields the standard temporal velocity auto-correlation function $C(t) = \langle v(0)v(t) \rangle$. Normalizing $C(x,t)$ by the particle density $P(x,t)$, we return to the original velocity-autocorrelation function:

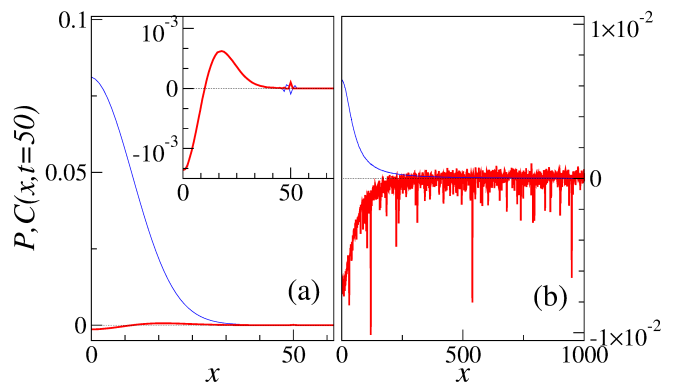$$\mathcal{C}_{vv}(x,t) = C(x,t)/P(x,t). \quad (54)$$

FIG. 12 (Color online) Propagators (thin blue line) and space-time velocity autocorrelation function (thick red line) at time $t = 50$ for two extreme cases of the random walk with random velocities, see Section III.A, with the flight-time PDF $\psi(\tau) = \delta(\tau-1)$, for (a) $h(v) = [\delta(v-u_0)+\delta(v-u_0)]/2$ and (b) $h(v)$ in the form of Cauchy distribution, Eq. (45). In the first case, the autocorrelation function is proportional to the second spatial derivative of the propagator, $C(x,t) \propto \triangle P(x,t)$ [see the inset where both functions are plotted together, with $\triangle P(x,t)$ weighted as in Eq. (55)], while in the second case $C(x,t) \sim -P(x,t)$. The functions were sampled with $N = 10^7$ realizations. The parameter $u_0=1$.

As for every model we considered so far, the integral transport equations can be derived for $P(v,x,t|v_0)$ and solved by using the Fourier-Laplace transforms. The definition of the velocity auto-correlation function contains two additional integrals with respect to the final and initial velocities, which makes the final answer more involved (Zaburdaev *et al.*, 2013).

However, the asymptotic analysis of the general answer in the limit of large time and space scales retrieves some surprisingly simple results. Consider first the Lévy walk regime of the velocity model, $h(v) = [\delta(v-v_0) + \delta(v+v_0)]/2$, with a power-law distributed flight time, Eq. (8). The density of particles is sandwiched between the two ballistic peaks. For the peaks we get $C(x = \pm v_0 t, t) = v_0^2 \Psi(t)\delta(x \pm v_0 t)/2$ and $\mathcal{C}_{v,v} = v_0^2$. For the central part of the propagator, in the regime of classical diffusion, $\gamma > 2$, the density of the correlation function is proportional to the first time derivative of the particle's density:

$$C_{\text{centr}}(x,t) = v_0^2 D \langle \tau \rangle \triangle P(x,t) = v_0^2 \langle \tau \rangle \frac{\partial P(x,t)}{\partial t}. \quad (55)$$

The above asymptotic result is valid for any flight time distribution with a finite second moment, see Fig. 12(a). Lets consider this result more closely. As mentioned above, by integrating the density of space-time velocity autocorrelation function over the coordinate we should obtain the standard temporal correlation function $C(t)$. In the long time limit, the integral of the central part is approaching zero [because of the Laplacian operator in Eq.(55)]. The only non-zero contribution comes from the ballistic peaks which lead to $C(t) = u_0^2 \Psi(t)$: velocities of particles remain correlated only during the
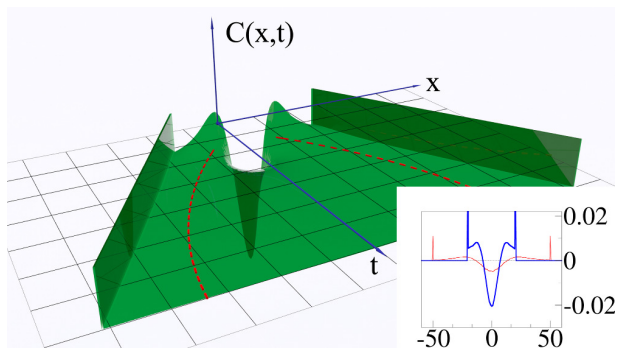
FIG. 13 (Color online) Space-time velocity autocorrelation function of Lévy walks in the superdiffusive regime. The space-time evolution of correlations shows a negative dip near $x = 0$ and two spreading maxima. The integral of the central part with respect to the coordinate is equal zero. The ballistic peaks carry the correlations of the particles which are still in their first flight. The red dashed lines indicate the positions of local maxima $x_{\mathrm{m}}^{\pm}$ on the $x - t$ plane which follow the power-law scaling $x_{\mathrm{m}}^{\pm} \propto \pm t^{1/\gamma}$, while the height of the maxima decays as $t^{-1-1/\gamma}$. The inset depicts spatial profiles of $C(x,t)$ for two different instants of time, $t = 20$ (heavy blue line) and 50 (light red line), $\gamma = 3/2$. From Zaburdaev *et al.* (2013).

flight time. If, for example, the flight time is exponentially distributed, the standard temporal velocity autocorrelation function decays very fast, $C(t) = v_0^2 e^{-t/\tau_0}$. If we look at the density of velocity-velocity autocorrelation at zero $x = 0$, from Eq.(55) it follows that $C(x = 0, t) = -v_0^2 \langle \tau \rangle (\pi D)^{-1/2} t^{-3/2}$. First of all, correlations at $x = 0$ are negative, and secondly, they decay in time algebraically like $t^{-3/2}$. This decay to zero is faster than that of the density of particles, $P(x = 0, t) \propto t^{-1/2}$, but still much slower than the exponential decay of the temporal correlation function. It highlights the fact that the space-time velocity correlation function provides access to long-lived correlations and therefore increases the chance of their detection in experiments.

For the regime of the superdiffusive Lévy walk, $1 < \gamma < 2$, the formula with the first time derivative remains valid. By further exploiting the properties of the time derivative we see that the velocity auto-correlation function is negative near the point $x = 0$, see Fig. 13. Upon the departure from the origin the correlation density becomes positive and produces two local maxima. These maxima are traveling with the power-law scaling $x_{\mathrm{m}}^{\pm} \propto \pm t^{1/\gamma}$, while the height of the maxima decays as $t^{-1-1/\gamma}$.

As we continue to move toward more anomalous behavior, for example for the ballistic regime of Lévy walks, the correlations decay in time even slower (Zaburdaev *et al.*, 2013). Finally, an example was given, when the velocity distribution of the particles was Lorentzian, see Section III.A. In that case the density of the space-time velocity autocorrelation function was proportional to the particle density, $C(x,t) \sim -P(x,t)$, see Fig. 12(b).

In all considered regimes there is a region of negative correlations at the vicinity of the starting point. This means that majority of particles found there are flying in the direction opposite to that of their initial motion. The shape of the "echo" region and the time-scaling of its width are model-specific characteristics. Interestingly, simulations of a stochastic process described by a system of Langevin equations in the regime of classical Brownian diffusion show analogous results (see (Zaburdaev *et al.*, 2013) and its Supplementary Material for additional plots), thus suggesting that these findings are applicable to a broad class of stochastic transport processes characterized by finite velocity of moving particles.

Here we considered only a simple initial condition, when all particles instantly change their velocity at $t = 0$. As a result, the temporal correlation function $C(t)$ obtained by the integration of the density of the space-time velocity correlations describes velocity correlations in a specific setting: initial velocity is always taken right after the reorientation event and the second velocity is measured after the lag time t. In general, the temporal velocity autocorrelation function depends on two arbitrary times t_1 and t_2, when the corresponding velocities of particles are measured. Such two-point correlation function was considered before in the context of CTRW (Barkai and Sokolov, 2007; Baule and Friedrich, 2007; Dechant *et al.*, 2014; Zaburdaev, 2008), and also for the case of Lévy walks (see Section VI.C and (Froemberg and Barkai, 2013a; Taktikos *et al.*, 2013)). This results call for the generalization of the space-time velocity correlation function to a broader class of initial conditions.

B. Exact solutions for ballistic random walks

The asymptotic analysis is very useful but in many cases it is still impossible to obtain the expression for the propagators in real time and space analytically. Interestingly, for random walk models which have the ballistic scaling, there is a particular method to calculate the inverse Fourier-Laplace transform without performing it directly. It immediately gives the shape of the scaling function $F(\xi)$, see Eq. (16). The method is similar to the one proposed by Godrèche and Luck (2001), and used for the analysis of the renewal process and the inversion of the double Laplace transform. The problem of finding the PDF in ballistic regimes is intimately related to the problem of time averages (Rebenshtok and Barkai, 2008), as the scaled position of the particle after time T is given by

$$x/T = \frac{1}{T} \int_0^T v(t) dt, \tag{56}$$

which is a time average of particle's velocity. In application to the random walk concept, the method of Godrèche and Luck has the following formulation. Assume that the propagator of the random walk model has the following

scaling form:

$$G(x,t) = \frac{1}{t} F\left(\frac{x}{t}\right). \qquad (57)$$

In the Fourier-Laplace space it can be represented as:

$$G(k,s) = \frac{1}{s} f\left(\frac{ik}{s}\right) = \frac{1}{s} f(\zeta); \quad \zeta = \frac{ik}{s}. \qquad (58)$$

Finally, by using the Sokhotsky-Weierstrass theorem (see Froemberg *et al.* (2014) for more details):

$$F(\xi) = -\frac{1}{\pi\xi} \lim_{\epsilon \to 0} \text{Im} f\left(-\frac{1}{\xi + i\epsilon}\right), \qquad (59)$$

where $\xi = x/t$ is the scaling variable. This formula allows us to compute the shape of the propagator without calculating of the inverse Fourier-Laplace transforms.

We first give an example corresponding to the standard Lévy walk model with a constant speed v and set it to unity for simplicity, $v = 1$. The asymptotic profile of the Green's function in the Fourier-Laplace space is given by Eq.(33) from which we can easily identify:

$$f(\zeta) = \frac{(1-\zeta)^{\gamma-1} + (1+\zeta)^{\gamma-1}}{(1-\zeta)^{\gamma} + (1+\zeta)^{\gamma}}. \qquad (60)$$

Now by using Eq.(59) we can find the shape of the scaling function to be:

$$\Phi(\xi) = \frac{\sin \pi\gamma}{\pi} \times$$
$$\frac{|\xi-1|^{\gamma}|\xi+1|^{\gamma-1} + |\xi+1|^{\gamma}|\xi-1|^{\gamma-1}}{|\xi-1|^{2\gamma} + |\xi+1|^{2\gamma} + 2|\xi-1|^{\gamma}|\xi+1|^{\gamma}\cos\pi\gamma} \qquad (61)$$

which is the Lamperti distribution (Lamperti, 1958). As another illustration we ask how the shape of the velocity distribution of a random walking particle affects the shape of the corresponding propagator. For that consider the model with random velocities, Section III.A, in the ballistic regime ($\gamma = 1/2$) with four different velocity distributions, $h(v)$: a) two delta peaks (Lévy walk regime), b) Gaussian, c) uniform on a symmetric bounded interval, and d) Lorentzian (Cauchy). Equation (59) gives analytical answers for the scaling function $F(x/t)$ for all four cases. Figure 13 shows that the velocity distribution has a pronounced effect on the shape of the particles' density. Namely, we see the familiar U-like profile for the standard Lévy walk model, more of a bell-shaped profile but still bounded by fronts for the uniform velocity distribution, and unbounded bell-shaped profile for the Gaussian velocity distribution. The Lorentzian case is special as it does not depend on the flight time distribution and has diverging moments.

We note here that this approach does not require the finite velocity of particles, it only relies on the existence of the ballistic scaling. Therefore it can be also applied to the coupled setups as wait/jump-first models (this is how the plots on Fig. 11 were obtained). We present
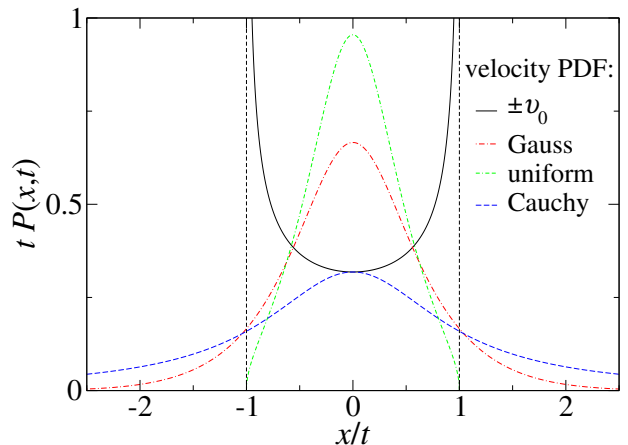

FIG. 14 (Color online) Exact solutions of ballistic Lévy walks. Here we plot analytical results obtained from Eq. 59 for the scaling functions of the random walks with random velocity model in the ballistic regime ($\gamma = 1/2$), for four different velocity distributions, two delta peaks corresponding to the Lévy walk (solid line), Gaussian (dash-dotted), uniform on an interval (double dash-dotted), and Cauchy (dashed). Adapted from Froemberg *et al.* (2014).

these analytical results to emphasize that even a model of random walks with random velocities can be thoroughly analyzed with the help of the combination of asymptotic analysis and elegant mathematical machinery. It would be challenging to try to extend or find similar approaches to other scaling regimes of random walks.

C. Infinite densities of Lévy walks

Many statistical properties of a Lévy walk process can be evaluated from the corresponding propagator, Eqs. (6,7). For superdiffusive sub-ballistic regimes the central part of the propagator is subjected to the generalized central limit theorem and thus it is given by the symmetric Lévy distribution $L_\gamma[x, \sigma(t)]$, with $\sigma(t) = (K_\gamma t)^{1/\gamma}$. However, this fundamental fact does not allow for calculations of the moments, starting from the second one, simply because they do not exist for Lévy distributions. The confinement of the process to the ballistic cone should be taken into account and in order to calculate higher-order moments one needs to known the behavior of the propagator at the vicinity of the ballistic fronts. These regions are out of the validity domain of the gCLT and a complementary theory is needed. The concept of infinite measure (Aaronson, 1997; Thaler and Zweimüller, 2006) provides with such theoretical framework (Rebenshtok *et al.*, 2014a,b)

In the intermediate region $t^{1/\gamma} < |x| < t$ the LW propagator scales as $P(x,t) \sim t/|x|^{1+\gamma}$. Since a power-law is a scale-free function, there is infinitely many different scaling transformations which match power-law tails of the propagators for different times, $t^{\xi_{\text{PDF}}} P(x/t^{\xi_x}, t)$, with linearly related scaling exponents $\xi_{\text{PDF}} = \xi_x(1+\gamma) - 1$.
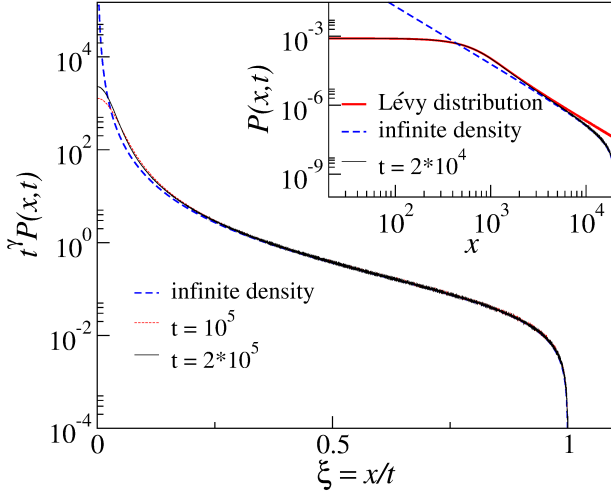
FIG. 15 (Color online) Ballistic scaling of the propagators of the Lévy walk model with random velocities, see Section III.B, for the velocity distribution $h(v)$ uniform on the interval $\in [-1, 1]$ and $\alpha = 3/2$. The corresponding infinite density (dashed blue line), Eq. (62), matches the tails of the rescaled propagators. Inset shows the propagator for a shorter time plotted together with a rescaled Lévy distribution (solid red line) and infinite density (dashed blue line). The propagator is barely visible due to the perfect matching of the theoretical curves at the central region near $x = 5000$. The propagators were sampled with $N = 10^{10}$ realizations. Adapted from Rebenshtok *et al.* (2014a)

When $\xi_x = 1/\gamma$ we have the familiar Lévy scaling, Eq. (16), with $\alpha = 1/\gamma$, which matches the central parts of the propagators. For $\xi_x = 1$ we have a "ballistic" scaling, $t^\gamma P(x/t, t)$, which matches the outmost fronts of the propagators. Therefore, this scaling is suitable for the analysis of the asymptotic evolutions of the high-order moments which is determined by the propagator tails. We next introduce a scaled ballistic variable, $\xi = x/t$ and define a density over this variable as (Rebenshtok *et al.*, 2014b)

$$\mathcal{I}(\xi) = \lim_{t \to \infty} t^\gamma P(x/t, t). \tag{62}$$

This function scales differently from the Lévy distribution $L_\gamma(x, \sigma(t))$ and it is non-normalizable[5], $\int_{-\infty}^{\infty} \mathcal{I}(\xi)d\xi = \infty$, because of the power-law singularity in the limit $\xi \to 0$, $\mathcal{I}(\xi) \simeq c_\gamma K_\gamma |\xi|^{-1-\gamma}$. For the general case of the Lévy walks with random velocities, the

infinite density is given by the following formula (Rebenshtok *et al.*, 2014a):

$$\mathcal{I}(\xi) = B \left[\frac{\gamma \mathcal{F}_\gamma(|\xi|)}{|\xi|^{1+\gamma}} - \frac{(\gamma - 1)\mathcal{F}_{\gamma-1}(|\xi|)}{|\xi|^\gamma} \right], \tag{63}$$

where

$$\mathcal{F}_\gamma(\xi) = \int_{|\xi|}^{\infty} dv\, v^\gamma h(v). \tag{64}$$

It is not surprising that, in contrast to the universal Lévy-like central part of the Green's function, the infinite density, which describes function's tails, is specific to the velocity distribution $h(v)$ (it is assumed that this PDF is not heavy tailed so the integral (64) is finite). It accounts for the particles with highly-correlated flying histories so that the velocity PDF is imprinted into the tails of the PDF $P(x, t)$. Two ends meet in the intermediate region where both functions scale similarly, $L_\gamma(x/\sigma(t)) \sim \mathcal{I}(x/t) \sim x^{-1-\gamma}$. For large t two densities match near perfectly at the point $x_c(t) = \left[\frac{c_\gamma}{L_\gamma(0)} \right]^{\frac{1}{1+\gamma}} (K_\gamma t)^{1/\gamma}$ so that the propagator $P(x, t)$ can be approximated with high accuracy by gluing two functions (properly scaled beforehand) at the point $x_c(t)$, see Fig. 14.

Now the fractional moments can be calculated as

$$\langle |x|^q \rangle \simeq \underbrace{2 \int_0^{x_c(t)} L_\gamma \left[\frac{x}{(K_\gamma t)^{1/\gamma}} \right] (K_\gamma t)^{-1/\gamma} x^q dx}_{\text{inner region}}$$
$$+ \underbrace{2 \int_{x_c(t)}^{\infty} \mathcal{I} \left(\frac{x}{t} \right) t^{-\gamma} x^q dx}_{\text{outer tails}}. \tag{65}$$

In the long-time limit, the lower limit of the second integral $x_c(t)/t \to 0$ while the upper limit of the first integral is a constant. For $q > \gamma$ the second integral is by far larger than the first, hence we may neglect the inner region and get

$$\langle |x|^q \rangle \sim 2t^{q+1-\gamma} \int_0^{\infty} \mathcal{I}(\xi) \xi^q d\xi \tag{66}$$

When $q < \gamma$ the contribution from the second integral is negligible in the limit $t \to \infty$ and the upper limit of the first integral is taken to infinity, hence, after a change of variables $y = x/\sigma(t)$, and using the symmetry $L_\gamma(y) = L_\gamma(-y)$, we are left with

$$\langle |x|^q \rangle \sim (K_\gamma t)^{\frac{q}{\gamma}} \int_{-\infty}^{\infty} L_\gamma(y)|y|^q dy. \tag{67}$$

These results prove that sub-ballistic Lévy walks belong to the class of strongly anomalous diffusion processes whose asymptotic moments satisfy Eq. (37) with $q\nu(q) = q/\gamma$ for $q < \gamma$ and $q\nu(q) = q + 1 - \gamma$ for $q > \gamma$, see Fig. 5. There is also a phase-transition-like crossover at the point $q_c = \gamma$ in terms of the moment prefactors

---

[5] The non-normalizable density function $\mathcal{I}(\xi)$ should not be thought as a *probability* density function (the latter is always normalizable). The ID relates to a mathematical concept of a spatially varying function, defined on a smooth manifold that is locally integrable almost everywhere. Non-normalizable densities are no strangers to physics; check, for example, for non-normalizable energy densities in black holes and non-normalizable densities of states in relativistic quantum dynamics.

M_q, see inset in Fig. 5. Finally, the knowledge of the both, the Lévy PDF and infinite density, allows one to calculate observables that are not integrable with respect to either of the two densities, for example $f(x) = 1 + x^2$ (Rebenshtok *et al.*, 2014a).

D. Memory effects and ergodicity breaking in Lévy walks

In general, a continuous time random walk models is a non-Markovian process, meaning that the future of a particle depends not only on particle's current state, namely its position and velocity, but also on its pre-history, like how long it was waiting, or how long it was flying already.

As a result, a CTRW process can not be fully characterized by its PDF, but requires the knowledge of all higher order correlation functions (Hänggi and Thomas, 1982). However, CTRWs and Lévy walk models we considered so far, where each next step is independent of the previous, represent the so-called semi-Markov processes. In a semi-Markov process, the points where jumps or velocity changes occur form a Markov chain; the renewal events at those points erase all previous memory. In between the renewal points, to predict the future of the particle, we need to know how long it was in its current state. In some cases, the limiting transport equations are consistent with Markovian dynamics, like in the case of normal diffusion Eq. (13) or superdiffusion Eqs. (22), and (23) preserve the continuity of evolution for the times exceeding the average waiting times. In other cases, when the mean time diverges, the asymptotic transport equations are obviously of a non-Markovian nature, as in the case of CTRW in the subdiffusive regime, when the corresponding transport equation has a fractional time derivative. A large body of work addressing the semi-Markov property and its consequences for the CTRW models exists and below we will look only at those of them which are pertinent to Lévy walks.

In the context of Lévy walks, there are two important interrelated issues which relate to the power law distributed flight times. The first issue concerns the effects of the initial distribution of particles with respect to their flight times on future evolution of the PDF $P(x,t)$ (Aquino *et al.*, 2004; Barkai, 2003; Barkai and Cheng, 2003; Sokolov *et al.*, 2001; Zaburdaev and Chukbar, 2003; Zaburdaev and Sokolov, 2009). The second issue is the weak ergodicity breaking and it points to the fact that time and ensemble averaged quantities can be different from each other (Bel and Barkai, 2005; Rebenshtok and Barkai, 2007, 2008).

The problem of the initial preparation of the system of particles is important for all random walk models. So far we always assumed that all particles were introduced to the system at $t = 0$, that is they had no history. In this case, the probabilities to make the first jump after a certain waiting time, or to make the first turn after a flight time, are governed by the same waiting time or flight time PDFs, $\psi(\tau)$. However, if at $t = 0$ a particle has already collected some "history", for example, it was sitting at a given point or it was in the state of flight for some time τ_1, then the PDF for it to make the first jump (first turn) at time τ is in general different from $\psi(\tau)$. This case is handled by the so-called renewal theory (in this simple case, it is just the implementation of the conditional probability formula), see Haus and Kehr (1987); Tunaley (1974):

$$\psi_{\text{first}}(\tau|\tau_1) = \frac{\psi(\tau + \tau_1)}{\Psi(\tau_1)}. \tag{68}$$

The only distribution function which is not affected by the pre-history is the exponential distribution and because of that is often called memoryless. In general, the initial distribution of particles over the flight or waiting times may affect the following evolution. An approach to incorporate this distribution was developed for CTRW model and can be extended to the Lévy walk case (Zaburdaev and Chukbar, 2003; Zaburdaev, 2008). Here we mention one important example of the memory effects. Assume that before starting observation we let the system evolve for time t_1 and then require that $t_1 \rightarrow \infty$. This is a so-called *equilibrated* [or stationary (Klafter and Zumofen, 1993)] setup where we assume that the system reaches a certain equilibrium before we start measuring it. In contrast, the setup where all particles are introduced to the system at $t = 0$ and do not have pre-histories is called a *non-equilibrated* [non-stationary (Klafter and Zumofen, 1993)] setup. For the equilibrated case, one has to imagine a system with an infinite number of particles in unbounded domain but with a fixed uniform density. Particles evolve according to their random walk model for an infinite time. At some time point which we denote as $t = 0$ we mark all particles located at $x = 0$ and then follow the evolution of marked particles only. It can be shown that in the equilibrated setup, the probability of making the *first* reorientation event after the observation started is given by the following PDF [see e.g., Denisov *et al.* (2012) for a simple derivation]:

$$\overline{\psi}(t) = \frac{1}{\langle \tau \rangle} \int\limits_0^\infty \psi(t + \tau) d\tau. \tag{69}$$

If the flight times are too long, such that the mean flight time diverges, there is no sense to speak about the equilibrated setup as it simply does not exist. The pre-history affects only the probability of the very first reorientation effect to occur; in terms of the transport equations, it will lead to the new terms on the right hand sides of Eqs. (25)-(27)

$$\nu(x,t) = \ldots + \overline{\psi}(t)\delta(|x| - vt)P_0 \tag{70}$$

$$P(x,t) = \ldots + \overline{\Psi}(t)\delta(|x| - vt)P_0, \tag{71}$$

and consequently to different propagators. Here the corresponding probability of not changing the direction till time t, $\overline{\Psi}(t)$, is given by the similar integration as in Eq.

(69): $\overline{\Psi}(t) = (1/\langle\tau\rangle)\int_0^\infty \Psi(t+\tau)d\tau$. Finally, the exponent in the power law tail of $\overline{\psi}(\tau) \propto t^{-\gamma}$ is smaller in the case of equilibrated setup than in the non-equilibrated case $\psi(\tau) \propto t^{-1-\gamma}$, meaning a longer lasting influence of the initial distribution on the consequent evolution. Understanding of these memory effects is important for the analysis of experimental data or comparison of theory and simulations, as we will exemplify when discussing applications.

The problem of weak ergodicity breaking (WEB) (Bouchaud, 1992) is of a great interest both in theoretical and experimental communities (Brokmann *et al.*, 2003; He *et al.*, 2008; Jeon *et al.*, 2011; Lubelski *et al.*, 2008; Margolin and Barkai, 2005; Weigel *et al.*, 2011). WEB, similarly to memory effects discussed above, is found in systems with temporal dynamics governed by power-law distributed time variables with diverging means (Barkai, 2008). Ergodicity breaking is called weak if the whole phase space of the system can be explored, but the ergodicity is never reached because the characteristic times involved in the corresponding process are always of the order or longer than the total measurement time. In practice it means that the time average of a certain quantity itself is random and can be characterized by a non-trivial distribution. In case of the fully ergodic system the distribution of time averages has a shape of the delta function at the value of the corresponding ensemble average. The most pronounced effects of WEB can be observed for subdiffusive systems (Bel and Barkai, 2005; He *et al.*, 2008; Lubelski *et al.*, 2008), however, Lévy walks, as they may involve flight time distributions with infinite flight times, also exhibit WEB. In several recent studies (Akimoto, 2012; Froemberg and Barkai, 2013b; Godec and Metzler, 2013a), the effects of WEB in Lévy walks were investigated on the example of the mean squared displacement calculated as time and ensemble average. The time averaged MSD is defined as:

$$\overline{\delta x^2(\tau)} = \frac{1}{(T-\tau)}\int\limits_0^{T-\tau}[x(t+\tau)-x(t)]^2 dt, \qquad (72)$$

where T is the measurement time and τ is the lag time. Several observations were made. In the superdiffusive sub-ballistic regime, the time averaged MSD for finite measurement time T shows different apparent scaling for large τ (but τ is still much smaller than T). Some of the individual trajectories can even demonstrate the subdiffusive behavior. Godec and Metzler (2013a) attribute this effect to the finiteness of the trajectories. Another quantity which can be constructed is the ensemble average of the time averaged MSD $\langle\overline{\delta x^2(\tau)}\rangle$. This quantity now can be compared with the ensemble averaged MSD, $\langle x^2(\tau)\rangle$, namely by calculating the ratio of the former to latter giving the so-called ergodicity breaking parameter, $\mathcal{EB} = \langle\overline{\delta x^2(\tau)}\rangle/\langle x^2(\tau)\rangle$. For the superdiffusive Lévy walk in the limit $\tau \to \infty$ it tends to a constant value $\mathcal{EB} = 1/(\gamma-1)$. To draw the connection to the previously discussed memory effects we note that the ensemble-time averaged MSD, $\langle\overline{\delta x^2(\tau)}\rangle$, corresponds to the ensemble averaged MSD of the equilibrated setup, whereas simple ensemble average MSD is calculated for the non-equilibrated setup (Klafter and Zumofen, 1993). In Froemberg and Barkai (2013b), the ballistic regime of Lévy walks was considered as well. In that case WEB effect is also present, but, surprisingly, is not as pronounced as in the superdiffusive case. The ensemble-time average can be also calculated analytically. Its leading term (assuming $\tau/T \ll 1$) is given by $\overline{\delta x^2(\tau)} \sim (v_0\tau)^2$. Note that the ensemble averaged MSD has a different pre-factor $\langle x^2(\tau)\rangle = (1-\gamma)(v_0\tau)^2$. Furthermore the fluctuations of the shifted quantity $\overline{\delta x^2(\tau)} - (v_0\tau)^2$ can also be quantified, see Froemberg and Barkai (2013b) for details.

Ergodicity breaking effects discussed here are essential for the analysis of the experimental data, particularly in biology, where due to the limited number of measurements one has to resort to the time averaging and always deals with trajectories of finite length. In addition, understanding of the fluctuations in time averaged observables can help to obtain more information about the underlying stochastic process (Dechant *et al.*, 2014; Schulz *et al.*, 2014). There is also a very recent work on Einstein relation, fluctuation dissipation, and linear response (Froemberg and Barkai, 2013b; Godec and Metzler, 2013b). We refer the interested reader to find out more details about these topics in a recent review by Metzler *et al.* (2014).

E. Langevin approach and fractional Kramers equation

In the Introduction we mentioned the Langevin equation as an approach to stochastic transport phenomena complimentary to the random walk paradigm. Random walks have their strength in the flexibility of the model construction and amenability of the corresponding transport equations to the analytical treatment. Langevin equations utilize the machinery of stochastic differential equations and provide a link to the Fokker-Planck equation (Risken, 1996). The Langevin equation was originally proposed in 1908 to describe the Brownian motion (Lemons and Gythiel, 1997). Since then it has grown into a powerful tool of modern physics (Coffey and Kalmykov, 2012). This success was certainly supported by rigorous mathematical foundations laid by mathematicians, such as N. Wiener, Itō, and Stratonovich. In many cases, the equivalence of random walks and the corresponding Langevin equations can be explicitly demonstrated in a proper limit. That includes also regimes of normal and anomalous diffusion, with both sub- and superdiffusion. This line of research led to the formulation of the fractional Fokker-Planck (Barkai, 2001; Barkai *et al.*, 2000b; Chechkin *et al.*, 2003; Heinsalu *et al.*, 2007; Metzler *et al.*, 1999) and Klein-Kramers equations (Barkai and Silbey, 2000; Dieterich *et al.*, 2008; Eule *et al.*, 2007; Friedrich *et al.*, 2006a; Metzler and Sokolov, 2002), and it remains an active field of research up to now.

One of the Langevin pathways to Lévy walks was proposed recently by Kessler and Barkai (2012) (we discuss it in more detail in Section V.E). In brief, the dynamics of the particle is governed by the Langevin equation with a standard white noise term but with a non-linear friction, Eq. (88). On a mesoscopic scale the trajectory of the particle, $\{x(t), p(t)\}$, can be divided into flights, that are events of unidirectional motion. Time duration of the i-th event, τ_i, is given by the time lag between two consecutive "turns" marked by sign alternations of the momentum $p(t)$. It was shown by Marksteiner *et al.* (1996) that, within a certain parameter range, the PDF of the flight time scales as $\psi(\tau) \propto \tau^{-1-\gamma}$, with a parameter-dependent exponent γ. The flight time and flight distance are coupled in a non-trivial way, such that the corresponding random walk description of the particle dynamics does not reduce to the simple Lévy walk model with linear coupling between x and t (Barkai *et al.*, 2014; Kessler and Barkai, 2012).

In attempt to model real-life continuous trajectories similar to those of Brownian motion but exhibiting anomalous diffusion, a Langevin equation with a special form of multiplicative noise term was suggested (Lubashevsky *et al.*, 2009a,b). A trajectory generated by this Langevin equation, when sampled at fixed time intervals, will reproduce the behaviour of the Lévy flight model.

Finally, to achieve a one-to-one correspondence of the Langevin picture and the Lévy walk model one can use the method of subordination (Fogedby, 1994). In this case an additional variable is introduced, which is called an operational time. The dynamics of velocity is happening in this operational time and can be tuned to produce the desired velocity distributions, $h(v)$. The real time is connected to the operational time via its own stochastic equation with a noise term which generates long traps in real time space. Those traps correspond to the long flight intervals as required for the Lévy walk model, see Eule *et al.* (2012) for more detail. This phenomenological approach allows to connect the world of Langevin equations to Lévy walks where the constant speed of a particle during a long time interval is crucial, remaining, at the same time, very different from a standard Brownian trajectory where the velocity is constantly changing.

A complementary approach to study anomalous stochastic transport is to generalize the Kramers-Fokker-Planck equation. Several versions of generalized Kramers-Fokker-Planck equations were suggested in the literature [they are summarized in (Eule *et al.*, 2007)]. Here we follow a scheme by Friedrich *et al.* (2006a) with a ballistically moving particle subjected to random kicks which alter its velocity. Provided the times between consecutive collisions are distributed as a power law, the fractional Kramers-Fokker-Planck equation for the joint position-velocity distribution, $f(\mathbf{r}, \mathbf{v}, t)$, can be obtained:

$$\left(\frac{\partial}{\partial t} + \mathbf{v}\nabla_{\mathbf{r}} + \mathbf{F}(\mathbf{r})\nabla_{\mathbf{v}}\right) f(\mathbf{r}, \mathbf{v}, t) = L_{FP}\mathcal{D}_t^{1-\gamma} f(\mathbf{r}, \mathbf{v}, t).$$
(73)

Here $\mathcal{L}_{FP}$ is the Fokker-Planck operator $L_{FP}f = \tilde{\gamma}\nabla_{\mathbf{v}} \cdot (\mathbf{v}f) + \kappa\triangle_{\mathbf{v}}f$, and $\mathcal{D}_t^{1-\gamma}$ is the fractional substantial derivative defined through its Laplace transform as $\mathcal{L}\left[\mathcal{D}_t^{1-\gamma}f(t)\right] = (s + \mathbf{v} \cdot \nabla_{\mathbf{r}} + \mathbf{F}(\mathbf{r}) \cdot \nabla_{\mathbf{v}})^{1-\gamma} f(s)$. Further, $\mathbf{F}(\mathbf{r})$ is the external force, $\tilde{\gamma}$ is the generalized friction coefficient, and κ is related to the amplitude of the noise in the corresponding Langevin equation for the velocity of the particle. For rigorous derivation and many technical details we refer to Carmi and Barkai (2011); Friedrich *et al.* (2006a,b). By appropriate modifications, the above equation can be simplified to give the equations of the random walk with random velocity model (Zaburdaev *et al.*, 2008) and of the Lévy walk model (Eule *et al.*, 2008). The genetic link between Lévy walks, Langevin equations, and fractional Fokker-Planck equations certainly needs to be investigated further (Lubashevsky *et al.*, 2009a,b; Magdziarz *et al.*, 2012; Turgeman and Barkai, 2009).

At this point it would be timely to mention two relevant approaches (which however fall beyond the scope of this review). That is the fractional Brownian motion, which is characterized by a Gaussian but time correlated noise (Mandelbrot and Ness, 1968), and the generalized Langevin equation, which contains an integral operator with a memory kernel on the right hand side of the equation governing the velocity increments (Zwanzig, 2001). Both approaches are useful in describing various transport processes across disciplines. They possess, however, very distinct features that are different from those of the random walk concept; in relation to the questions already discussed in this review, we would like to direct the reader to Eliazar and Shlesinger (2013); Magdziarz *et al.* (2009); Meroz *et al.* (2013).

V. LÉVY WALKS IN PHYSICS

Physics is a natural habitat of random walk models (Fernandez *et al.*, 1992; de Gennes, 1979; Weiss, 1994). During last twenty five years, the Lévy walk model has found a number of applications, mostly in classical chaos and nonlinear hydrodynamics (Klafter *et al.*, 1996; Klafter and Sokolov, 2011; Shlesinger *et al.*, 1999). Geisel and Thomae (1984) were the first to consider an intermittent ballistic motion with power-law flight-time PDFs in the context of deterministic chaos. Later on, Geisel *et al.* (1985) studied a model of the rotational phase dynamics in a Josephson junction, by using a one-dimensional map

$$x_{n+1} = g(x_n), \tag{74}$$

assuming discrete translational and reflection symmetries,

$$g(x + N) = g(x) + N, \quad g(-x) = -g(x). \tag{75}$$

where N denotes the number of the unit box, $[N-1, N]$. With this setup, the definition of the map is required only for the reduced range $0 \leq x \leq 1$. It can be extended
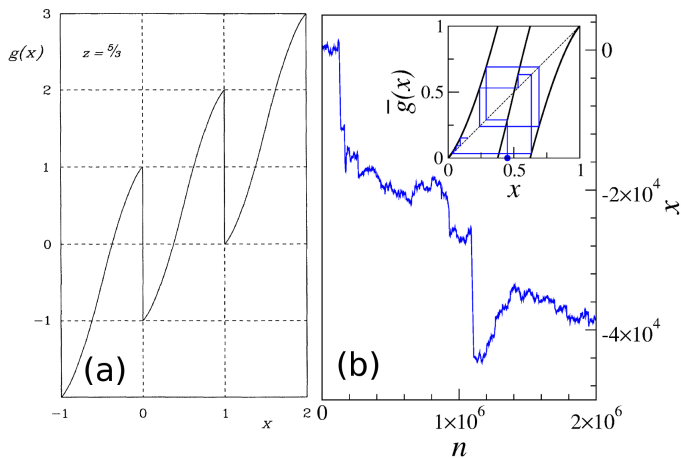
FIG. 16 (Color online) (a) Map $g(x)$, Eqs. (74-76), for $z = 5/3$. Adapted from (Zumofen and Klafter, 1993); (b) A trajectory $x(n)$ obtained by iterating the map from the initial point $x(0) = 0.45$. The inset shows the reduced map $\bar{g}(x)$, Eq. (76), with first ten iterations of the initial point $x(0)$ (•). The branch on the left (right) part is responsible for a decrement (an increment) of the cell number $N = \mathsf{int}(x)$ produced by the extended map $g(x)$. The parameter $\epsilon = 10^{-4}$.

then over $x \in [-\infty, \infty]$ by using symmetries in Eq. (75). Geisel *et al.* (1985) used a nonlinear map,

$$\bar{g}(x) = \begin{cases} (1+\epsilon)x + ax^z - 1, & 0 \le x \le 1/2 \\ 2 - (1+\epsilon)(1-x) - a(1-x)^z, & 1/2 \le x \le 1 \end{cases} \tag{76}$$

where ϵ is a small constant and $a = 2^z(1 - \epsilon/2)$. The profile of the corresponding extended map $g(x)$ for $z = 5/3$ is shown in Fig. 16(a). Because of the power-law form of the second term on the right hand side of Eq. (76), the reduced variable x mod 1 tends to cluster near the semi-stable points $x_N = N$. Once entered into the vicinity of one of these points, a trajectory performs a uni-rotational motion with a near constant rate $|x_{n+1} - x_n| = 1$. The rotation direction depends on the point to which the trajectory stuck, $v = 1$ when it stuck to $x_N^+ = N - 0$ [$x = 1$ in the reduced map $\bar{g}(x)$] and $v = -1$ when to $x_N^- = N + 0$ [$x = 0$ in the reduced map $\bar{g}(x)$]. It was found that a histogram of the numbers of iterations, or the time, if we set $t = n$, spent by the system in a rotation state, yields a long-tailed distribution $\psi(t) \propto t^{-z/(z-1)}$. The results of a numerical sampling reveal that the MSD $\langle x^2(t) \rangle$ scales as in Eq. (35), with $\gamma = 1/(z-1)$. It was then shown to be a clear-cut case of a Lévy walk with the constant speed $v = 1$ and the exponent γ (Shlesinger and Klafter, 1985), see Fig. 16(b). A complete evaluation of the diffusion in the intermittent maps within the Lévy walk framework was presented by Zumofen and Klafter (1993). The next "dynamical" realization of the Lévy walk was found in Hamiltonian chaotic systems (Klafter and Zumofen, 1994; Shlesinger *et al.*, 1993; Zumofen and Klafter, 1994a). This was a case when the LW concept perfectly matched a peculiar dynamical effect, in appearance similar to the intermittency in the dissipative maps

with power-law singularities (Geisel *et al.*, 1987; MacKay *et al.*, 1984a). The machinery behind the Hamiltonian stickiness is related to specific fractal structures living in the phase space of chaotic Hamiltonian systems (MacKay *et al.*, 1984b; Meiss, 1992). We will discuss this issue in more detail in the next section.

With this section we are not up to a comprehensive historical review. We want to present Lévy walks in physics as something (re)emergent and promising rather than something residual and completed. In the following subsections we will concentrate on the most recent advances and results, both theoretical and experimental, which underline the potential and universality of the concept.

A. Lévy walks in single-particle Hamiltonian systems

The subject of Lévy walks in low-dimensional Hamiltonian chaos is already twenty years old (Klafter and Zumofen, 1994; Zumofen and Klafter, 1994a). We start with a brief outline of it not because of the historical reason but because it will help to understand better the recent developments that will be discussed next.

The phase space of a non-integrable single-particle Hamiltonian system is *mixed* and consists of different invariant manifolds, that are chaotic layers, regular islands, tori, etc. (Sagdeev *et al.*, 1992). The i-th manifold can be characterized by an averaged value of any observable, for example velocity, $v_i = \langle v_i(t) \rangle_{t \to \infty}$. The average velocity of a manifold might be nonzero and for a regular island it is determined by the winding number of the elliptic orbit at the island center. A chaotic layer is well separated from regular manifolds by KAM-tori (Sagdeev *et al.*, 1992) so that a trajectory initiated inside the layer cannot enter a regular island even when the latter is embedded into a chaotic sea. A "coastal area" near the island is structured by *cantori* (MacKay *et al.*, 1984b), which form partial barriers for the trajectories. Once entered into the region enclosed by a cantorus, a trajectory will be trapped in the vicinity of the corresponding island for a long time. During this sticking event (Meiss and Ott, 1986), the trajectory reproduces the dynamics of the orbits located inside the island. If the corresponding island is transporting, $v_i \ne 0$, the sticking event produces a long ballistic flight with velocity v_i. It has been found that power-law tails of sticking time PDFs, $\psi(\tau) \propto \tau^{-1-\gamma}$, is a general feature of Hamiltonian chaos which is related to the self-similar hierarchical structure of cantori (Geisel *et al.*, 1987; Meiss, 1992; Meiss and Ott, 1986). With this finding all needed ingredients were collected and a link between "strange kinetics" of Hamiltonian chaos and Lévy walks was established (Shlesinger *et al.*, 1993).

In a Hamiltonian system possessing the time-reversal symmetry, ballistic islands always exist in pairs and have identical sticking time PDFs. If, in addition, the long-time dynamics of the system is governed by only two
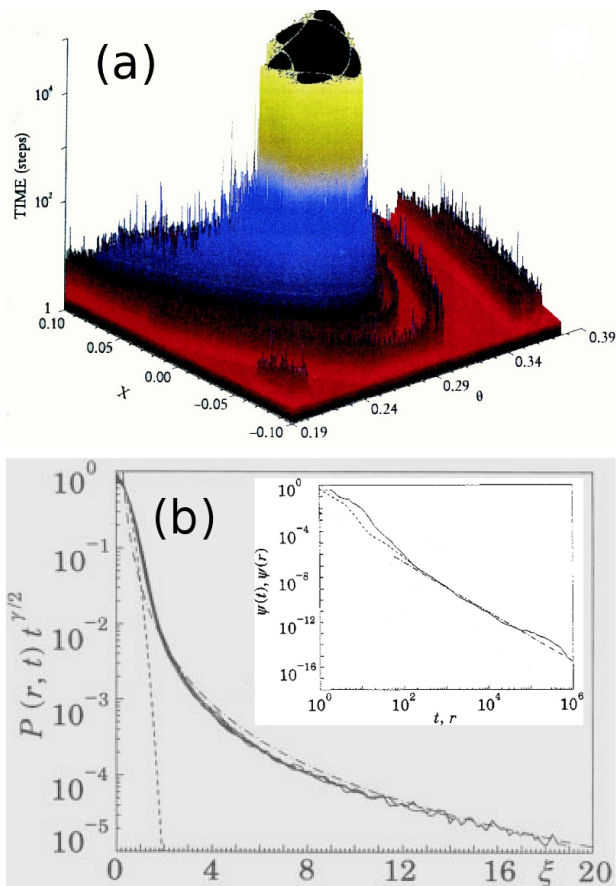
FIG. 17 (Color online) Lévy walks in the standard map. (a) Time $t_{\text{exit}}(x, \theta)$ it takes for a trajectory initiated at the point (x, θ) to exit from a vicinity of a regular island around the period-five orbit (black area on the top of the distribution). (b) The rescaled propagators for different time, $t = 100, 200, 400, 800, 1600$, $\xi = x/t^{1/\gamma}$. The dashed line is a Gaussian fit and the dashed-dotted line is a power law fit $f(\xi) \propto \xi^{-1-\gamma}$. The inset shows the sticking-time (solid line), $\psi(t)$, and the flight-length (dashed line), $\psi(x)$, PDFs at the vicinity of the period-five island. The dashed dotted-line is a power-law with exponent $\gamma = 1.2$. The spatial variable x is denoted r in the original work. The y-axis label on (b) should read as $P(r,t)t^{1/\gamma}$. Adapted from Zumofen and Klafter (1994a).

symmetry-related sticky ballistic islands, with a sticking time exponent γ, then the system dynamics will realize the standard Lévy walk, Fig. 1(b). Zumofen and Klafter (1994a) considered the kicked-rotor map, an archetypical Hamiltonian model (Sagdeev *et al.*, 1992),

$$x_{n+1} = x_n + K \sin(2\pi\theta), \quad \theta_{n+1} = \theta_n + x_{n+1}, \quad (77)$$

where K is the stochasticity parameter, as an example. For $K = 1.03$ the system phase space represents a chaotic sea which extends over the whole x-region. The long-time dynamics of the system is governed by two symmetry-related islands enclosing period-five elliptic orbits with velocities $v = \pm 1$. The islands are sticky, see Fig. 17(a), and the locations of the cantori are marked by the sudden

increase of the sticking times. The corresponding sticking time PDF, see inset on Fig. 17(b), for $t \gtrsim 10^2$ follows approximately a power law with an exponent $\gamma = 1.2$. Fig. 17(b) shows propagators obtained for different times after they were scaled as in Eq. (16), with exponent $\alpha = 1/\gamma$. The curves fall on top of each other thus indicating the scaling expected for the propagators of Lévy walk, see inset in Fig. 2.

A Lévy-walk kinetics has also been found in continuous ac-driven one-dimensional (Denisov *et al.*, 2002b; Glück *et al.*, 1998) and stationary two-dimensional (Klafter and Zumofen, 1994) Hamiltonian systems. There the key mechanism responsible for the appearance of anomalous transport was the cantori-induced stickiness. There are still ongoing debates on the universality of sticking-time exponent(s) at the asymptotic limit $t \to \infty$, with a number of pros and cons for different "universal" values (Chirikov and Shepelyansky, 1999; Cristadoro and Ketzmerick, 2008; Shepelyansky, 2010; Venegeroles, 2009; Weiss *et al.*, 2002). The Lévy walk can stand this uncertainty: If a PDF of sticking times is well approximated by a power law with a particular exponent γ over some substantial time interval (for example, over several decades in t) then the corresponding propagator for these times will scale as in Eq. (16), with the scaling exponent $\alpha = 1/\gamma$.

It is noteworthy that in Hamiltonian systems only subballistic super-diffusion (see Section II.A 2) is possible in the asymptotic limit. This follows from the Kac theorem on the finiteness of recurrence time in Hamiltonian systems (Kac, 1959; Zaslavsky, 2002). Therefore all sticky ballistic manifolds should have finite mean sticking times, so that the corresponding sticking-time PDFs (which are the flight-time PDFs of the corresponding Lévy walks), $\psi(\tau) \propto \tau^{-1-\gamma}$, are characterized by exponents in the range $1 < \gamma \leq 2$ (Denisov *et al.*, 2002b).

Two-dimensional chaotic advection is another field where the chaotic Hamiltonian phase space, with all its trademarks, including cantori and the stickiness phenomenon, appears (Aref *et al.*, 2014). On the theory level, the dynamics of a chaotic flow can be modeled with symplectic equations and the flow stream function as a Hamiltonian. The path of a passive tracer in the flow can be seen as a trajectory of the Hamiltonian system. Periodic flow modulations lead to the appearance of mixed phase space and regular islands. That idea was behind the first experimental observation of the Lévy walk in a real physical system. In their experiment, Solomon *et al.* (1993) used a rotating annulus tank filed up with fluid. The flow was generated by pumping the fluid into and out of the annulus through the holes in its bottom. This resulted in the appearance of the stable two-dimensional flow pattern on the surface of the fluid. Rotational motion of the tracer, monitored by by using tracer's azimuthal angle, consisted of ballistic episodes interrupted by trappings of the tracer by periodic chain of vortices, see Fig. 18.

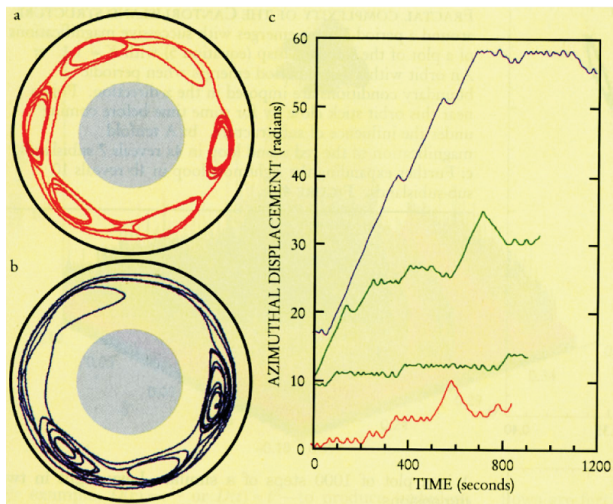It followed from the measurements that ballistic flights

FIG. 18 (Color online) Tracer dynamics in a chaotic flow. The flow produces a regular chain of six stable vortices which can trap the tracer as it circles ballistically around the annulus. Two short-time trajectories are shown on the left part of the figure. The corresponding azimuthal dynamics is presented on the right panel: while trajectory (a) (red, lowest on the graph) was trapped by the chain during all the observation time, trajectory (b) (blue, upper on the graph) shows that the tracer produced a long ballistic flight before being trapped. Adapted from (Klafter *et al.*, 1996).

had near constant velocities and the flight-time PDFs followed power-law asymptotics (Solomon *et al.*, 1994), see Fig. 19. At the same time, the sticking-time PDFs revealed either an exponential decay or power-law tails with exponent $\gamma_{st} > 1$ so that the mean sticking time is finite. Therefore, following our classification, see Fig. 1, the process can be taken as a Lévy walk with rests. However, there was a feature: Because of the annulus rotation, ballistic motion happened predominantly in one direction, clockwise or counterclockwise, depending on the rotation direction. This modification of the walk process can be absorbed into the theory by introducing bias in the standard Lévy walk model, e. g. by making ballistic flights in the positive direction less probable than in the negative one. The corresponding update was made by Weeks and Swinney (1998) and the model outcomes were found to be in a good agreement with the experimental measurements. We also refer the reader to the works by del Castillo Negrete (1998) and Isichenko (1992) for a theoretical overview of "anomalous advection" and dynamical mechanisms behind it.

A potential of the Lévy walk model for generalizations can be illustrated with *Hamiltonian ratchets*, ac-driven Hamiltonian systems which are able to generate a constant current in the absence of a bias (Denisov and Flach, 2001; Denisov *et al.*, 2002a; Schanz *et al.*, 2005, 2001). A directed chaotic transport appears due to violation of the time reversal-symmetry with a zero-mean drive (Denisov *et al.*, 2014). The set of regular islands, submerged into the chaotic layer, becomes asymmetric,
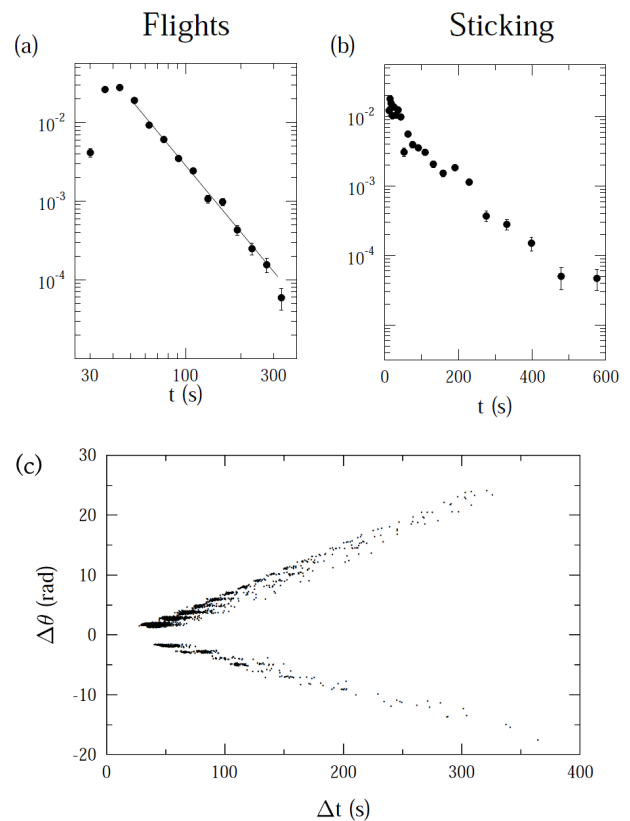

FIG. 19 Statistical characteristics of the tracer diffusion in an ac-driven chaotic flow. (a) Flight- and (b) sticking-time PDFs obtained for a flow with the six-vortex lattice, see Fig. 18. Line corresponds to a power law $t^{-1-\gamma}$, with $\gamma = 1.5$. (c) Flight length $\triangle\theta$ vs flight duration $\triangle t$. The fork-like structure reveals that all flights have near constant velocity. Adapted from (Weeks, 1997).

so that there are islands with nonzero velocities which do not have symmetry-related twins. This leads to the violation of the balance between ballistic flights in opposite directions and the appearance of a strong current (Denisov and Flach, 2001). The asymmetric generalization of the Lévy walk process by Weeks and Swinney (1998) is able to capture many features of the Hamiltonian ratchet dynamics (Denisov *et al.*, 2004, 2001).

B. Lévy walks in many-particle Hamiltonian systems

In many-particle systems with unbounded interaction potentials, such as nonlinear chains and lattices, it is no longer reasonable to talk about diffusion of particles. The individual particle dynamics has an oscillatory character due to the confinement induced by the interaction with its neighbors. The collective system dynamics creates a "tissue" which can react to small perturbations locally affecting its dynamics. The perturbation transport defines overall energy, correlation and information transport through a lattice (Giacomelli *et al.*, 2000; Helfand,

1960; Primo *et al.*, 2007; Torcini *et al.*, 1995; Torcini and Lepri, 1997).

Consider a many-particle system at microcanonical equilibrium, with a Hamiltonian

$$H_{\text{total}}(\{x_i, p_i\}) = \sum_{i=1}^{N} H_i, \qquad (78)$$

where $H_i = H(x_i, x_{i-1}, x_{i+1}, p_i)$ is the energy of the i-th particle with position x_i and momentum p_i. It is also assumed that the Hamiltonian guarantees the preservation of the zero total momentum of the system, $P = \sum_{i=1}^{N} p_i = 0$. At the initial time $t = 0$ one of the bulk particles receives an external perturbation. The system gains a small amount of extra energy E_P which is conserved due to the Hamiltonian character of the system evolution. However, the perturbation does spread as the perturbation energy is shared by a constantly growing number of particles. Remarkably, the spreading is universally limited by a finite velocity, $v_0 < \infty$, that at a given time t the perturbation is almost completely confined to the interval $[-v_0 t, v_0 t]$ ("almost" means that outside the cone the perturbation is exponentially diminished). The fundamental fact of the cone's existence, so-called "Lieb-Robinson bound" for classical systems, has a status of a mathematical existence theorem (Marchioro *et al.*, 1978; Nachtergaele *et al.*, 2009). Altogether, that was a strong hint to consider the perturbation spreading as a diffusion process, treat the normalized local excess of energy $\triangle E(i,t)$, $\Sigma_{i=1}^{N} \triangle E(i,t) = E_p$, as a PDF, $\varrho(i,t) = \overline{\triangle E(i,t)}/E_p$ ($\overline{\cdots}$ denotes a microcanonical average), and estimate its second moment.

For a one-dimensional hard-point gas with alternating masses, a protozoan Hamiltonian many-particle model (Casati and Ford, 1976), it was found that the mean squared displacement $\sigma^2(t) = \Sigma_{i=1}^{N} i^2 \varrho(i,t)$ scaled as $\sigma^2(t) \propto t^\mu$ with the exponent μ very close to 4/3 (Cipriani *et al.*, 2005). Moreover, a quasi-PDF $\varrho(i,t)$ appeared to be the exact propagator of a Lévy walk with velocity fluctuations, subsection III.B, and exponent $\gamma = 3 - \mu = 5/3$, if we set $i \equiv x$, see Fig. 20. Zaburdaev *et al.* (2011a); Zaburdaev *et al.* (2012) further strengthened this finding by showing that the scaling of the ballistic peaks is identical to that predicted by the Lévy walk model, Eq. (50). Perturbation profiles for different values of microcanonical "temperature", energy per particle ε, perfectly matched each other by assuming that the averaged velocity of the walk and the fluctuations variance both scale as $v_0, D_v \propto \sqrt{\varepsilon}$. Similar results were obtained for a FPU β chain by using local energy-energy correlation function $e(i,t)$ (Zhao, 2006) instead of a finite perturbation. This switch was induced by the fact that it is not feasible to sample the evolution of perturbations in FPU-type systems due to emerging statistical fluctuations. Although less sharp than in the case of hard-point gas, the results obtained for the times $t < 10^4$ revealed the correspondence between the correlation function profiles and the propagators of a Lévy walk with fluctuating
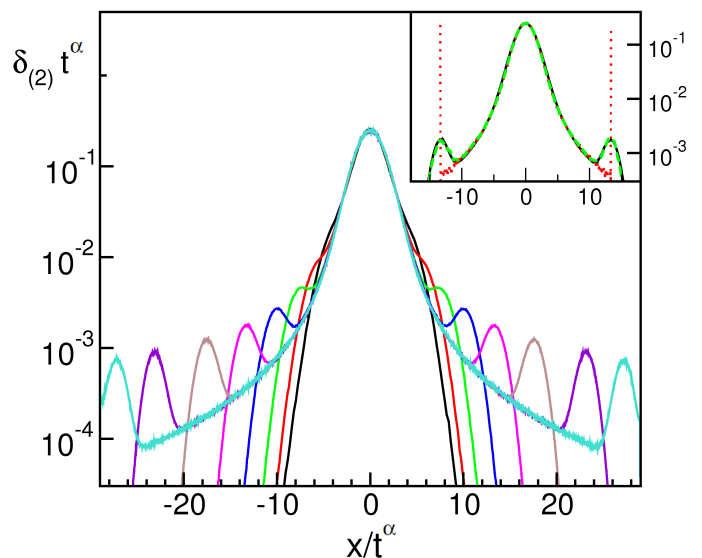

FIG. 20 (Color online) Lévy walks in a hard-point gas. Perturbation profiles $\varrho(i,t)$ (denoted by $\delta_{(2)}(i,t)$ in the original publication) at $t = 40, 80, 160, 320, 640, 1280, 2560,$ and 3840 (the width increases with time) for the energy per particle $\varepsilon = 1$, rescaled as in Eq. (16) with the exponent $\alpha = 1/\gamma = 3/5$. In the inset, the profile at $t = 640$ (solid line) is compared with the propagators of the standard Lévy with the velocity $v = 1$ (dotted line) and a fluctuating velocities with $D_v = 0.036$ (dashed line). Adapted from Cipriani *et al.* (2005).

velocity and exponent $\gamma = 5/3$ (Zaburdaev *et al.*, 2011a; Zaburdaev *et al.*, 2012).

There is a genetic link between the problem of energy diffusion and the issue of deterministic heat conduction (Helfand, 1960; Liu *et al.*, 2014, 2012). The latter is typically anomalous in most of nonlinear chains, meaning that the thermal conductivity, κ_T, scales with the length of a chain L as $\kappa_T \propto L^\eta$, with η between 0 (normal heat conduction) and 1 (ballistic heat conduction) (Lepri *et al.*, 2003). Denisov *et al.* (2003) built up a model of a dynamical heat channel in which energy is carried by an ensemble of non-interacting Lévy walkers. Relatively simple evaluation led to the linear relation between the exponents,

$$\eta = 3 - \gamma. \qquad (79)$$

There are still ongoing debates both on the (non)universality of Fourier exponent η and the validity of the single-particle Lévy walk approach to the heat conduction by many-particle chains (Lepri *et al.*, 2008; Liu *et al.*, 2012). Meanwhile the Lévy walk model has been used to reproduce the temperature profiles of finite chains (Dhar *et al.*, 2013; Lepri and Politi, 2011) and analyze heat fluctuations in conducting rings (Dhar *et al.*, 2013). Very recently, Vermeersch *et al.* (2014) proposed an interesting interpretation of the interfacial thermal transport through metal-semiconductor interfaces in term of exponentially truncated Lévy flights.

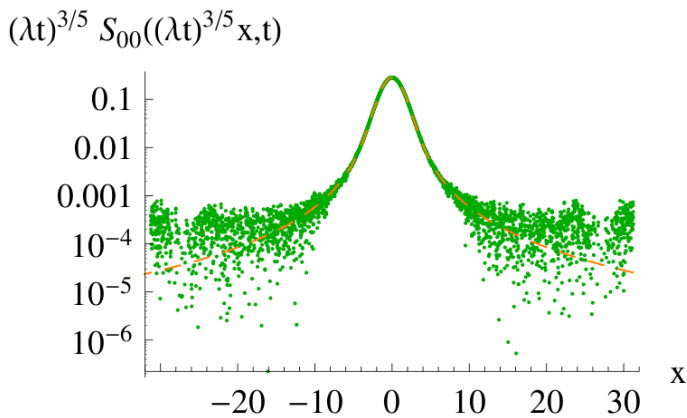$(\lambda t)^{3/5} \, S_{00}((\lambda t)^{3/5} x, t)$

FIG. 21 (Color online) Heat peak for a hard-point gas with alternating masses at time $t = 1024$. The dashed orange curve is the Lévy distribution $L_\gamma(x)$ with $\gamma = 5/3$. Adapted from Mendl and Spohn (2014).

Similar to the problem of the light transmission (see Section V.C), the set-up of the performed experiments does not allow to differentiate in a clear-cut manner between Lévy flights and Lévy walks, yet experimentalists could think about new experiments that can do.

The findings presented by Cipriani *et al.* (2005); Zaburdaev *et al.* (2011a) are phenomenological. To understand the mechanisms which sculpt Lévy kinetics out of many-particle dynamics, the problem should be considered in a broader context. van Beijeren (2012) used a hydrodynamic approach to build a mode-coupling theory for the Fourier components of the densities of conserved quantities, that are number of particles, total momentum, and energy. A linear transformation splits the transport over three channels facilitated by the three different modes, a heat mode and two sound modes propagating in opposite directions. Thus, instead of a single energy-energy correlator curve for a given time, as in Fig. 20, the hydrodynamic approach produces three profiles (two of them, for the sound modes, are related by the inversion $x \to -x$). The key result by van Beijeren (2012) is that the scaling of the ballistic sound peaks is of the Kardar-Parisi-Zhang (KPZ) universality class (Kardar *et al.*, 1986). The anomalous scaling of the central heat peak with the exponent $\gamma = 5/3$ was predicted, which corresponds to the anomalous scaling of the conductivity $\kappa_T \propto L^{1/3}$ (Lepri *et al.*, 2003). Very recently Spohn (2014) presented a complete version of the hydrodynamic formalism which addresses also the dynamics of the heat peak in more detail. Das *et al.* (2014); Mendl and Spohn (2014) have found for FPU chains and the hard-point gas the Lévy scaling for the correlator of their heat modes (see Fig. 21) and confirmed the KPZ-type scaling for the correlator of their sound modes. The Lévy-like profiles for the heat mode exhibit cut-offs at the points $x = \pm ct$, where c is the speed of sound. It is tempting to think that further progress in this direction can provide with a "hydrodynamic" foundation of Lévy walks.

C. Lévy flights of light and Lévy walks of photons

When passing through a medium, light is subjected to multiple scattering by medium inhomogeneities. Physics of this process depends on the characteristic size of inhomogeneities and different scattering mechanisms can coexist. For example, scattering by molecules (Rayleigh scattering) and by water droplets (Mie scattering) work together in a cloudy sky (Kerker, 1969). In some cases one particular mechanism dominates and thus specifies characteristic scales of the path length between consecutive scattering events (for example Mie scattering dominates inside a cloud). If a medium is a fractal (Mandelbrot, 1982) than the structure of its inhomogeneities is scale-free [a stratocumulus cloud is a good example (Cahalan *et al.*, 1994)]. The path of a photon inside a fractal media can be represented as a random walk consisting of free-path segments connecting subsequent scattering points with the PDF of the segment length in a power-law form (Davis and Marshak, 1997). The question now is shall we use the Lévy flight or Lévy walk to correctly model the process? If we are interested in the stationary transmission through the medium only then the answer is "either" (Buldyrev *et al.*, 2001).

Consider a propagation of a light beam through a slab of thickness L, with a photon free-path PDF $p(\ell) \sim \ell^{-1-\gamma}$. A local stationary transmission on the output surface is defined by all the trajectories leading to the corresponding point from the illuminated spot on the entry side. The total transmission is given by the integral over the local transmission and equals the probability of the absorption of a photon that starts at the illuminated spot by the absorption boundary on the opposite side of the slab[6]. Within this setup two approaches are equivalent. The total path length of a Lévy flight corresponds to the total traveling time of a Lévy walk, and results obtained with both models are interchangeable (Buldyrev *et al.*, 2001). By using a one-dimensional Lévy flight model[7] with $1 < \gamma \leq 2$, Davis and Marshak (1997) derived the transmission as a function of L,

$$T(L) = \frac{1}{1 + (L/\bar{\ell})^{\gamma/2}} \, , \tag{80}$$

where $\bar{\ell}$ is the mean free path and the unity in the denominator regularizes the expression at $L = 0$. In the continuous limit $L \gg \bar{\ell}$, the problem can be recast in terms of the fractional diffusion equation, Eq. (21), and, by treating the particle PDF as the light intensity, the

---

[6] The absorption effects are neglected within the framework of the approach. A photon that entered the slab will appear on the opposite side almost surely in the asymptotic limit $t \to \infty$.

[7] The problem setup considered by Davis and Marshak (1997) assumed the scattering probability peak in the forward x-direction. It was shown that the directional correlations in scattering angles can be absorbed into a rescaling of the free path within the one-dimensional framework, see Appendix in the cited work.

scaling in Eq. (80) can be obtained. Identically, the scaling could be derived within the Lévy walk framework by using the integral Eqs. (25)-(28) for the PDF of walking photons (Drysdale and Robinson, 1998). Photons move with finite velocity in any medium and therefore the Lévy walk is physically more adequate to model the photon dynamics than the Lévy flight. However, in the context of the transmission problem and from the mathematical point of view the difference between the two approaches is absent. The difference could become tangible when the problem setup is changed and, for example, auto-correlation (Section IV.A) and/or interference effects are taken into account. It remains for future work to set up the corresponding experiments. Below we overview the up-to-date experimental results.

Solar light transmission by cloudy skies. The first attempt to get insight into the morphology of a scattering media by utilizing the Lévy flight concept was made by Pfeilsticker (1999). He used statistical data obtained by measuring the mean geometrical paths of photons coming from a cloudy sky. By assuming the fractal cloud morphology and resorting to the scaling Eq. (80), the flight-length exponent was estimated as $\gamma \simeq 1.74 \div 1.78$. Pheilsticker found that the exponent value depends on the cloud type: it tends to 1.5 for convective clouds and to 2 for stratiform clouds.

Photon transmission through a Lévy glass. Modern technologies provide the possibility to synthesize scattering materials with a tunable fractal structure (Tsujii, 2008). One of the recent advances is the creation of *Lévy glass*, a polymer matrix with embedded high-refractive-index scattering nanoparticles (Barthelemy *et al.*, 2008). The matrix also contains a set of glass microspheres with a power-law diameter distribution, $p(\varnothing) \sim \varnothing^{-\eta-1}$, Fig. 22(a). The microspheres do not scatter because their refractive index is the same as of the host polymer and therefore scattering happens on nanoparticles only. The photon transport inside a Lévy glass is dominated by long "jumps" performed by the photon when it propagates through the glass spheres, Fig. 22(b). When the diameter distribution of the spheres is sampled exponentially in $\varnothing$ space, the jump-length PDF scales as $p(\ell) \sim \ell^{-1-\gamma}$, with $\gamma = \eta - 1$ (Bertolotti *et al.*, 2010). This is a clear-cut case of the Lévy walk(flight) of photons. Measurements performed with a Cauchy glass, $\gamma = 1$, by illuminating the slab with a narrow collimated laser beam, corroborated the scaling given by Eq. (80), see Fig. 22(c).

Very recently, Savo *et al.* (2014) reported on an experimental retrieval of the scaling exponent α, Eqs. (16, 36), by analyzing the scaling of the *time-resolved* transmission with L. The performed measurements verified the universal relation between the three exponents, $\alpha = 1/\gamma = 1/(\eta - 1)$, thus strengthening the position of Lévy walk (flight) formalism as an adequate theoretical approach to the process of photon (light) diffusion through fractal media.

An interesting aspect of the photon diffusion inside a Lévy glass is the role of a quenched disorder. The dis-
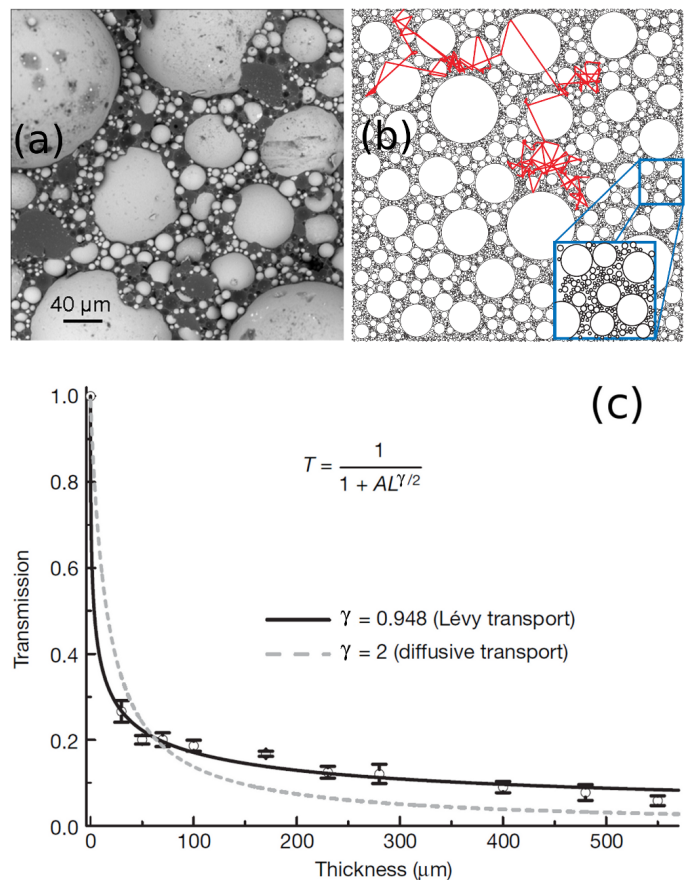

FIG. 22 (Color online) Lévy flights of photons in a Lévy glass. (a) Electron micrograph of a Lévy glass. The gray zones are interiors of the glass spheres, whereas the darker area corresponds to the polymer matrix. Scattering nanoparticles are too small to be resolved. (b) A sketch of a photon walk inside a two-dimensional version of a Lévy glass. Inset shows the scale invariance of the glass. (c) Measured transmission through a Lévy glass slab as a function of the slab thickness. Gray dashed curve is obtained with Eq. (80) for $\gamma = 1$ (normal diffusion) while black line obtained for $\gamma = 0.948$. Note that the exponent γ is denoted α in the original publications. Adapted from Barthelemy *et al.* (2008); Burresi *et al.* (2012).

tribution of glass spheres in a matrix does not evolve in time and so there is a room for correlations between flight directions and angles. By using a one-dimensional chain of barriers with a power-law spacing distribution, Beenakker *et al.* (2009) found that a walk along the chain is not the standard uncorrelated Lévy walk because of the strong correlations of subsequent step sizes. Similar results have been obtained by Burioni *et al.* (2010) and Vezzani *et al.* (2011). However, by using a two-dimensional model of a Lévy glass, Barthelemy *et al.* (2010) demonstrated that the influence of the quenched disorder can be neglected (in a sense that it can be accounted by a simple parameter tuning) when stepping into higher dimensions. Therefore the transport of photons in two- and three-dimensional Lévy glasses is close to an uncorrelated Levy walk [although this could also change when
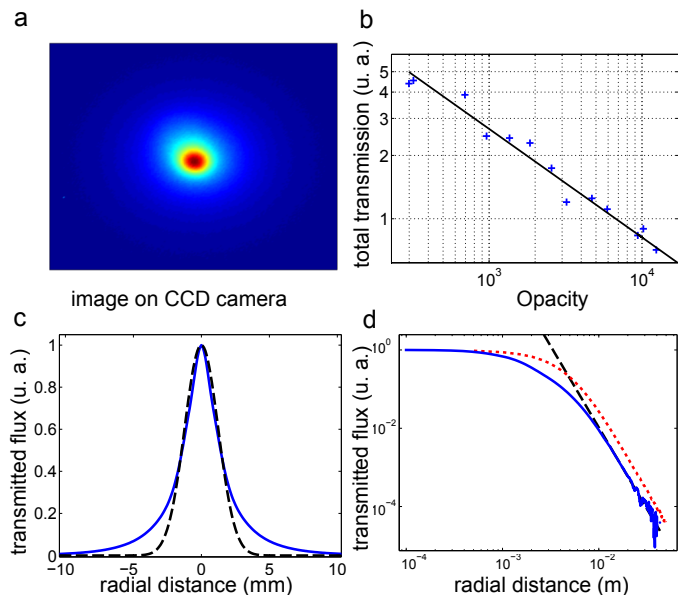
FIG. 23 (Color online) Photon transmission through a hot rubidium vapor. (a) The radial profile of the outcoming light on the charge-coupled device camera. (b) Blue crosses show experimentally measured transmission as a function of the opacity. The power-law fit $T \propto O^{-0.516}$ is shown by solid curve. (c) Experimental radial profile of the light transmitted through the vapor chamber (blue solid line) is compared with a Gaussian distribution with the same width at half maximum (black dashed line). (d) Radial profile of the transmitted light. Black dashed line is a power-law fit $I(r) \propto r^{-4.03}$. Adapted from Baudouin *et al.* (2014b).

a scattering media is perfectly self-similar and represents a regular fractal, as shown by Buonsante *et al.* (2011)].

Lévy flights of photons in atomic vapors. The two considered realizations of Lévy walks of light assumed the elastic scattering of photons. The needed power law distributions are produced by the fractal spatial inhomogeneity of scattering media and the corresponding flight-time exponents are linearly related to characteristic fractal exponents. In the case of inelastic scattering, the distance traveled by a photon depends on its frequency, which changes after every scattering event (which is in fact an absorption/emission). The spatial inhomogeneity is no longer needed and a power law distribution of flight-length can be obtained from the *spectral* inhomogeneity of the medium (Molisch and Oehry, 1998). In an atomic vapor (Baudouin *et al.*, 2014a) the absorption probability of a photon with a frequency ω at a distance r from its emission point is $p(\omega|r) = \Phi(\omega)\exp[-\Phi(\omega)r]$, where $\Phi(\omega)$ is the absorption spectrum of the atoms. The average absorption probability can be obtained as a frequency-average of $p(\omega|r)$ weighted with an emission spectrum $\Theta(\omega)$ (Holstein, 1947; Molisch and Oehry, 1998),

$$p(r) = \int_0^\infty \Theta(\omega)\Phi(\omega)e^{-\Phi(\omega)r}d\omega, \tag{81}$$

When emission and absorption spectra are identical, the Doppler spectrum $\Phi_D(\omega) = \exp(-\omega^2)/\sqrt{\pi}$ leads to $p(r) \sim r^{-2}[\ln(r)]^{-1/2}$, while the Cauchy spectrum $\Phi_C(\omega) = 1/[\pi(1 + \omega^2)]$ yields $p(r) \sim r^{-3/2}$. Pereira *et al.* (2004) proposed this as a means to realize a three-dimensional Lévy flight of photons in a hot atomic vapor where the spectra-equality condition may hold. They have also raised two important points. Firstly, in a high opacity atomic vapor many elastic scattering events happen before an inelastic scattering event occurs. This is a natural call for an extended intermittent model in which Lévy walks are alternated with periods of Brownian diffusion (see also Section VII.B where such processes appear in the context of animal search). Secondly, they pointed out that in lab vapors the time of flight is negligible compared to the waiting time between absorption and emission events. Therefore the use of Lévy flight model, Fig. 1(a), is well-justified. However, as noted by Pereira *et al.* (2004), in interstellar gases the flight time can be larger than the characteristic absorption/emission time and the Lévy walk will be more appropriate in the astrophysical context.

By using a specially designed experimental set-up, Mercadier *et al.* (2009) measured the first step length distribution of Doppler-broadened photons which enter a hot rubidium vapor. The obtained PDF follows a power law with $\gamma = 1.41$. The step-length PDF changes after each scattering event while remaining a near perfect power-law. The dependence of the exponent $\alpha(n) = \gamma(n) + 1$ on the number n of scattering events saturates to a value close to 2, as expected from the theory (Pereira *et al.*, 2004). Recently, Baudouin *et al.* (2014b) measured transmission through a hot rubidium vapor by changing the opacity of the media, $O = L/\bar{\ell}$, over two decades. This was realized by controlling the density of atoms (and thus $\bar{\ell}$) by adjusting the temperature inside the vapor chamber. The results fit the dependence predicted by Eq. (80) with the exponent $\gamma \simeq 1.01$, Fig. 23(d). The radial profile of the transmitted light has a power law tail, $I(r) \propto r^{-3-\mu}$, as expected from the Lévy-based theory developed in the paper, Fig. 23(c-d). By comparing these results with the single step length PDFs obtained before, Baudouin *et al.* (2014b) stated an excellent agreement with a Lévy-walk approach.

D. Blinking quantum dots

Blinking quantum dots serve another realizations of the ballistic Lévy walk. Similar to Lévy flights of light, photons are again involved but in a different way.

A quantum dot (QD) is a nano crystal made out of semi-conducting material and is several nanometers in size (Alivisatos, 1996). The size is crucial for determining the specific properties of QDs which are governed by quantum effects and are on the border between bulk and molecular behavior. One of the important features of QDs is the so-called quantum confinement, when the
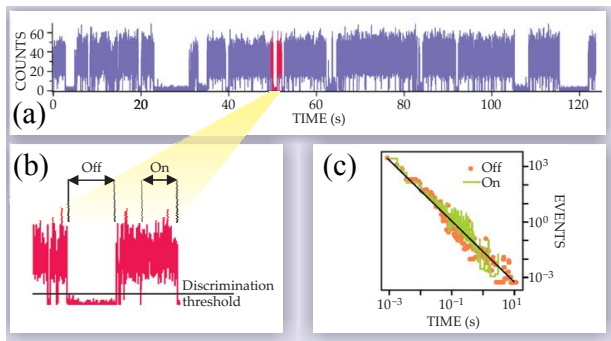
FIG. 24 (Color online) Blinking quantum dots. Panel (a) shows a sample trace of a quantum dot fluorescence. A zoom in part (b) shows how a threshold is defined, which allows to identify the periods of on and off times. The PDFs of those times are shown on (c) and have a clear power-law dependence with the same tail exponent for on and off times. The solid black line indicates a slope of 1.65, i. e. $\gamma = 0.65$. Adapted from Stefani *et al.* (2009).

exciton Bohr radius is of the order of the object size, leading to the discrete energy levels and a band gap which depends on the size of the object. When under the laser light with energy above the band gap, QDs can adsorb light by creating and exciton pair and then re-emit a photon when the exciton decays. The frequency of the emitted light is increasing with decreasing QD size and can be accurately tuned in applications. One of the important QDs applications is bio-imaging; in addition to their small size, QDs have higher brightness as compared to organic fluorescent dyes and show minimal photobleaching. However, there is one interesting effect: QDs blink (Nirmal *et al.*, 1996). Experimentally it was found that quantum dots alternate periods of fluorescence with no emission of photons, and the durations of these periods are not exponentially distributed but instead have a fat tailed power-law distribution with diverging average time. A quantum dot can fluoresce or be completely dark during the whole measurement time, which can be on the order of hours. Current experimental results provide the *on* and *off* times statistics spanning four orders of magnitude. In Fig. 24 one realization of the QD fluorescence intensity track is shown. By defining a certain threshold in the intensity, a sequence of on and off times can be identified and characterized. Many experiments with different QD materials and at different temperatures show power law distributions of those times, and in many cases the exponent is nearly the same for both of them: $\gamma \simeq 0.5$ (Margolin *et al.*, 2005). Therefore the blinking dynamics of a QD can be described as a two state model, where the durations of phases in each state (on, $I(t) = 1$, and off, $I(t) = 0$) are distributed as power laws with diverging means. As we discussed in Section IV.D, systems with such distributions exhibit memory effects, aging and weak ergodicity breaking. Interestingly, the problem of blinking nanodot can be mapped onto the Lévy walk model. Consider the fluorescence intensity $I(t)$ and define its time average as:

$$\bar{I} = \frac{\int_0^T I(t)dt}{T} \tag{82}$$

As we learned from Section IV.D, for the weak ergodicity breaking problems the time average is itself a random variable with a certain distribution. It can be shown, that the PDF of the time averaged intensity $P(\bar{I})$ is given by the Lamperti distribution (Lamperti, 1958; Margolin *et al.*, 2005):

$$P(\bar{I}) = \frac{\pi^{-1} \sin(\pi\gamma) \, \bar{I}^{\gamma-1} \left(1 - \bar{I}\right)^{\gamma-1}}{\bar{I}^{2\gamma} + \left(1 - \bar{I}\right)^{2\gamma} + 2\bar{I}^\gamma \left(1 - \bar{I}\right)^\gamma \cos(\pi\gamma)} \tag{83}$$

We know this distribution from the analysis of the ballistic Lévy walk model, and it is easy to draw an analogy. In the ballistic regime of the Lévy walk, we can define a time averaged position of the particle x/T as an integral from 0 to T of the particles velocity $v(t)$, see Eq. (56). As in quantum dots, the time spent in each velocity state has a power-law distribution with infinite mean. The only difference to the QD blinking problem is that the velocity of particles can have values of $v(t) = \pm v_0$, while the intensity switches between 0 and 1. As a result, in case of Lévy walks, the PDF $P(x/T)$ is symmetric around zero, whereas for the time average intensity it is shifted and has a support from 0 to 1. One particular example of $\gamma = 1/2$ gives a simple particular case of the Lamperti distribution, see Eq. (34) and Fig. 3. An intuitive expectation that the QD will be half time on and half time off appears to be least probable: the corresponding PDF has a minimum at $\bar{I} = 1/2$. Instead the $P(\bar{I})$ has a divergent behavior at $\bar{I} = 0$ and $\bar{I} = 1$ (similarly to the divergence of the PDFs at ballistic fronts in case of Lévy walks). Therefore a quantum dot is either on or off for most of the observation time.

The particular mechanism responsible for the appearance of the power-law distributed blinking times in quantum dots remains unknown. There are several working models which relate the statistics of on and off times to the dynamics of exciton pair including its transport, diffusion, and trapping [see Stefani *et al.* (2009) for an overview], but none of the models are able to describe all available experimental observations. For the context of this review it is important that the experimental data on blinking QD can be directly mapped to the model of Lévy walks in the ballistic regime (Margolin *et al.*, 2006). We can speculate that the analytical results available for the Lévy walk model with random velocities could be useful for the interpretation of experiments with QDs with a whole distribution of intensities and not just two levels. Reciprocally, a possible correlation between consequent long on (off) times, when a long on (off) time is followed with higher probability by another long on (off) time (Stefani *et al.*, 2009), calls for further generalizations of the Lévy walk model.

E. Lévy walks of cold atoms

Lévy distributions are known in the field of cold atom optics since 1990s, when Bardou *et al.* (1994) and Reichel *et al.* (1995) discussed the relation between the process of the so-called subrecoil laser cooling (Aspect *et al.*, 1988) and anomalous diffusion in terms of Lévy flights. Lévy walks appeared in cold atom optics in the context of Sisyphus cooling of atoms loaded into an optical bi-potential created by two counterpropagating linearly polarized laser beams (Dalibard and Cohen-Tannoudji, 1989). There are two internal atomic states and atoms with different internal states feel potentials of different polarizations. The laser-induced transitions of an atom between its internal states influence translational motion of the atom along the bi-potential. Elaborated within the Monte Carlo wave function framework, this connection was shown to be responsible for Lévy walk-like dynamics of atoms (Marksteiner *et al.*, 1996). Katori *et al.* (1997) measured the mean squared displacement of Mg ions in a bi-potential optical lattice and found the scaling $\sigma^2(t) \propto t^\mu$ with the exponent $\mu > 1$ for potential depths below the critical value. Sagi *et al.* (2012) performed more sophisticated experiments and measured the spreading of a packet of cold Rb atoms in optical lattices of different depths. The obtained atomic distributions scaled with the characteristic scaling, Eq. (16), Fig. 25(a), and their shapes could be nicely fit by Lévy distributions, Fig. 25(b). However, a Lévy walk description did not work well in this case, because in both, experiments and Monte Carlo wave function simulations, strong correlations between velocities and durations of atom flights were found.

Marksteiner *et al.* (1996) derived that on the semiclassical level the distribution $W(x, p, t)$ of atoms can be described by the Kramers equation

$$\frac{\partial W}{\partial t} + p\frac{\partial W}{\partial x} = \left[D\frac{\partial^2}{\partial p^2} - \frac{\partial}{\partial p}F(p)\right]W, \qquad (84)$$

with the cooling force (Castin *et al.*, 1991)

$$F(p) = -\frac{p}{1 + p^2}, \qquad (85)$$

where momentum is expressed in dimensionless units p/p_c, with the capture momentum p_c set to unity. For small momenta the force is of the conventional linear form, $F(p) \sim -p$, while $F(p) \sim -1/p$ for large p so that the atom becomes frictionless at the high-momentum limit. The diffusion constant D combines all relevant parameters such as the depth of the optical potential, recoil energy, see below. The equilibrium momentum-momentum correlation function corresponding to Eq. (84) scales as $t^{-\lambda}$, with the exponent

$$\lambda = (1/2D) - 3/2. \qquad (86)$$

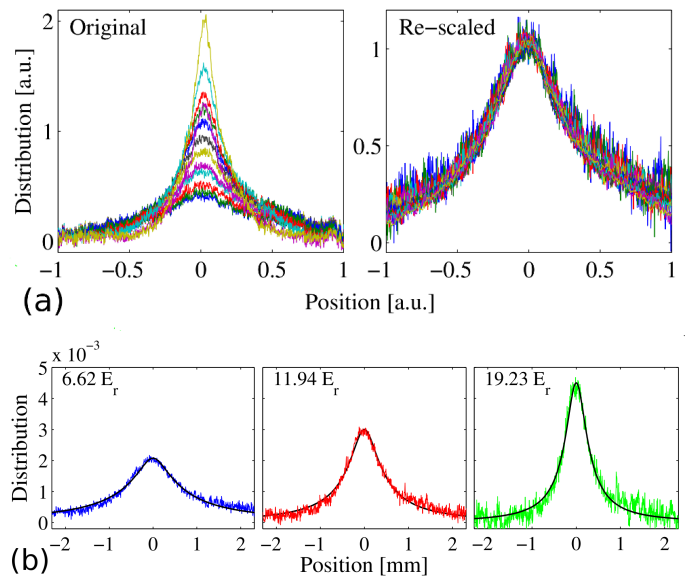The control parameter,

$$D = cE_R/U_0. \qquad (87)$$

FIG. 25 (Color online) Lévy walks of atoms in optical lattices. (a) Atomic distributions obtained for different times, $t \in [10 - 40]$ ms, before (left) and after the scaling transformation (16) with exponent $\alpha = 0.8$ (right). (b) Atomic distributions after 30 ms of spreading for three different optical potential depths. Lines correspond to Lévy distributions with depth-specific exponents. Adapted from Sagi *et al.* (2012).

depends on the recoil energy E_R and the depth of the optical lattice potential U_0. The constant c is specific to the type of atom/ion cooled, with the typical value around 10. Therefore, one could, by tuning the potential depth U_0 while keeping all other parameters fixed, control the exponent λ and switch between the regimes of normal and anomalous atom diffusion.

When $\lambda < 1$, the integral of the correlation function over time diverges and an anomalously fast diffusion appears. Equilibrium velocity distribution for Eq. (84) has a form of the Tsallis distribution (Douglas *et al.*, 2006; Lutz, 2003). Although interesting as an indication of a strong deviation from the Boltzmann-Gibbs thermodynamics (Lutz and Renzoni, 2013), these distributions themselves do not provide sufficient insight into the diffusion of atoms in the real space.

By unraveling the Kramers equation (84) into a Langevin equation with a white Gaussian noise as a drive,

$$\dot{p} = F(p) + \sqrt{2D}\zeta(t), \qquad (88)$$
$$\dot{x} = p, \qquad (89)$$

Kessler and Barkai (2012) analyzed the atom diffusion from the microscopic point of view. The theory developed by Barkai *et al.* (2014) predicts the existence of three phases in the dynamics, generated by Eqs. (88-89), depending on the value of D. Namely, it can exhibit normal diffusion, Lévy-walk superdiffusion, and Richardson's diffusion (Richardson, 1926a), when the MSD scales as $\sigma(t) \propto t^3$. The existence of the Lévy walk regime was proved analytically for the range $1/5 < D < 1$. In the
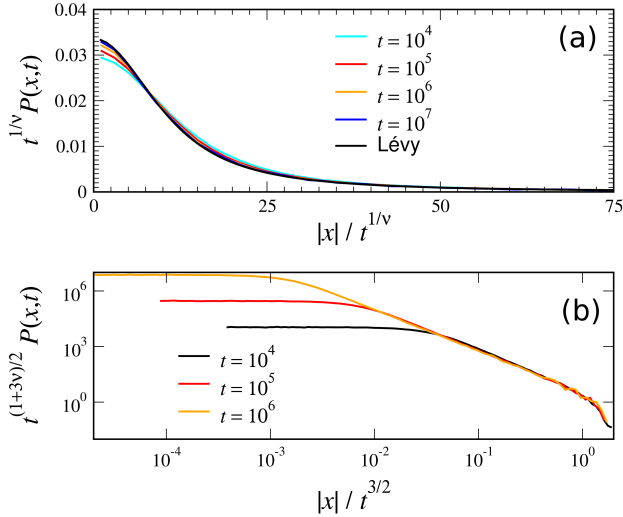
FIG. 26 (Color online) Scaling of the propagators $P(x,t)$ of the stochastic process, Eqs. (88,89), modelling the diffusion of cold atoms. The scaling exponent γ (denoted by ν in the original publications) is $(1+D)/3D$. (a) With the increase of time the rescaled profiles start to fall onto the Lévy distribution $L_\gamma(\xi)$. (b) Another scaling reveals the the cutoff induced by a nonlinear space-time coupling, Eq. (90). The parameter $D = 2/5$. Adapted from Kessler and Barkai (2012).

asymptotic limit of large t, the central part of the propagator $P(x,t)$ scales with the distinctive scaling, Eq. (16), where $\Phi(\xi) = L_\gamma(\xi)$, and $\gamma = (1 + D)/3D$. The coupled transition probably is different form that for the standard Lévy walk, Eq. (26), and has the form (Barkai *et al.*, 2014; Kessler and Barkai, 2012)

$$\phi(y,\tau) = \psi(\tau)p(y|\tau), \qquad (90)$$

with the conditional PDF $p(y|\tau) \sim \tau^{-3/2}B(y/\tau^{3/2})$. The normalized nonlinear function $B(x)$ is responsible for the cutoff of the propagator tails, so that all moments of the process are finite. Together with the mode-coupling theory of the energy transport in classical nonlinear chains (Section V.B), these results pave the way toward physical foundations of Lévy walks.

VI. LÉVY WALKS IN BIOLOGY

From rather complex but objective systems of physics, we are shifting to the field of biology and biophysics where effects and phenomena are much harder to quantify because of their intrinsic diversity and variability. In recent years, the topic of Lévy walks resonated in research communities working on motility of living organisms, their foraging, and search strategies. By the level of debates, the topic may even be called controversial. Fortunately our review is preceded by two very recent monographs devoted to these subjects (Méndez *et al.*, 2014; Viswanathan *et al.*, 2011). Here we are presenting our point of view through the prism of the Lévy walk

framework and point to the examples that are directly relevant to this model. Before passing to particular examples we would like to outline the general complexity of the problem in question.

A. Motility is a complex issue across many scales

Motility spans many scales, ranging from swimming micron-sized bacteria to albatrosses which can travel hundreds of kilometers at a time. Motility involves interactions of moving animals with their environment and habitats, which in most cases is hard to quantify or predict. In ecology, the interest in motility usually does not arise *per se* but in relation to some greater issues, for example, questions of how animals search for food, how they navigate home, how they find each other to mate or to agglomerate into colonies, and others.

In a very interesting twist, Lévy walks are involved in a particular topic of effectiveness of search and foraging strategies. Lévy walks are argued to be the most efficient search strategy *under certain conditions* imposed on the distribution and properties of targets. There is a constantly growing number of accounts where Lévy statistics is reported for the trajectories of animals. Quite often these results get criticized or disputed, based on insufficient data, an inconsistent analysis, or just out of different beliefs. As a side effect of these still ongoing discussions, new papers constantly appear where researchers report the analysis of the motion patterns of yet another living species and claim that the patterns *do* or *do not* look as Lévy flight or Lévy walk trajectories. There is even a philosophical flavor in this discussion (Baron, 2014). The possible reasons of this controversy are manifold. Below we summarize them from rather evident to more complex levels.

i) *Difference in sizes, forms of locomotion, habitats etc.* All these difference dictate different experimental techniques and also call for different statistical techniques. As pointed out by Méndez *et al.* (2014), on the micron scales of single cells, positional data can be acquired with high space and time resolution leading to almost continuous recorded trajectories. Such observations are common in a lab since 1970s. Tracking of big animals in their habitats is a much harder task due to complex interactions of the animals with the environment and large spatial scales they travel over. This field advanced only recently, to a greater extent due to the miniaturization and growing accuracy of the portable GPS devices. Therefore there is much less and sparser statistical data for big animals. Still, while it is possible to follow 1500 individual sperm cells at a time (Su *et al.*, 2012), this number remains unrealistic for sharks or deers. There is a data-driven gap in the applied methodology. Some researchers are trying to use Langevin-type equations for continuous tracks while others prefer more coarse-grained random walk models for the trajectories recorded with limited resolution. Currently the gap is narrowing, as there are examples of

random walks used to model the motility of bacteria and attempts to apply the Langevin machinery to analyze the trajectories of bumblebees and beetles.

ii) *Complex trajectories.* Some trajectories resemble neither Lévy flights nor Lévy walks but are still modeled as such. These are usually almost smooth continuos tracks of cells or other organisms (Dieterich *et al.*, 2008; de Jager *et al.*, 2011; Levandowsky *et al.*, 1997). There is often a problem of how to define a flight or a step of a random walk for such tracks, to resolve which several methods were suggested (Humphries *et al.*, 2013; Raichlen *et al.*, 2014; Rhee *et al.*, 2011; Turchin, 1998). The proposed random walk models often are of academic interest only, since most of the information encoded in continuous trajectories is lost or disregarded. These approaches provide, however, some statistical characteristics of the foraging patterns that can be compared with those for the known search strategies. An alternative approach is to look into the microscopic details of motility patterns by using, for example, Langevin dynamics (Lenz *et al.*, 2013; Selmeczi *et al.*, 2008; Zaburdaev *et al.*, 2011b), and then pose a question of how it can lead to the appearance of the Lévy like behaviour on larger spatial scales (Lubashevsky *et al.*, 2009b). In a few cases, the information provided by trajectories was sufficient to suggest biological mechanisms of the motility, as was demonstrated for some cells and bacteria (Gibiansky *et al.*, 2010; Jin *et al.*, 2011; Li *et al.*, 2008; Marathe *et al.*, 2014; Zaburdaev *et al.*, 2014).

iii) *Lévy flight vs. Lévy walk.* Although it is evident that living organisms can only move with a finite speed, there is a big subset of studies where the Lévy flight is used to model the observed trajectories. Some papers mention both approaches, walks and flights, interchangeably, but then they mostly consider the statistics of displacements at fixed time intervals or the MSD. The distribution of displacements at fixed time intervals in fact yields a velocity distribution (López-López *et al.*, 2013), and therefore suggests a very different model of random walks with random velocities; as we have seen already, its properties are different from both the Lévy flight and Lévy walk models. We also know that the MSD of a Lévy flight diverges and therefore the corresponding model is not suitable for the analysis of the MSDs obtained from the experimental data. The ignorance to the difference between the Lévy flight and Lévy walk concepts does not add positively to the clarity of the issue.

iv) *Other biological reasons.* As we have mentioned, whether a bacterium or a deer, both interact with the environment. The more complex the organism is, the more rich and unpredictable are the effects of this interaction. While lab conditions for bacteria or cell experiments can be controlled to a high degree, the question of how much of deer's motion is influenced by the type of a forest the deer moves in, is much harder to disentangle. Individuals may have different responses to the same stimuli, because, for example, they can be at different developmental stages. Therefore it should not be forgotten that
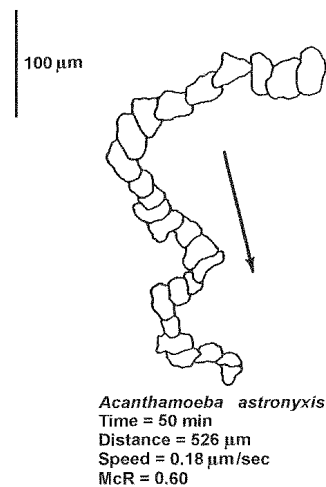

FIG. 27 A sample trajectory of soil amoeba showing outline of the cell at 1 minute intervals. Adapted from Levandowsky *et al.* (1997).

some effects which look like anomalous behaviour for the ensemble of organisms, may come about only as a result of variability between the individuals, where each individual behaves quite normally but on its own scale, see a book by Méndez *et al.* (2014) and original works by Hapca *et al.* (2009); Petrovskii *et al.* (2011).

It is certainly beyond our goals and abilities to resolve all these challenging issues in this review. We can only welcome attempts to summarize and critically address these points by Méndez *et al.* (2014); Selmeczi *et al.* (2008). We hope that the theoretical background provided in this review will help to introduce the Lévy walk model (and its appropriate modifications) to the community of biologists and biophysicists with more rigor so that it can be applied to the collected data in a proper way.

B. Soil amoeba

One of the first mentions of the Lévy walk model in biological context was made in the work on crawling amoeba by Levandowsky *et al.* (1997). Amoeba are uni-cellular organisms which can move on surfaces and three-dimensional media by growing cell protrusions called pseudopodia. In Levandowsky *et al.* (1997), 17 amoeba isolates were tracked with a help of a microscope and a video recorder. Different traces of the overall duration $15 - 60$ min were recorded with a time step of 1 or 2 minutes. Considered species represented a range of sizes 10 to 100 microns and average speeds 0.16 to 1.3 µm/s. This means that cells roughly moved about one cell size per one step (one minute), see Fig. 27. After each step, the authors measured turning angles, velocity distribution and the MSD. For all observed cells the MSD scaled as $\langle x^2 \rangle \propto t^\mu$ with $\mu \sim 1.5 - 1.9$, which

led the authors to the conclusion that the Lévy walk could be a good candidate for a model. The obtained histograms of turning angles indicated little directional change. The authors also stated that their tracking was not long enough to check whether cells switch to the normal diffusion at longer times. Although not a clear-cut example of the Lévy walk, this was the first and balanced assessment of the experimental observations. After two decades of similar research one could suggest that the Ornstein-Uhlenbeck process, i. e. a Langevin equation for velocity increments containing friction and random force (Risken, 1996), could be a reasonable alternative approach. The corresponding stochastic process is characterized by an exponentially decaying velocity auto-correlation function, and if the observation time is less or of the order of the correlation time the MSD behaves almost ballistically and only at later times switches to diffusive behavior, see similar results for beetles (Reynolds *et al.*, 2013). A recent comprehensive study of *Dictyostelium discoideum* amoeba motility considered several possible mechanisms, including the generalized Langevin equation with a memory kernel, nontrivial fluctuations, and a more microscopic, zig-zag motion strategy (Li *et al.*, 2008).

C. Run and tumble of bacteria

Until recently, motion of a swimming *E.coli* bacteria was considered as a clear example of the standard diffusion. The diffusive dynamics naturally follows from the mesoscopic picture of random walks describing the run and tumble motion (Berg, 1993, 2004). *E.coli* have multiple flagella, helical filaments which rotate and thus propel the cell in the fluid. Because of the microscopic size of the cell, the swimming occurs at low Reynolds numbers, which has its implications on the physics of the process (Lauga and Goldstein, 2012; Purcell, 1977). Molecular motors can rotate flagella in two opposite directions, clockwise (CW) and counterclockwise (CCW). In CCW mode multiple flagella form a bundle and the cell swims following almost a straight path, which is called a "run". When one or several motors switch the direction to CW, the bundle dissolves and the cell rotates almost on the same spot, so called "tumble" phase. When the bundle forms again in the CCW mode, the cell begins its next run. The angle between the directions of the two consequent runs is not completely random but has a non-uniform distribution with a mean around 70°. *E.coli* are rod shaped bacteria of about two microns long, the average run time is one second and the corresponding almost constant speed is $\sim 20\mu m/s$. Therefore the length of a run is roughly ten times the cell body length. Tumbles are approximately ten times shorter than the runs and usually neglected in theoretical models. Since the motion occurs in a fluid, runs are not entirely straight but are subjected to the effects of the rotational diffusion. If, for a moment, we neglect the rotational diffusion, the
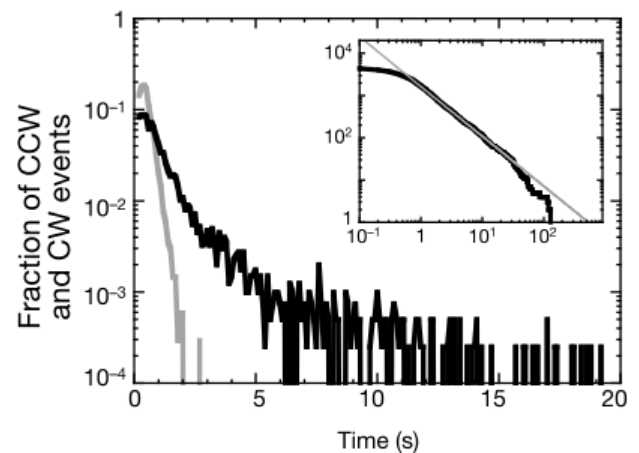

FIG. 28 Distributions of run and tumble times of *E.coli* bacteria. Counterclockwise (CCW) rotation (black line) corresponds to the run of bacteria, whereas clockwise (CW) rotation (gray line) corresponds to tumbling. Measurements are presented for a single bacterium. While tumbling times are shorter and well described by the exponential distribution, the durations of CCW rotations exhibit a long non-exponential tail which can be fitted by a power law. The inset shows the cumulative distribution function for CCW rotation times and the gray line is the power law with an exponent ~ 2.2. From Korobkova *et al.* (2004).

swimming cell can be seen as a biological realization of the Lévy walk model: it moves with an almost constant velocity, then tumbles and chooses a new swimming direction. The experimentally measured run time distribution of *E.coli* was usually described by an exponential distribution (Berg, 2004). However, in a recent experiment with individual tethered cells by Korobkova *et al.* (2004), it was shown that the PDFs of durations of CCW rotation of flagella (corresponds to run of the cell) fit the power law distribution with an exponent $\gamma = 1.2$, see Fig. 28.

It was also shown theoretically that the genetic circuit responsible for the duration of motor rotation in CCW direction can generate power-law distributed times in the presence of chemical signal fluctuations (Matthäus *et al.*, 2011). Experiments with tethered cells suggest that power-law distributed run times could be also observed in individual swimming cells, but there is no experimental confirmation of this yet.

To encompass the possibility of the power-law distributed run times, Lévy walk model is the natural choice to describe the dispersal of idealized *E.coli* bacteria (by neglecting the effects of rotational diffusion during the runs) in two or three dimensions.

Interestingly, many bacteria (and some eukaryotic cells) swimming in fluid or moving by other means on surfaces produce similar patterns, reminiscent of the run-and-tumble motion. Those include, for example, run-and-reverse pattern, where the direction of the next run is opposite to the previous one, or run-reverse-flick motion, where reversals are alternated with ran-
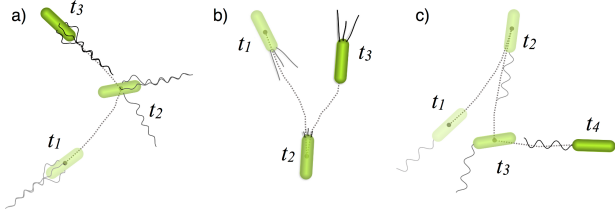
FIG. 29 (Color online) Different motility patterns of bacteria: (a) run and tumble motion, where straight runs are alternated by tumbling events; the angle between the consecutive runs can have a certain preferred value (b) run reverse, where the next always has an opposite direction (c) run reverse and flick, where reversals strictly alternate with completely randomizing turn, similar to *E. coli*, in other words it is an alternation of (a) and (b) that makes up a more complex pattern of (c). From Taktikos *et al.* (2013).

dom turns (Taktikos *et al.*, 2013; Xie *et al.*, 2011), see Fig.29(c). Experimentally such trajectories are often observed within the single focal plane of the microscope or in a confined planar geometry. These biologically relevant motility patterns suggest an alternative description of a Lévy walk process in two dimensions, namely via the angle determining the orientation of the cell velocity, $\phi(t)$: $\mathbf{v}(t) = v(\cos\phi(t), \sin\phi(t))$. The time evolution of the angle can be split into two components, abrupt angular changes during the reorientation events and an independent component of the noise leading to the rotational diffusion, $\phi(t) = \phi_{\text{rw}}(t) + \phi_{\text{rot}}(t)$. $\phi_{\text{rw}}(t)$ characterizes a one dimensional CTRW in the angle space. The run-and-tumble motion is characterized by waiting times when the angle does not change (run) and random jumps according to the turning angle distribution (tumble). For example, in case of run-and-reverse, the jumps are of the size $\pm\pi$. Therefore the problem of the Lévy walk in two dimensions can be mapped onto a one-dimensional CTRW process for the angle. It has interesting consequences for the calculation of the standard quantities as, for example, the velocity autocorrelation function or the MSD. The velocity correlation function of bacteria's velocities at times t_1 and t_2, $C(t_1, t_2)$ is given by:

$$C(t_1, t_2) = \langle \mathbf{v}(t_1)\mathbf{v}(t_2) \rangle = v^2 \left\langle e^{-i[\phi(t_2) - \phi(t_1)]} \right\rangle. \quad (91)$$

The contribution to correlations coming from the rotational diffusion is well known and appears as an exponential pre-factor, a more non-trivial part is the random walking component of the angle. It can be shown that

$$C_{\text{rw}}(t_1, t_2) = v^2 \int_{-\infty}^{+\infty} d\phi_1 \int_{-\infty}^{+\infty} d\delta\phi e^{-i\delta\phi} P(\phi_1, t_1; \delta\phi, t_2). \quad (92)$$

Here, $P(\phi_1, t_1; \delta\phi, t_2)$ is the joint probability density to find a cell moving in direction ϕ_1 at time t_1 and direction $\phi_1 + \triangle\phi$ at time t_2. It is easy to see that the above Eq. (92) is the double Fourier transform with respect to ϕ_1 and $\delta\phi$, where the corresponding coordinates in Fourier space are set to $k_1 = 0$ and $k_2 = 1$, respectively.

Therefore, to find the velocity autocorrelation function one needs to find the two-point PDF for the random walk of the angle. It is a non-trivial, especially for the case of power-law distributed waiting times, but exactly solvable problem (Barkai and Sokolov, 2007; Baule and Friedrich, 2007; Dechant *et al.*, 2014; Zaburdaev, 2008). The MSD can now be calculated by using the Kubo relation:

$$\langle [\mathbf{r}(t) - \mathbf{r}(0)]^2 \rangle = \int_0^t dt_1 \int_0^t dt_2 \, \langle \mathbf{v}(t_1) \cdot \mathbf{v}(t_2) \rangle. \quad (93)$$

There are two important particular cases of the above general formulas. For the exponentially distributed run times, $\psi_{\text{run}}(\tau) = \tau_{\text{run}}^{-1} \exp(-\tau/\tau_{\text{run}})$, many things simplify dramatically and yield the following answer for the MSD:

$$\langle [\mathbf{r}(t) - \mathbf{r}(0)]^2 \rangle_{\text{rw}} = 2v^2 \widetilde{\tau}^2 \left(\frac{t}{\widetilde{\tau}} - 1 + e^{-t/\widetilde{\tau}} \right), \quad (94)$$

where the effective decorrelation time $\widetilde{\tau}$ depends on the average run time, τ_{run}, and the average cosine of the turning angle, $\cos\phi_0$ (Lovely and Dahlquist, 1975):

$$\widetilde{\tau} = \frac{\tau_{\text{run}}}{1 - \cos\phi_0}. \quad (95)$$

For *E.coli*, $\cos\phi_0 \simeq 0.33$ whereas for reversing cells it is equal to -1. The Eq. (94) is a well known result for the Ornstein-Uhlenbeck process (Risken, 1996) which we already mentioned before, but here it was derived from the Lévy walk model and not from the Langevin equation. For short times $t \lesssim \widetilde{\tau}$ the MSD scales ballistically and then turns to the diffusive regime. In case of the power-law distributed run times (as in Eq. (8)) with $1 < \gamma < 2$, the MSD scales as $t^{3-\gamma}$, a well known result. An interesting observation is that in the superdiffusive regime the turning angle distribution plays no role (unless the turning angle is not zero) in the asymptotic regime.

To finalize this section we discuss two more modifications of the Lévy walk used to model motility of bacteria. Above we mentioned the run-reverse and flick motility pattern which was reported for *V.alginolyticus* bacteria by Xie *et al.* (2011). In this case, the reversals are alternating with completely randomizing turns with $\cos\phi_0 = 0$. In *V.alginolyticus* this happens because its single flagellum is unstable, when switching from CW to CCW rotation. The durations of runs after flick and reversals may also be governed by two different distributions. When translated into a CTRW model for the angle, that means that jumps with two distributions for the jump amplitude and waiting times are alternating. As a remarkable difference to the model with a single turning angle distribution where the velocity correlation function is always positive, run-reverse-flick model has an interval of negative velocity correlations (Taktikos *et al.*, 2013).

For another type of swimming bacteria, *P. putida*, it was found that cells predominantly adopted the run-and-reverse pattern, but, in addition, the speed of a single cell changed roughly by a factor of two between forward and

backward swimming directions (Theves *et al.*, 2013). For the corresponding one dimensional Lévy walk model with two alternating speeds that would result in the back and forth motion, but with the ballistic scaling in the direction of the higher speed. The cells swimming in a fluid are subjected to fluctuations and therefore the rotational diffusion regularizes the ballistic scaling. As a result, bacteria undergoing run-and-reverse motion with alternating velocities, diffuse faster than bacteria showing run-and-reverse behavior but with a constant intermediate velocity.

The above examples demonstrate that the class of Lévy walk models provides a perspective tool for the mesoscopic description of the bacterial motility. Whether the involved times are anomalously long or exponentially distributed, Lévy walk framework is flexible and can be adjusted to the needs of a particular problem – rotational diffusion during runs, different turning angles and speeds, pausing during tumbles – while remaining in the domain of analytically solvable models.

D. Short note on chemotaxis

Bacteria, amoeba, sperms and many other cells and microorganisms are known to be able to perform chemotaxis: they can actively alternate motility in response to the gradients of certain chemicals, signaling molecules, nutrients, or waste products. Different organisms adopt different chemotactic strategies (Eisenbach and Lengeler, 2004). Larger cells, such as amoeba, can detect the gradients across their own cell body length via multiple chemoreceptors. Reacting to the occupancy of those receptors, amoeba can preferentially grow the pseudopodia in the corresponding direction and therefore continuously reorient during its motion. Bacteria are too small to do that and instead use a temporal integration of the chemical concentration which they experience along the trajectory. The chemical signal is passed on to the genetic pathway which regulates the flagella motor reversals (we are omitting a lot of interesting biological details, which, at least for *E.coli*, are well understood (Berg, 2004)). If a cell swims in the direction of increasing concentration of the favorable signal it extends its run phase. The response of the cell to the pulses of certain chemicals was measured experimentally by observing the frequency of motor reversals; it revealed a non-trivial two lobed response function, showing the properties of adaptation (Celani and Vergassola, 2010; Segall *et al.*, 1986). By assuming that tumbles follow after exponentially distributed run time, the rate of tumbling events in the presence of the signaling chemical with not too strong variations can be represented as:

$$\lambda(t) = \lambda_0 \left(1 - \int_{-\infty}^{t} dt' c(t') R(t - t') \right), \qquad (96)$$

where $\lambda_0 = 1/\tau_{\mathrm{run}}$ is the cell's tumbling rate in a homogeneous environment, $c(t)$ is the concentration of the
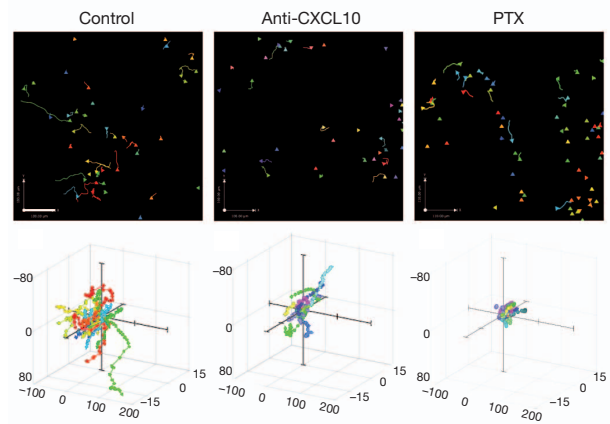

FIG. 30 (Color online) (top) Tracks of T-cells recorded by two-photon fluorescence microscopy in three different experimental conditions. (bottom) Reconstructed three-dimensional trajectories of individual cells. Adapted from Harris *et al.* (2012).

chemical along the path, and $R(t)$ is the memory or response function of bacteria obtained from the experiments. de Gennes (2004) used this formula and the random walk model of run and tumble to calculate analytically the resulting average drift velocity along the small gradients of $c(x)$. This approach can be generalized to all above discussed motility patterns of bacteria and shows the importance of the theoretical modeling by means of simple random walks. One of the open questions in this field is how to generalize the de Genes' approach to a general distribution of tumbling events, going beyond the exponential function and including the power-laws.

E. T-cells

In a recent experimental study by Harris *et al.* (2012), the migration of CD8$^+$ T-cells in the brain explant of mice was analyzed. CD8$^+$ T-cells are a special type of white blood cells which are responsible for killing cancer cells, those infected by viruses, or otherwise damaged or abnormal cells. Direct contact of the T-cell and the target cell is required for killing the abnormal cell. In this study, T-cells were targeting the cells infected by a parasite *T. gondii* which invades the cells of the central nervous system and causes the toxoplasmosis infection. T-cells which produce a fluorescent protein were imaged in 3D by using two-photon microscopy of the brain explant of mice with chronic toxoplasmic encephalitis in different experimental conditions. As one of the important factors involved in the regulation of T-cells motility, a small signaling protein, chemokine CXCL10, was noted. By varying the concentration of this chemokine the authors showed that T-cells were changing the average speed but not other statistical characteristics of their trajectories. Along with the standard MSD measurements, several additional properties of the acquired
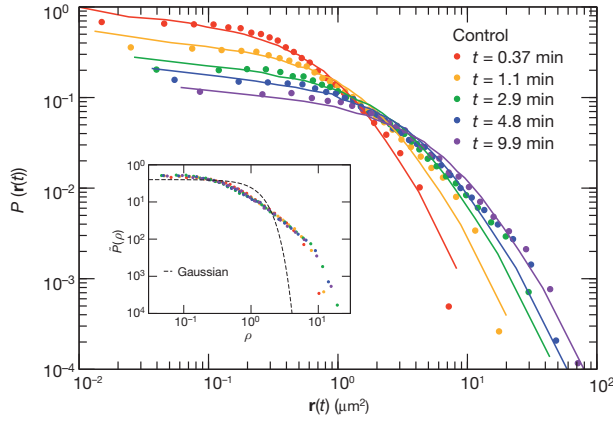
FIG. 31 (Color online) PDF of T-cells' displacements for the control case at different time points. Symbols denote the experimental data, and lines are fits according to the generalized Lévy walk model. The inset shows that the profiles, rescaled according to $\tilde{P} = t^{\alpha}P$ and $\rho = r/t^{\alpha}$ with $\alpha = 0.63$, collapse on top of each other. From Harris *et al.* (2012).

trajectories were analyzed: PDF of displacements at different times and its scaling properties, correlation function of cell displacements, and overall shape of the tracks. MSD showed a clear superdiffusive behaviour with the exponent 1.4: $\langle \mathbf{r}^2(t) \rangle \propto t^{1.4}$. Consistent with previous observations of runs and pauses in lymphocytes the authors suggested the model of Lévy walks with rests as the working hypothesis. Indeed by comparing this model with more than 10 other possible random walk models, it was shown to give the best representation of the experimental data (it is suggested to read the extensive, almost 20 pages, Supplementary material to the original paper). In Fig. 30 we show the representation of 3D tracks and in Fig. 31 the PDF of cell' displacements at different times (corresponds to the Control case in Fig. 30).

Rescaled profiles convincingly fall onto a single master curve. In the concluding remarks of the paper, it is mentioned that the Lévy walk model for the motility of T-cells is consistent with the idea of more effective search, as compared to Brownian motion in case of sparse targets. Overall it is one of the most thorough trajectory analyses to date which leads to the Lévy walk model. Probably because ten other models were shown to fail to reproduce the experimental data, it effectively exhausted the arsenal of arguments from the opponents of the Lévy walk foraging hypothesis [as a counterexample, see a trail of publications on the Lévy walk of mussels (de Jager *et al.*, 2011)].

It is instructive to look at the scales involved in this study. A typical duration of the recorded trajectories was $15 - 30$ min with average moving speeds of 3 to 6 μm/min, depending on the levels of the chemokine. With a size of the T-cell about 10 microns, similarly to the case of amoeba, cells travelled a couple of tens of their sizes. For bacteria that would correspond to a distance of a single run. However, for the case of T-cells that might
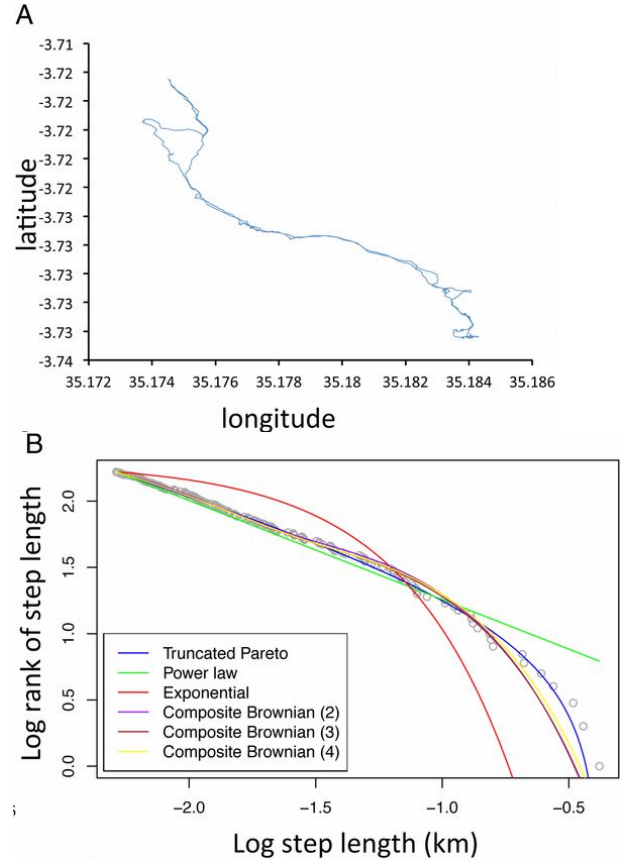

FIG. 32 (Color online) Lévy walks of Hadza hunter-gatherers. (a) A representative trajectory of a Hadza hunter-gatherer bout obtained by GPS tracking. (b) The PDF of displacements during outbound parts of bouts, showing Lévy statistics in about a half of all cases. Symbols represent the experimental data and lines correspond to different theoretical approximations to this distribution. Adapted from Raichlen *et al.* (2014).

be the relevant scale for finding the infected cells, and undoubtedly it is very intriguing that Lévy walks can be evoked in this context.

F. Humans

Humans are most sophisticated organisms whose motility is governed by complex environmental, sociological, technological, and urban factors. The field of human mobility is an active domain of research because of its evident connection to real-life applications. Development of transportation systems, design of mobile networks, prevention of contagious disease spreading, all these issues are linked to the human mobility. Starting from dollar bill tracking by Brockmann *et al.* (2006) and to mobile phone tracking by the group of Barabási (Gonzalez *et al.*, 2008), and to a recent study of influenza virus spreading by Brockmann and Helbing (2013), works on this topic gained a lot of attention, also in the public domain and
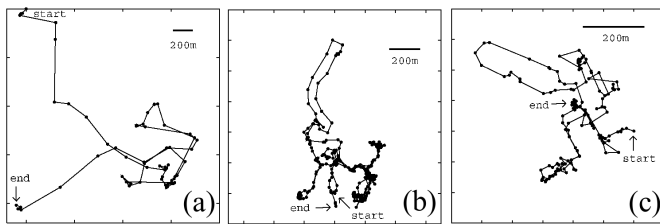
FIG. 33 (Color online) GPS data on human movements during their daily activities in three different locations: (a) a University campus, (b) Disney World theme park, and (c) a state fair. Adapted from Rhee *et al.* (2011).

media. Here we will review three empirical studies with very different settings, in which the Lévy walk patterns were found.

An interesting experiment is described by Méndez *et al.* (2014) on the page 275 of their book. Nineteen blindfolded volunteers were ordered to search for targets randomly distributed over a soccer field. Each searcher was followed by a person who was recording the moving times of the searcher between the reorientation events. As an observed process it is a good example of the standard random walk with constant velocity. Searchers were not priorly informed of the purpose of the study, and about what was going to be measured. Each searcher was given ten minutes of time, and a prize was awarded to a person finding most of the targets. After a certain target was found on the field, it was returned to the field but displaced by a 1.5 m distance in a random direction. In total there were 200 targets with a characteristic size of 1 meter, distributed on a filed of the size 100×50 meters. Interestingly, after the data was analyzed and pooled according to the number of collected targets, $(0-1, 2-4, 5-8)$, and the distribution of run times was plotted, it appeared that the first two groups had an exponentially distributed run times, whereas the third group had a distribution reminiscent of the power law with an exponent of the tail $\mu = 2.3$ [that corresponds to $\gamma = 1.3$ in our notations for the flight time distribution, Eq. (8)]. Certainly, the span of run times was only about one order of magnitude (there could be no runs longer than ~ 2 min because of the size of the field) and statistical tests could not give a clear preference to the power-law fit. Nevertheless, it is still very remarkable how the deviation from the exponential distribution arose and how this deviations correlated with the number of targets found.

While the previous example might look like a fun experiment, some people rely on search for their survival. In another recent study by Raichlen *et al.* (2014), human hunters-gatherers Hadza in northern Tanzania were shown to use Lévy walks in about a half of their foraging bouts, see Fig. 32. The Hadza hunter-gatherers have no modern tools or developed agriculture, they hunt with bow and arrow, and collect wild plant food. 44 subjects were monitored with the help of GPS devices during their foraging bouts for several days and at different seasons. The authors analyzed the step length distribution for outbound bouts (defined as travel between the camp and the furtherest away from the starting point). The steps were defined either by pauses or by turning angles, which in turn were analyzed with different threshold values from $0°$ to $180°$ with a step of $10°$. The obtained data were tested against Lévy walks, Brownian motion, or composite Brownian motion combining up to 4 exponential distributions. In around 50% of all bouts the distribution of step lengths was best described either by a power-law or a truncated power-law with tail exponents 1.9 and 1.5, respectively. The Lévy walk behavior appeared in both male and female subgroups despite the fact that they often had different goals of their bouts: hunting and searching for wild honey, or collecting berries and plant foods. The MSD of the corresponding tracks also showed an anomalous superdiffusive behavior. Inclusion of round bounds did not change the results significantly. The authors argued that the human foragers, despite their higher cognitive complexity, still follow the same search pattern as used by other animals. Furthermore, the similar motion pattern of humans arises in much more complex urban environments, as we discuss next.

In a comprehensive study of (Rhee *et al.*, 2011), 226 daily GPS traces were collected from 101 volunteers in five different outdoor sites: two university campuses, state fair, theme park Disney World, and New York metropolitan area (see sample tracks in Fig. 33).

They acquired data with high space resolution of 3 meters and time step of 10 seconds, one of the most precise tracking to date. The following quantities were extracted from the traces: flight length, pause time, direction, and velocity. The authors used three different methods to define the flights on the smoothed data: rectangular (when a piece of trajectory between the two end points does not leave the boundary of a certain width from the line connecting those two points), based on the turning angle, and marked by pausing events. For all locations it was found that (truncated) power-law distribution fitted the data better than other model distributions. In comparison to previously discussed examples here the span of flight lengths covers four orders of magnitude. The tail exponents of those distributions were found to be in the range 1.2-1.9 based on pausing definitions of flights, see Fig. 34.

Only in the case of the state fair, the exponential distribution was not so different from the power-law. Authors explain this by the truncation of the step length, as the state fair was indeed the smallest location of all five. The pausing events were also power-law distributed with a heavy tail exponents in the range $2.3 - 3.5$. The velocity of displacements was close to constant for short displacements, but increased steeply for larger travels. The reason behind this was that longer excursions could be made by using ground transportation, which was faster than walking. In terms of developing the appropriate Lévy walk type model that would require to introduce an addi-
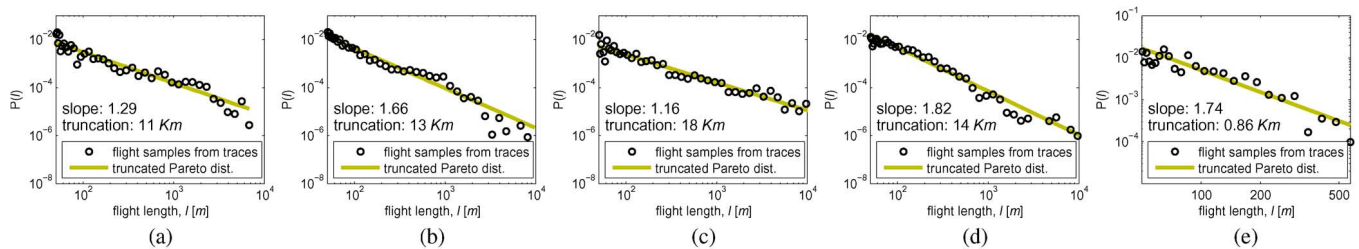
FIG. 34 (Color online) Distribution of human displacements. Step length distribution fitted with truncated Pareto distributions using the pause-based model to define the step lengths. (a) Campus I. (b) Campus II. (c) New York City. (d) Disney World. (e) State Fair. Reproduced from Rhee *et al.* (2011).

tional coupling between the distance and velocity, which can be read out from the experimental data. The MSD for all five locations always had two regimes: superdiffusive at short times, less than 30 min to 1 hour, and subdiffusive afterwards. The superdiffusion is explained by long excursions, whereas the subdiffusive scaling was caused by the bounded travel domain and also due to the fact that humans do not do a completely random walk, but rather travel to certain destinations and often return to the same points, like home, office, or class. Because of similar factors, mobility of humans is certainly more complex than just a Lévy walk, but still this model appears to be one of the bests to describe human relocations as if they were a truly random process.

To finalize this subsection we return to one of the first and influential studies of human travel data approximated by the dispersal of dollar banknotes. Some fraction of dollar bills in the US carry a stamp encouraging a person who gets a hold of it to visit a dedicated webpage, enter the bill number, current date, and location, and see its past trace. Brockmann *et al.* (2006) used the databank of banknote traces and proposed a Lévy flight model combined with anomalously long traps, leading to a fractional diffusion equation, Eq. (21). Although one could argue that instantaneous jumps might be not the most adequate representation of human travel, which on the vast scales of North America could happen by car, bus, train or air fair, each having its typical speed, for the data acquired it was practically impossible to take into account the finite velocity of travelers. Therefore, formally this study is outside our focus, but certainly deserves mentioning as one of the first works in this field. As the techniques of following individuals continue to progress, it is to be expected that in the near future we will learn more about the human mobility.

G. Bumblebees, seabirds, monkeys, and others

As we mentioned in the beginning of this section, the amount of data on animal motions was constantly growing during the last decade. Not every new paper reports a Lévy walk motion pattern as a result, but at least tries to relate the observed motion patterns to the Lévy walk

model. Current research trends in ecology were greatly influenced by the idea that under some circumstances a superdiffusive Lévy walk can be an advantageous search strategy when compared to classical Brownian-like diffusion pattern. We will review the search problem in the next section, and here we briefly list very diverse and interesting examples of data on animal tracking.

Insects. Insects can be traced by using different methods, such as traps, video cameras, entomological radars, or scanning harmonic radars combined with miniature transponders attached to individual insects. To the date, there is an impressive list of insects which were studied with respect to their motility patterns: ants (Schultheiss and Cheng, 2013), bumblebees (Lenz *et al.*, 2013), honeybees (Reynolds *et al.*, 2007), moth (Cardé *et al.*, 2012), beetles (Reynolds *et al.*, 2013), stoneflies (Knighton *et al.*, 2014), and fruit flies (Cole, 1995; Reynolds and Frye, 2007).

Sea animals. Underwater creatures are much more difficult to follow and in general are traced by small, pressure-sensitive data-logging tags giving the depth information, or by high-frequency acoustic transmitter in combination with a directional hydrophone, or with satellite relayed data loggers. The list of tracked species is also quite long: various sharks, penguins, tuna (Sims *et al.*, 2008), turtles (Dodge *et al.*, 2014; Hays *et al.*, 2006), dolphins (Bailey and Thompson, 2006), mussels (de Jager *et al.*, 2011), cuttlefish, octopus, various rays, sole and anglerfish (Wearmouth *et al.*, 2014), jelly fish (Hays *et al.*, 2012), grey seals (Austin *et al.*, 2004), and, finally, fishermen (Bertrand *et al.*, 2007).

Birds. Birds are usually tracked with the help of small GPS loggers attached to their bodies. One of the first studies in the field was done on wandering and black-browed albatrosses (Edwards *et al.*, 2007; Humphries *et al.*, 2012; Viswanathan *et al.*, 1996) with several more to follow on pelagic seabird Corys shearwaters (Focardi and Cecere, 2014), frigatebirds (De Monte *et al.*, 2012), and Egyptian vultures (López-López *et al.*, 2013).

Mammals. Most of observations of mammals foraging on terrain is done via visual contact and approximate GPS location determined by an observer using range finders. Several kinds of animals were tracked by this method: baboons (Schreier and Grove, 2014), spider

monkeys (Ramos-Fernández *et al.*, 2004), fallow deer (Focardi *et al.*, 2009), jackals (Atkinson *et al.*, 2002), reindeer (Marell *et al.*, 2002), langurs (Vandercone *et al.*, 2013), and bearded sakis (Shaffer, 2014).

VII. LÉVY WALKS AND SEARCH STRATEGIES

Searching and foraging is enormously important in the ecological context and it is not surprising that more and more physicists and mathematicians contribute to this field. A growing database allows to propose and test various models with increasing level of detail and complexity. The first mentioning of Lévy walks being advantageous in search as compared to classical random walks belongs to Shlesinger and Klafter (Shlesinger *et al.*, 1986). Further on, Lévy-walk hunting strategy in the context of feeding behavior in grazing microzooplankton was discussed by Levandowsky *et al.* (1988). It is widely recognized now that two papers by the group of Stanley, first on the Lévy flights of albatrosses (Viswanathan *et al.*, 1996), and three years latter on optimality of the Lévy search (Viswanathan *et al.*, 1999), lead to the birth of the new interdisciplinary field dealing with quantitative analysis of animal motility patterns and optimality of search. The maturity of the field is marked by several comprehensive monographs on the topic (Bénichou *et al.*, 2011; Méndez *et al.*, 2014; Viswanathan *et al.*, 2011), and the field itself spreads beyond animals and humans to robotics, see Section VII.C.

The problem of animal search is complex, as well characterized by Shlesinger (2009): "*Actual search patterns of animals will depend on many factors: amount of energy expended in different modes of travel; the probability of finding food during various locomotions (flying, running, walking, hopping, etc); whether a single animal or a group is executing the search; day or night conditions; topography; weather; fixed food sources (water and vegetation) or moving targets (prey); homogeneous or scarce food sources; whether the animal randomly searches for food or has knowledge of food locations.*" As an idealization of these features, when there is no prior information about the location of targets and complex interactions of a searcher with the environment and its prey, a so-called random search approach is used, which assumes that the searcher adopts a certain random motion pattern. The superdiffusive Lévy walk was proposed as an optimal search strategy (Viswanathan *et al.*, 1999) in case of sparse non-destructive targets, see below. However, validity and the straightforward use of the Lévy walk concept for the analysis of animal search patterns was questioned both experimentally and theoretically (Benhamou, 2007; Bénichou *et al.*, 2006, 2007; Edwards *et al.*, 2007; Jansen *et al.*, 2012; Plank and Codling, 2009; Reynolds *et al.*, 2014). For an opinion on "Should foraging animals really adopt Lévy strategies?", see a recent review in Bénichou *et al.* (2011). The resolution of this issue is out of our scope. Yet we do be-

lieve that there is a balanced middle point between the two extremes, "Lévy" and "no Lévy", which follows from the universal principle: mathematics and physics can not take place of Nature but they certainly can help to understand the former. Indeed, wandering albatrosses "do not care about math" (Travis, 2007) and it is naive to think that a bird utilizes a Lévy walk when preying, by independently drawing a length of the next flight from a PDF with power law tails. Lévy walk-like motion patterns are not necessarily produced by a Lévy walk process[8]. Moreover, patterns themselves – even when they look very similar to those obtained in theory – could not identify complex mechanisms of animal locomotion that produced them. This does not contradict the fact that the Lévy walk concept represents a powerful tool for *quantification* and *analysis* of statistical data and provides with more insights into animal foraging strategies than the conventional Brownian-based approach (Buchanan, 2008).

In the next three subsections we overview the current state of the field. A special emphasis is put on the original paper by Viswanathan *et al.* (1999) which greatly promoted the Lévy walk model as an advantageous search strategy.

A. Lévy walk as an optimal search strategy

Viswanathan *et al.* (1999) considered a walker which performed a Lévy walk in two dimensions and searched for targets, randomly distributed in space with a density ρ. The searcher can detect targets at the sight radius r. If a walker sees a target it proceeds straight to it. If there is no target in sight it chooses a random direction and moves for a random time with a fixed speed. If no target is found during a flight a new flight starts in an another random direction. The distribution of flight distances is chosen in the power-law form $g(l) \propto l^{-\mu}$. Due to a simple coupling $l = v\tau$ we can identify

$$\mu = \gamma + 1, \qquad (97)$$

where γ denotes the tail exponent of the flight time distribution, Eq. (8). As we discussed in the first section, $\mu > 3$ will result in the finite mean squared length of the jump and normal diffusive dispersal. A regime of $1 < \mu < 3$ corresponds to the superdiffusive Lévy walks. In this model, it is important that the searcher keeps looking for a target while moving and that the current flight is terminated if the target is found. One of the ways to define the efficiency of the search is by the ratio of the number of targets found to the time spent in search or,

---

[8] In a recent study of trace fossils, Sims *et al.* (2014) shown that the artificial trails produced by following three simple rules, (i) "do not cross your trail", (ii) "stay close to it", and (iii) "make *U*-turns", appeared to be Lévy walk patterns when analyzed with the conventional methods used in the field.

in case of constant speed, to the total distance traveled:

$$\eta = \frac{1}{\langle l \rangle N}, \qquad (98)$$

where $\langle l \rangle$ is the mean flight distance and N is the average number of flights between the two successive targets. The only characteristic scale of the problem is given by an average distance between two detected targets, $\lambda = (2r\rho)^{-1}$. With its help, the mean flight distance can be approximated as:

$$\langle l \rangle = \frac{\int_r^\lambda l \cdot l^{-\mu} dl + \lambda \int_\lambda^\infty l^{-\mu} dl}{\int_r^\infty l^{-\mu} dl} \qquad (99)$$

The first term in the nominator arises from the usual definition of the average flight length, but it has an upper bound of the typical distance between the two found targets. These flights do not terminate at the target. The second term counts the flights which were chosen to be longer than λ but do terminate after the target encounter. The denominator is a normalizing factor. Next, the mean number of steps between the two successive targets needs to be found. At this point it is important to distinguish between two possible scenarios: targets can be either destroyed after being found (destructive case), or they become temporally depleted but can be revisited at later times (non-destructive). In these two cases, the average number of steps between two successive destructive and non-destructive targets can be estimated as [for detailed explanation see original paper by Viswanathan *et al.* (1999)]:

$$N_{\mathrm{d}} \simeq (\lambda/r)^{\mu-1}; \quad N_{\mathrm{n}} \simeq (\lambda/r)^{(\mu-1)/2}. \qquad (100)$$

Now the question of optimality may be asked: Is there an optimal value of μ which leads to maximal number of found targets, but keeps the length of excursions sufficiently short? If targets are plentiful, $\lambda \lesssim r$, then $N_{\mathrm{d}} \approx N_{\mathrm{n}} \approx 1$ and $\langle l \rangle \approx \lambda$. In that case the search efficiency does not depend on μ at all. In the case of sparse resources, $\lambda \gg r$, situation is different. For destructive foraging the efficiency is maximal for smallest μ meaning that moving along one straight line is the best strategy in that case. However, situation is more interesting in case of non-destructive search. By substituting the expressions for $\langle l \rangle$, Eq.(99), and for the number of steps N_{n}, Eq. (100), into equation (98), and equating its derivative with respect to μ to zero, we obtain the optimal value of the power-law exponent:

$$\mu_{\mathrm{opt}} = 2 - 1/[\ln(\lambda/r)]^2. \qquad (101)$$

The second term is a small correction in case of sparse targets, so roughly the exponent of $\mu \approx 2$ ($\gamma \approx 1$) arises as a solution. This value of power-law tail of the traveled distances corresponds to the border regime between superdiffusive and ballistic Lévy walks. Qualitatively the advantage of Lévy walks with $\mu \approx 2$ is explained by a compromise between diffusive trajectories returning to the same target zone ($\mu > 3$) and ballistic motion ($\mu \sim 1$) which is the best strategy to explore space. This result greatly promoted the notion of Lévy walks as an optimal search strategy in the case of randomly distributed, non-destructive, sparse targets.

One could question whether the assumptions made when formulating the above search model are realistic. An animal, even a protozoan, is a much more intellectual being than a point-like particle driven by a finite-length algorithm. After all, why should a donkey leave a water pond in the oasis (a non-destructive target following the nomenclature) he has once found in a desert? Well, another could answer, the donkey has other needs also and he will turn to satisfy them once he has quenched his thirst and appeased his hunger; for example, he might like to find a mating partner. It is a perfectly correct argument but it goes far beyond the premises of the model. Animal search is a multi-layered activity determined by a vast number of external and internal (instincts, etc.) factors and it is impossible to catch even most essential of them with a simple stochastic model. The good point is that the model introduced by Viswanathan *et al.* (1999) allows for a gradual complexification and can absorb new assumptions and conditions. Since the paper was published, many modifications were proposed, which include, for example, moving or/and regenerating, patchy targets (Bénichou *et al.*, 2011; Palyulin *et al.*, 2014). It was also found that, in some situations like searching for a single target in confinement (Tejedor *et al.*, 2012), or under the presence of a bias (Palyulin *et al.*, 2014), persistent random walks or Brownian strategies perform better than Lévy walks.

B. Intermittent search strategies

A simple assumption that animals or humans have lower search capabilities when they are moving fast lead to the idea of the so-called *intermittent search*, when periods of localized diffusive-like search activity are altered with ballistic relocation to a new spot (searching for a lost key in an apartment is a good example). The intermittence has been detected in motion patterns of biological species ranging from protists to primates (Bartumeus, 2007; Bénichou *et al.*, 2011). Different research fields contributed with different theories, as, for example, ecologists discussed phases of "tactical habitat utilization" (local search events) and "strategic displacements" (ballistic relocations) (Gautestad and Mysterud, 2006), while experts on random walks served a spectrum of phenomenological models (Bénichou *et al.*, 2011). For us, further extensions of the standard Lévy walk model which are motivated by these studies are of interest.

Lomholt *et al.* (2008) suggested that an intermittent search in which the relocation happens according to the Lévy walk could lead to a more efficient search than, for example, exponentially distributed displacements be-

tween the diffusive search phases. From the point of view of modeling, such process might be called a composite process. The Lévy walk is not simply diluted with resting events, when a walker is immobile, like the process shown on Fig. 1(c), but it is alternated with periods of different activity, for example, diffusion. Such processes are not new in the field of random walks but they experienced a revival of interest because of the new context. Bartumeus *et al.* (2003) claimed that precisely this type of search strategy is realized by *Oxyrrhis marina*, a dinoflagellate living in the sea depth, when it preys on a microzooplankton. Namely, when the prey decreases in abundance, a predator switches from a slow-rate Brownian motion, characterized by an exponential PDF of flight time, to a helical Lévy motion, characterized by an inverse square power-law PDF.

In addition to the analysis of search patterns of biological species, the formalism of composite random walks allows to find analytic solutions for the density of particles and calculate the scaling of the corresponding MSD. In a recent paper by Thiel *et al.* (2012), a composite random walk was used to describe the run-and-tumble dynamics where the durations of the tumbles were explicitly taken into account and the runs were assumed to have a heavy tailed flight-time PDF. It was also assumed that during tumbling events particles perform normal diffusion. Depending on the interplay between the tail of the flight times and durations of the tumbling phases (which also could, in principle, be characterized by a tunable power-law distribution) the MSD was shown to span the regimes from the normal diffusion to ballistic superdiffusion.

C. Lévy walks for intelligent robotics: following suit

Biological systems are a constant source of inspiration for the robot designers. It is not a surprise then that the wave of studies on Lévy-walk foraging and animal search strategies has attracted attention of the researchers working in the field of robotics. The current aim of the *Lévy robotics* is twofold. First, it is a development of new nature-inspired search algorithms for autonomous mobile robots (Fujisawa and Dobata, 2013; Keeter *et al.*, 2012; Lenagh and Dasgupta, 2010; Nurzaman *et al.*, 2009; Pasternak *et al.*, 2009; Sutantyo *et al.*, 2010, 2013). A complementary research line aims at the understanding of how Lévy-walk motion patterns emerge from combinations of different external factors and theoretical assumptions on animal strategies and behavior (Fricke *et al.*, 2013).

An idea to combine Lévy walks with chemotaxis in order to produce "Lévy-taxis", a search algorithm for an autonomous agent to find a source of chemical contamination in a turbulent aquatic environment, was proposed by Pasternak *et al.* (2009). It is not a typical search task because the searcher should scan a constantly changing chemical field and follow plumes in order to find their origin. In the computational studies, a virtual AUV
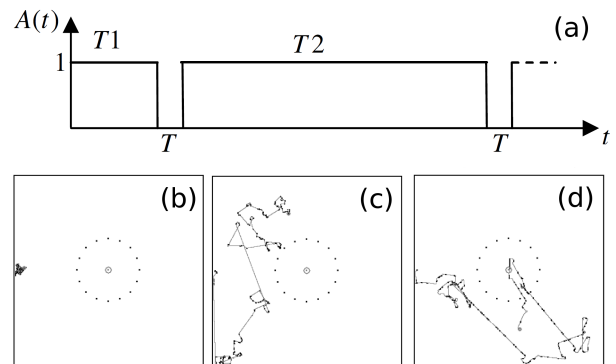

FIG. 35 Performance of a sonotactic robot. (a) Activity of the robot: Durations $T1, T2, ...$ follow a power-law tail distribution while the duration of re-orientation events T is constant; (b-d) Trajectories of the robot using the sonotaxis strategy (b), the Lévy walk (c) and the combination of the two (d). Speaker (small solid circle) is located at the center of the squared test area (box) and dashed line encircles the area with sound gradient above a threshold. The starting point is located at the middle of the left box border. Adapted from Nurzaman *et al.* (2009).

(Autonomous Underwater Vehicle), floating in a virtual two-dimensional river-like turbulent flow, contaminated from a point-like source, was used. Events of unidirectional motion, characterized by a power-law distribution of their lengths and a wrapped Cauchy distribution of their direction angles, were intermingled with short re-orientation events. During the latter the vehicle was randomly choosing a new movement direction along the local concentration upstream flow. This strategy somehow corresponds to a Lévy walk in a flow-oriented reference frame. When compared to other strategies, based on Brownian walk, simple Lévy walk, correlated Brownian walk and a brute-force zig-zag scanning, Lévy-taxis outperformed all of them, both in terms of detection success rate and detection speed.

Another searching strategy for a mobile robot, a sequence of Lévy walks alternated with taxis events, was proposed by Nurzaman *et al.* (2009). In computer simulations, the robot task was to locate a loudspeaker by using the information on the local sound intensity obtained from a robot-mounted microphone. The loudspeaker was stationary and the robot's speed v was constant. The robot orientation was defined by the angle θ. The robot dynamics was governed by three stochastic equations,

$$\begin{bmatrix} \dot{x}(t) \\ \dot{y}(t) \\ \dot{\theta}(t) \end{bmatrix} = A(t) \begin{bmatrix} v\cos\theta(t) \\ v\sin\theta(t) \\ 0 \end{bmatrix} + [1 - A(t)] \begin{bmatrix} 0 \\ 0 \\ \varepsilon_\theta(t) \end{bmatrix} \quad (102)$$

where the Cartesian coordinates $x(t)$ and $y(t)$ specify the position of the robot at time t. Activity $A(t)$ is a dichotomous function switching between 1 and 0 so that the robot is either moving forward with velocity v (activity is "1") or is choosing randomly a new direction of motion (activity is "0"). When the duration of a sin-
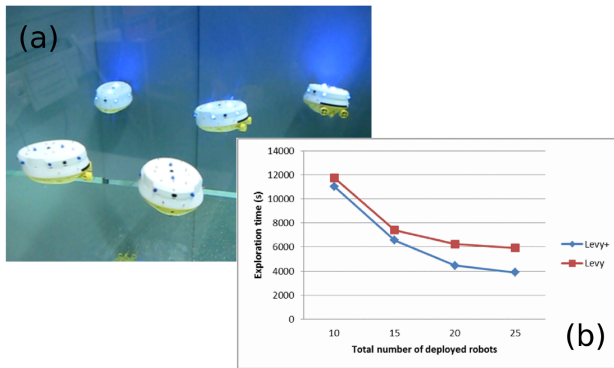
FIG. 36 Collective multi-robot exploration. (a) Autonomous underwater vehicles used in the experiments; (b) Targets searching experimental results: Exploration time vs number of robots for two strategies, with independent Lévy searchers (red line) and and interacting Lévy searchers (blue line). Adapted from Sutantyo *et al.* (2013).

gle 1-event is distributed according to a power-law, see Fig. 35(a), the robot performs a two-dimensional version of the Lévy walk with rests shown on Fig. 1(c). Alternatively, a stochastic sonotaxis strategy by using which the robot tried to locate and move towards the loudspeaker was probed. However, neither of the two strategies was able to accomplish the task when used alone. The sonotaxis turned out to be effective in a close vicinity of the speaker only, and did not work when the sound gradient was small, see Fig. 35(a). The Lévy walk did not care about the sound intensity by default and produced unbiased wandering only, Fig. 35(b). The combination of the two solved the problem: the Lévy walk first brought the robot to the area where the sound-intensity gradient was high enough and from there the sonotaxis strategy was able to lead the robot to the loudspeaker, Fig. 35(c). A *Lévy looped search* algorithm to locate *mobile* targets with a swarm of non-interacting robots was proposed by Lenagh and Dasgupta (2010). The idea was to replace straight ballistic segments with loops so that each searcher returns to its initial position. The length of each loop was sampled from a power-law distribution, whereas the starting angle was sampled from the uniform distribution in the interval $[0, 2\pi]$. The reported results showed that the looped search outperformed the standard Lévy search in tracking mobile targets.

The idea that a search efficiency can be increased by using a number of autonomous agents is natural and relevant in many contexts. It is evident, for example, that the search time is inversely proportional to the number of independent searchers provided all other conditions remain the same. However, if an interaction or exchange of information between the searchers is allowed, the search time can be decreased even further. Swarm communication is widely used among animals and insects, and it is known among biologists and roboticists as "stigmergy"

(Beckers *et al.*, 1994). A multi-robot searching algorithm based on a combination of a Lévy walk and an artificial potential field inducing repulsion among robots, was proposed and tested by Sutantyo *et al.* (2010). The obtained results for up to twenty robots showed that the repulsion increases search efficiency in terms of the search time. It is noteworthy that the effect diminishes with increase of the robot number, because crowding robots start to change their directions earlier than expected from the governing power-law distribution. Experimental results obtained for two Lévy-swimming AUVs in a 3-d aquatic testbed (Keeter *et al.*, 2012) show that in this case the best performance corresponds to a simple divide-and-conquer strategy, when the tank is divided into two equal volumes and each submarine scouts its assigned region only. However this situation may change when the number of AUVs is larger than two so that communication between searchers could be beneficial. Group Lévy foraging with an artificial pheromone communication between robots was studied recently by Fujisawa and Dobata (2013). Each robot had a tank filled with a "pheromone" (alcohol) which was sprayed around by a micropump. Rovers also carried alcohol and touch sensors and their motion was controlled by a program which took into account the local pheromone concentration. The swarm foraging efficiency peaked when the robots were programmed beforehand to perform a Lévy walk in the absence of the communication. Multi-robot underwater exploration and target location were studied with a swarm of Lévy-swimming AUVs by Sutantyo *et al.* (2013), see Fig. 36(a). Interaction between the robots was introduced by using a modification of the Firefly Optimization, an algorithm popular in the field of particle swarm optimization (Kennedy and Eberhart, 2001). The "attractiveness" of each AUV was defined by the time since the robot last found a target; it increased every time a target was located and then slowly decayed. The task was for each searcher to find all the targets. The results of the experiments showed that the interaction decreases the averaged search time substantially, see Fig. 36(b).

Finally, an attempt to get insight into the machinery causing the emergence of Lévy walk-like patterns in the motion of different biological species was made recently by Fricke *et al.* (2013). Inspired by the results obtained for T-cells (Harris *et al.*, 2012), see Section VI.E, researchers from the University of New Mexico and Santa Fe Institute used six small rovers, equipped with ultrasound sensors, compasses, and cameras. This navigation set enabled each robot to find patches of resources distributed over 2-d area. Tunable adaptive algorithms based on five different search strategies were tested. It turned out that the algorithm using correlated random walks, in which correlations between consequent step angles of a rover depend on the target last observed by the rover, produces Lévy-like motion patterns.

Lévy robotics is only one example that illustrates the practical value of the LW-concept. We do believe that

there are more to come and discuss potential candidates in the final section of the review.

VIII. OUTLOOK

Lévy walk concept is almost in its thirties and now possibly at the beginning of the most interesting phase of its life. The gradually developing theoretical framework was there in time to support the burst of applications across different fields. As can be seen from the previous sections, most of the empirical data obtained with cold atoms, nanostructured media, quantum dots, and ecology emerged only recently. Lévy walks remain in a stage of active development, and we now see them being used in robotics and mobile communication technologies (Lee *et al.*, 2013). In this concluding section we would like to discuss some open problems in the field, and to sketch what we think are the next perspectives and challenges.

For the physicists, probably one of the central questions is to understand how the Lévy walk, which is a mathematical model, emerges in diverse physical phenomena. There is a certain progress in this respect in the fields of classical many-particle chaos (Mendl and Spohn, 2014) and cold atom dynamics (Barkai *et al.*, 2014). In the problem of light diffusion in hot atomic vapors, general principles of light emission/absorption were suggested to be relevant mechanisms (Baudouin *et al.*, 2014b). In experimental plasma physics, the anomalous nonlocal transport is regularly reported in various works, but its origin remains a subject of ongoing debates. This can be partially explained by the high complexity of modern plasma experiments which are often performed in nonequilibrium regimes, involve nonlinear interactions, formation of large coherent structures, etc. We can see that even simple approximations of plasma ion dynamics by using the Lévy walk immediately call for non-linear space-time couplings (Gustafson and Ricci, 2012; Zimbardo *et al.*, 2000).

Most of the analytical results presented in this review are restricted to one-dimension. This reflects the current situation on the theory front. Although the analysis can be formally generalized to higher dimensions by replacing the Fourier coordinate with a Fourier vector, $k \rightarrow \mathbf{k}$, this technical step will immediately pose a number of questions. For example, a two-dimensional Lévy walk can be defined in two different intuitive ways, namely, as a process when (i) the length of the upcoming flight and its random *orientation* are both chosen from continuous PDFs (like in the case of run and tumble of bacteria, Section VI.C) or, alternatively, (ii) a random displacement is chosen independently but always *along* one of the two basis vectors. How do the propagators of these processes look like? Evidently, because of the isotropy of the first process, the corresponding propagator will be circular symmetric, $P(\mathbf{r}, t) = P(r, t)$, $r = \sqrt{x^2 + y^2}$, see left panel of Fig. 37(a). It is tempting to say that in this case the problem can be reduced to the one-
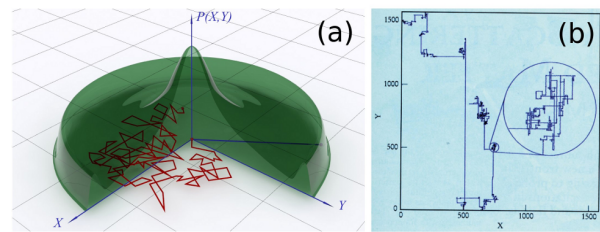

FIG. 37 (Color online) Two intuitive generalizations of the Lévy walk to two dimensions. Both models are characterized by power-law pdfs of the flight time, but in (a) an "isotropic" model the direction of a flight is given by a random angle uniformly distributed on the interval $[0, 2\pi]$, while in (b) a "lattice" model ballistic flights happen only along one of the two basis vectors of a square lattice. The latter process was observed when tracking trajectories of a Hamiltonian particle moving over an egg-grate potential (Klafter and Zumofen, 1994). Figure (b) is adapted from (Klafter *et al.*, 1996).

dimensional setup by simply taking $|x|$ with r in the propagator. However it has yet to be clarified which equation governs the evolution of $P(r, t)$. A LW process of the type (ii) has been observed in numerical studies of the superdiffusion in two-dimensional chaotic Hamiltonian systems by Klafter and Zumofen (1994), see right panel of Fig. 37(b). It was shown that at the asymptotic limit and far from the center $\mathbf{r} = 0$, the corresponding propagator factorizes, $P(\mathbf{r}, t) \simeq P(x, t/2)P(y, t/2)$, where $\mathbf{r} = x \cdot \mathbf{e}_x + y \cdot \mathbf{e}_y$ and $P(x, t)$, $P(y, t)$ are one-dimensional propagators. This type of two-dimensional Lévy walks with the exponent $\gamma = 2$ is relevant for the description of the diffusion in Sinai billiards with infinite horizon (Bouchaud and Georges, 1990), as it has been shown recently by Cristadoro *et al.* (2014).

As a next step one can consider Lévy walks on lattices of different geometries and try to elucidate the effects of the underlying geometry on the corresponding propagators. This question is particularly motivated by the experimental studies of light propagation in regular foams, where, due to the effect of total internal reflection, the light gets trapped in the liquid phase of the foam (Gittings *et al.*, 2004). Theoretically it was shown that, in the case of a honeycomb foam lattice, the light propagation can be superdiffusive (Schmiedeberg *et al.*, 2005; Schmiedeberg and Stark, 2006).

An issue of correlated Lévy walks not only constitutes a theoretical challenge but is of relevance in the context of several recent experiments. One example is the diffusion of light in Lévy glasses, Section V.C, where the quenched disorder of scatterers may induce correlations between the flights. Independently, this question was posed by theoreticians some time ago, see Barkai *et al.* (2000a); Kutner and Maass (1997, 1998); Levitz (1997), and still requires further analytical investigation. Correlated ballistic Lévy walk could also serve as an advanced model to account for the correlations in blinking times of quantum dots (Stefani *et al.*, 2009).

A fundamental characteristic of any random walk process is the so-called first passage time, which defines how soon a random walker would visit a point located at a certain distance from the origin, see book by Redner (2001). The first passage time problem for Lévy walks naturally occurs in the context of searching strategies, where it quantifies the time it takes to hit a target. Many of the results obtained for the first passage time and related problems for the standard random walks (Redner, 2001) were generalized to subdiffusion and Lévy flights. At the same time, the problem of the first passage time for Lévy walks remains largely unexplored (Korabel and Barkai, 2011).

As already mentioned, the origins of Lévy walks in biology and ecological context is an unsettled issue. Although some examples exist that show how the power-law distributed run times emerge from the underlying genetic circuits of bacteria (Matthäus *et al.*, 2011), it remains to be seen whether similar evidences can be found for more complex organisms that exhibit Lévy walk-like behavior. In meantime, Lévy walk strategies are implemented to construct robots that can assist humans in finding sources of contamination, and to develop efficient strategies to rescue people from disaster areas (Akpoyibo *et al.*, 2014). The concept of Lévy foraging has made its way into the field of criminology, potentially leading to implications in predictive policing. Johnson (2014) used criminal records of more than a thousand offenders who committed series of crimes and found that the distribution of distances between the consequent events was consistent with Lévy walk dynamics. There is also an interview with a burglar which corroborates the Lévy walk behavior as an optimal *evading* strategy and relates it to the perception of risk to be caught. In a very recent paper titled "Voles don't take taxis", Pease (2014) comments on the work of Johnson (2014) and puts it in the context of modern quantitative criminology research.

To conclude, we provide an overview of the theoretical aspects of a simple but remarkably flexible model of Lévy walks. We illustrated theoretical considerations with a variety of examples where the model and its offspring served to quantify the stochastic transport phenomena and help elucidate underlying mechanisms. We would like to think that this review will stimulate researchers from even more distant fields to use the model in their studies and thus will help to advance Lévy walks into new unexplored territories.

Acknowledgments

References

Aaronson, J., 1997, *An Introduction to Infinite Ergodic Theory* (American Mathematical Society, Providence).

Akimoto, T., 2012, Phys. Rev. Lett. **108**, 164101.

Akpoyibo, S. E., R. G. Lakshmi Narayanan, and O. C. Ibe, 2014, International Journal of Computer Networks & Communications **6**, 1.

Alivisatos, A. P., 1996, Science **271**, 933.

de Anna, P., T. Le Borgne, M. Dentz, A. M. Tartakovsky, D. Bolster, and P. Davy, 2013, Phys. Rev. Lett. **110**, 184502.

Aquino, G., M. Bologna, P. Grigolini, and B. J. West, 2004, Phys. Rev. E **70**, 036105.

Aref, H., *et al.*, 2014, arXiv:1403.2953.

Artuso, R., and G. Cristadoro, 2003, Phys. Rev. Lett. **90**, 244101.

Aspect, A., E. Arimondo, R. Kaiser, N. Vansteenkiste, and C. Cohen-Tannoudji, 1988, Phys. Rev. Lett. **61**, 826.

Atkinson, R. P. D., C. J. Rhodes, D. W. Macdonald, and R. M. Anderson, 2002, Oikos **98**, 134.

Austin, D., W. D. Bowen, and J. I. McMillan, 2004, Oikos **105**, 15.

Bachelier, L., 1900, Annales Scientifiques de l'École Normale Supérieur **III**, 21.

Bailey, H., and P. Thompson, 2006, J. Anim. Ecol. **75**, 456.

Bakunin, O. G., 2003, Physics-Uspekhi **46**, 309.

Balescu, R., 2005, *Aspects of Anomalous Transport in Plasmas* (Taylor & Francis, London).

Bardou, F., J.-P. Bouchaud, A. Aspect, and C. Cohen-Tannoudji, 2001, *Lévy Statistics and Laser Cooling* (Cambridge University Press, Cambridge, UK).

Bardou, F., J. P. Bouchaud, O. Emile, A. Aspect, and C. Cohen-Tannoudji, 1994, Phys. Rev. Lett. **72**, 203.

Barkai, E., 2001, Phys. Rev. E **63**, 046118.

Barkai, E., 2002, Chem. Phys. **284**, 13.

Barkai, E., 2003, Phys. Rev. Lett. **90**, 104101.

Barkai, E., 2008, in *Anomalous Transport: Foundations and Applications*, edited by R. Klages, G. Raddons, and I.M. Sokolov (Wiley-VCH, Weinheim), p. 213–240.

Barkai, E., E. Aghion, and D. Kessler, 2014, Phys. Rev. X **4**, 021036.

Barkai, E., and Y.-C. Cheng, 2003, J. Chem. Phys. **118**, 6167.

Barkai, E., V. Fleurov, and J. Klafter, 2000a, Phys. Rev. E **61**, 1164.

Barkai, E., and J. Klafter, 1998, in *Chaos, Kinetics and Nonlinear Dynamics in Fluids and Plasmas*, edited by S. Benkadda and G.M. Zaslavsky (Springer, Berlin/Heidelberg), pp. 373–393.

Barkai, E., R. Metzler, and J. Klafter, 2000b, Phys. Rev. E **61**, 132.

Barkai, E., A. V. Naumov, Y. G. Vainer, M. Bauer, and L. Kador, 2003, Phys. Rev. Lett. **91**, 075502.

Barkai, E., and R. Silbey, 2000, J. Phys. Chem. B **104**, 3866.

Barkai, E., and I. M. Sokolov, 2007, J. Stat. Mech-Theory E **2007**, P08001.

Baron, S., 2014, Synthese **191**, 459.

Barthelemy, P., J. Bertolotti, K. Vynck, S. Lepri, and D. S. Wiersma, 2010, Phys. Rev. E **82**, 011101.

Barthelemy, P., J. Bertolotti, and D. S. Wiersma, 2008, Nature (London) **453**, 495.

Bartumeus, F., 2007, Fractals **15**, 151.

Bartumeus, F., F. Peters, S. Pueyo, C. Marrasé, and J. Catalan, 2003, Proc. Nat. Acad. Sci. USA **100**, 12771.

Baudouin, Q., W. Guerin, and R. Kaiser, 2014a, in *Annual Review of Cold Atoms and Molecules*, edited by K. Madison, K. Bongs, L. D. Carr, A. M. Rey, and H. Zhai (World Scientific, Singapore), pp. 251–313.

Baudouin, Q., R. Pierrat, A. Eloy, E. J. Nunes-Pereira, P.-A. Cuniasse, N. Mercadier, and R. Kaiser, 2014b, Phys. Rev. E **90**, 052114.

Baule, A., and R. Friedrich, 2007, Europhys. Lett. **77**, 10002.

Becker-Kern, P., M. M. Meerschaert, and H.-P. Scheffler, 2004, Ann. Probab. **32**, 730.

Beckers, R., O. E. Holland, and J. Deneubourg, 1994, Artif. Life **4**, 181.

Beenakker, C. W. J., C. W. Groth, and A. R. Akhmerov, 2009, Phys. Rev. B **79**, 024204.

van Beijeren, H., 2012, Phys. Rev. Lett. **108**, 180601.

Bel, G., and E. Barkai, 2005, Phys. Rev. Lett. **94**, 240602.

Ben-Naim, E., B. Machta, and J. Machta, 2005, Phys. Rev. E **72**, 021302.

Benhamou, S., 2007, Ecology **88**, 1962.

Bénichou, O., C. Loverdo, M. Moreau, and R. Voituriez, 2006, Phys. Rev. E **74**, 020102.

Bénichou, O., C. Loverdo, M. Moreau, and R. Voituriez, 2007, J. Phys. Condens. Matter **19**, 065141.

Bénichou, O., C. Loverdo, M. Moreau, and R. Voituriez, 2011, Rev. Mod. Phys. **83**, 81.

Berg, H., 1993, *Random Walks in Biology* (Princeton University Press, Princeton, NJ).

Berg, H., 2004, *E. coli in Motion* (Springer, New York).

Bernoulli, J., 1713, *Ars conjectandi, opus posthumum. Accedit Tractatus de seriebus infinitis, et epistola gallicé scripta de ludo pilae reticularis* (Thurneysen Brothers, Basel).

Bertolotti, J., K. Vynck, L. Pattelli, P. Barthelemy, S. Lepri, and D. S. Wiersma, 2010, Adv. Funct. Mater. **20**, 965.

Bertrand, S., A. Bertrand, R. Guevara-Carrasco, and F. Gerlotto, 2007, Ecol. Appl. **17**, 331.

Bouchaud, J., 1995, in *Lévy Flights and Related Topics in Physics*, edited by M. F. Shlesinger, G. M. Zaslavsky, and U. Frisch (Springer, Berlin/Heidelberg), pp. 237–250.

Bouchaud, J.-P., 1992, J. Phys. I **2**, 1705.

Bouchaud, J.-P., and A. Georges, 1990, Phys. Rep. **195**, 127.

Brockmann, D., and T. Geisel, 2003, Phys. Rev. Lett. **91**, 048303.

Brockmann, D., and D. Helbing, 2013, Science **342**, 1337.

Brockmann, D., L. Hufnagel, and T. Geisel, 2006, Nature (London) **439**, 462.

Brokmann, X., J.-P. Hermier, G. Messin, P. Desbiolles, J.-P. Bouchaud, and M. Dahan, 2003, Phys. Rev. Lett. **90**, 120601.

Brown, R., 1828, Phil. Mag. **4**, 161.

Buchanan, M., 2008, Nature **453**, 714.

Buldyrev, S. V., S. Havlin, A. Y. Kazakov, M. G. E. da Luz, E. P. Raposo, H. E. Stanley, and G. M. Viswanathan, 2001, Phys. Rev. E **64**, 041108.

Buonsante, P., R. Burioni, and A. Vezzani, 2011, Phys. Rev. E **84**, 021105.

Burioni, R., L. Caniparoli, and A. Vezzani, 2010, Phys. Rev. E **81**, 060101.

Burresi, M., R. Radhalakshmi, V.and Savo, J. Bertolotti, K. Vynck, and D. S. Wiersma, 2012, Phys. Rev. Lett. **108**, 110604.

Cahalan, R. F., W. Ridgway, W. J. Wiscombe, T. L. Bell, and J. B. Snider, 1994, J. Atmos. Sci. **51**, 2434.

Cardé, R. T., A. M. Cardé, and R. D. Girling, 2012, J. Anim. Ecol. **81**, 268.

Carmi, S., and E. Barkai, 2011, Phys. Rev. E **84**, 061104.

Casati, G., and J. Ford, 1976, J. Comput. Phys. **20**, 97–109.

Castiglione, P., A. Mazzino, P. Muratore-Ginanneschi, and A. Vulpiani, 1999, Physica D **134**, 75.

del Castillo Negrete, D., 1998, Phys. Fluid. **10**, 576.

Castin, Y., J. Dalibard, and C. Cohen-Tannoudji, 1991, in *Proceedings of the workshop "Light Induced Kinetic Effects on Atom, Ions and Molecules"*, Elba Island, Italy, edited by L. Moi, S. Gozzini, C. Gabbanini, E. Arimondo, and F. Strumia (ETS Editrice, Pisa), pp. 5–24.

Celani, A., and M. Vergassola, 2010, Proc. Nat. Acad. Sci. USA **107**, 1391.

Chechkin, A. V., J. Klafter, and I. M. Sokolov, 2003, Europhys. Lett. **63**, 326.

Chirikov, B. V., and D. L. Shepelyansky, 1999, Phys. Rev. Lett. **82**, 528.

Chukbar, K., 1995, J. Exp. Theor. Phys. **108**, 1025.

Chukbar, K., 1999, Plasma Phys. Rep. **25**, 77.

Cipriani, P., S. Denisov, and A. Politi, 2005, Phys. Rev. Lett. **94**, 244301.

Clauset, A., C. Shalizi, and M. Newman, 2009, SIAM Rev. **51**, 661.

Coffey, W. T., and Y. P. Kalmykov, 2012, *The Langevin Equation: With Applications to Stochastic Problems in Physics, Chemistry, and Electrical Engineering* (World Scientific, Singapore).

Cole, B. J., 1995, Anim. Behav. **50**, 1317.

Cristadoro, G., T. Gilbert, M. Lenci, and D. P. Sanders, 2014, Phys. Rev. E **90**, 050102(R).

Cristadoro, G., and R. Ketzmerick, 2008, Phys. Rev. Lett. **100**, 184101.

Dalibard, J., and C. Cohen-Tannoudji, 1989, J. Opt. Soc. Am. B **6**, 2023.

Das, S. G., A. Dhar, C. B. Saito, K.and Mendl, and H. Spohn, 2014, Phys. Rev. E **90**, 012124.

Davis, A., and A. Marshak, 1997, in *Fractal Frontiers*, edited by M. M. Novak and T. G. Dewey (World Scientific, Singapore), pp. 63–72.

Davydov, B. I., 1934, Dokl. Akad. Nauk SSSR **2**, 474.

De Monte, S., C. Cotté, F. d'Ovidio, M. Lévy, M. Le Corre, and H. Weimerskirch, 2012, J. R. Soc. Interface **9**, 3351.

Dechant, A., E. Lutz, D. A. Kessler, and E. Barkai, 2014, Phys. Rev. X **4**, 011022.

Denisov, S., and S. Flach, 2001, Phys. Rev. E **64**, 056236.

Denisov, S., S. Flach, O. Y. A. A. Ovchinnikov, and Y. Zolotaryuk, 2002a, Phys. Rev. E **66**, 041104.

Denisov, S., S. Flach, and P. Hänggi, 2014, Phys. Rep. **538**, 77.

Denisov, S., J. Klafter, and M. Urbakh, 2002b, Phys. Rev. E **66**, 046217.

Denisov, S., J. Klafter, and M. Urbakh, 2003, Phys. Rev. Lett. **91**, 194301.

Denisov, S., J. Klafter, and M. Urbakh, 2004, Physica D **187**,

89.

Denisov, S., J. Klafter, M. Urbakh, and S. Flach, 2001, Physica D **170**, 131.

Denisov, S., V. Zaburdaev, and P. Hänggi, 2012, Phys. Rev. E **85**, 031148.

Dhar, A., K. Saito, and B. Derrida, 2013, Phys. Rev. E **87**, 010103.

Dieterich, P., R. Klages, R. Preuss, and A. Schwab, 2008, Proc. Nat. Acad. Sci. USA **105**, 459.

Dodge, K. L., B. Galuardi, T. J. Miller, and M. E. Lutcavage, 2014, PLoS ONE **9**, e91726.

Douglas, P., S. Bergamini, and F. Renzoni, 2006, Phys. Rev. Lett. **96**, 110601.

Drysdale, P. M., and P. A. Robinson, 1998, Phys. Rev. E **58**, 5382.

Dunkel, J., and P. Hänggi, 2009, Phys. Rep. **471**, 1–73.

Dunkel, J., P. Hänggi, and S. Hilbert, 2009, Nat. Phys. **5**, 741–747.

Edwards, A. M., R. A. Phillips, N. W. Watkins, M. P. Freeman, E. J. Murphy, V. Afanasyev, S. Buldyrev, M. G. E. da Luz, E. P. Raposo, H. E. Stanley, and G. M. Viswanathan, 2007, Nature (London) **449**, 1044.

Einstein, A., 1905, Ann. Phys. **322**, 549.

Eisenbach, M., and J. Lengeler, 2004, *Chemotaxis* (Imperial College Press, London).

Eliazar, I. I., and M. F. Shlesinger, 2013, Phys. Rep. **527**, 101.

Erdélyi, A., 1954, *Tables of Integral Transforms*, Vol. 1 (McGraw-Hill, New York).

Eule, S., R. Friedrich, and F. Jenko, 2008, J. Chem. Phys. **129**, 174308.

Eule, S., R. Friedrich, F. Jenko, and D. Kleinhans, 2007, J. Phys. Chem. B **111**, 11474.

Eule, S., V. Zaburdaev, R. Friedrich, and T. Geisel, 2012, Phys. Rev. E **86**, 041134.

Fernandez, R., J. Fröhlich, and A. D. Sokal, 1992, *Random Walks, Critical Phenomena, and Triviality in Quantum Field Theory* (Springer, Berlin/Heidelberg).

Fischer, H., 2010, *A History of the Central Limit Theorem: From Classical to Modern Probability Theory* (Springer, New York).

Focardi, S., and J. G. Cecere, 2014, J. Anim. Ecol. **83**, 353.

Focardi, S., P. Montanaro, and E. Pecchioli, 2009, PLoS ONE **4**, e6587.

Fogedby, H. C., 1994, Phys. Rev. E **50**, 1657.

Fourier, J. B. J., 1822, *Théorie Analytique De La Chaleur* (F. Didot, Paris).

Fricke, G. M., F. Asperti-Boursin, J. Hecker, J. Cannon, and M. Moses, 2013, in *Advances in Artificial Life, ECAL 2013*, Taormina, Italy, edited by P. Liò, O. Miglino, G. Nicosia, S. Nolfi, and M. Pavone (MIT Press, Cambridge, MA), pp. 1009–1016.

Friedrich, R., F. Jenko, A. Baule, and S. Eule, 2006a, Phys. Rev. Lett. **96**, 230601.

Friedrich, R., F. Jenko, A. Baule, and S. Eule, 2006b, Phys. Rev. E **74**, 041103.

Froemberg, D., and E. Barkai, 2013a, Eur. Phys. J. B **86**, 1.

Froemberg, D., and E. Barkai, 2013b, Phys. Rev. E **87**, 030104.

Froemberg, D., M. Schmiedeberg, E. Barkai, and V. Zaburdaev, 2014, arXiv:1412.0984 .

Fujisawa, R., and S. Dobata, 2013, in *Proceedings of the 2013 IEEE/SICE International Symposium on System Integration*, Kobe, Japan, (IEEE), pp. 808–813.

Fürth, R., 1920, Z. Phys. **2**, 244.

Gal, N., and D. Weihs, 2010, Phys. Rev. E **81**, 020903.

Gautestad, A. O., and I. Mysterud, 2006, Ecol. Complex. **3**, 44.

Geisel, T., J. Nierwetberg, and A. Zacherl, 1985, Phys. Rev. Lett. **54**, 616.

Geisel, T., and S. Thomae, 1984, Phys. Rev. Lett. **52**, 1936.

Geisel, T., A. Zacherl, and G. Radons, 1987, Phys. Rev. Lett. **59**, 2503.

de Gennes, P.-G., 1979, *Scaling Concepts in Polymer Physics* (Cornell University Press, New York).

de Gennes, P.-G., 2004, Eur. Biophys. J. **33**, 691.

Giacomelli, G., R. Hegger, A. Politi, and M. Vassalli, 2000, Phys. Rev. Lett. **85**, 3616.

Gibiansky, M. L., J. C. Conrad, F. Jin, V. D. Gordon, D. A. Motto, M. A. Mathewson, W. Stopka, D. C. Zelasko, J. D. Shrout, and G. C. L. Wong, 2010, Science **330**, 197.

Gittings, A., R. Bandyopadhyay, and D. Durian, 2004, Europhys. Lett. **65**, 414.

Glück, M., A. R. Kolovsky, and H. J. Korsch, 1998, Physica D **116**, 283.

Gnedenko, B., and A. Kolmogorov, 1954, *Limit distributions for sums ofindependent random variables* (Addison-Wesley, Reading, MA).

Godec, A., and R. Metzler, 2013a, Phys. Rev. Lett. **110**, 020603.

Godec, A., and R. Metzler, 2013b, Phys. Rev. E **88**, 012116.

Godrèche, C., and J. Luck, 2001, J. Stat. Phys. **104**, 489.

Goldstein, S., 1951, Q. J. Mech. Appl. Math. **4**, 129.

Gonzalez, M. C., C. A. Hidalgo, and A.-L. Barabasi, 2008, Nature (London) **453**, 779.

Grinstead, C., and J. Snell, 1997, *Introduction to Probability* (American Mathematical Society, Providence, RI).

Gustafson, K., and P. Ricci, 2012, Phys. Plasmas **19**, 032304.

Hänggi, P., and H. Thomas, 1982, Phys. Rep. **88**, 207.

Hapca, S., J. Crawford, and I. Young, 2009, J. R. Soc. Interface **6**, 111.

Harris, T. H., E. J. Banigan, D. A. Christian, C. Konradt, E. D. Tait Wojno, K. Norose, E. H. Wilson, B. John, W. Weninger, A. D. Luster, A. J. Liu, and C. A. Hunter, 2012, Nature (London) **486**, 545.

Hasegawa, A., K. Mima, and M. Duong-van, 1985, Phys. Rev. Lett. **54**, 2608.

Haus, J., and K. Kehr, 1987, Phys. Rep. **150**, 263.

Havlin, S., and D. Ben-Avraham, 1987, Adv. Phys. **36**, 695.

Hays, G. C., T. Bastian, T. K. Doyle, S. Fossette, A. C. Gleiss, M. B. Gravenor, V. J. Hobson, N. E. Humphries, M. K. S. Lilley, N. Pade, and D. W. Sims, 2012, Proc. Biol. Sci. **279**, 465.

Hays, G. C., V. J. Hobson, J. Metcalfe, D. Righton, and D. W. Sims, 2006, Ecology **87**, 2647.

He, Y., S. Burov, R. Metzler, and E. Barkai, 2008, Phys. Rev. Lett. **101**, 058101.

Heinsalu, E., M. Patriarca, I. Goychuk, and P. Hänggi, 2007, Phys. Rev. Lett. **99**, 120602.

Helfand, E., 1960, Phys. Rev. **119**, 1.

Holstein, T., 1947, Phys. Rev. **72**, 1212.

Humphries, N. E., H. Weimerskirch, N. Queiroz, E. J. Southall, and D. W. Sims, 2012, Proc. Nat. Acad. Sci. USA **109**, 7169.

Humphries, N. E., H. Weimerskirch, and D. W. Sims, 2013, Methods in Ecology and Evolution **4**, 930.

Isichenko, M. B., 1992, Rev. Mod. Phys. **64**, 961.

de Jager, M., F. J. Weissing, P. M. J. Herman, B. A. Nolet,

and J. van de Koppel, 2011, Science **332**, 1551.

Jansen, V. A. A., A. Mashanova, and S. Petrovskii, 2012, Science **335**, 918.

Jeon, J.-H., V. Tejedor, S. Burov, E. Barkai, C. Selhuber-Unkel, K. Berg-Sørensen, L. Oddershede, and R. Metzler, 2011, Phys. Rev. Lett. **106**, 048103.

Jin, F., J. C. Conrad, M. Gibiansky, and G. C. L. Wong, 2011, Proc. Nat. Acad. Sci. USA **108**, 12617.

Johnson, S. D., 2014, Legal Criminol. Psych. **19**, 193.

Jurlewicz, A., P. Kern, M. Meerschaert, and H.-P. Scheffler, 2012, Computers & Mathematics with Applications **64**, 3021.

Kac, N., 1959, *Statistical Independence in Probability, Analysis, and Number Theory* (Wiley, New York).

Karatsas, I., and S. Shreve, 1997, *Brownian Motion and Stochastic Calculus*, 2nd ed., (Springer, New York).

Kardar, M., G. Parisi, and Y.-C. Zhang, 1986, Phys. Rev. Lett. **56**, 889.

Katori, H., S. Schlipf, and H. Walther, 1997, Phys. Rev. Lett. **79**, 2221.

Keeter, M., D. Moore, R. Muller, E. Nieters, J. Flenner, S. Martonosi, A. Bertozzi, A. Percus, and R. Levy, 2012, in *American Control Conference (ACC), 2012*, Montreal, QC (IEEE), pp. 3154–3160.

Kennedy, J., and R. Eberhart, 2001, *Swarm Intelligence* (Morgan Kaufmann, Burlington, MA).

Kerker, M., 1969, *The Scattering of Light and Other Electromagnetic Radiation* (Academic Press, New York).

Kessler, D. A., and E. Barkai, 2012, Phys. Rev. Lett. **108**, 230602.

Kilbas, A., H. M. Srivastava, and J. J. Trujillo, 2006, *Theory and Applications of Fractional Differential Equations* (Elsevier, Amsterdam).

Klafter, J., A. Blumen, and M. F. Shlesinger, 1987, Phys. Rev. A **35**, 3081.

Klafter, J., M. F. Shlesinger, and G. Zumofen, 1996, Phys. Today **49**, 33.

Klafter, J., and R. Silbey, 1980, Phys. Rev. Lett. **44**, 55.

Klafter, J., and I. Sokolov, 2011, *First Steps in Random Walks: From Tools to Applications* (Oxford University Press, Oxford).

Klafter, J., and G. Zumofen, 1993, Physica A **196**, 102.

Klafter, J., and G. Zumofen, 1994, Phys. Rev. E **49**, 4873.

Klauder, J. R., and P. W. Anderson, 1962, Phys. Rev. **125**, 912.

Knighton, J., T. Dapkey, and J. Cruz, 2014, Ecol. Inform. **19**, 1.

Korabel, N., and E. Barkai, 2011, J. Stat. Mech-Theory E. **2011**, P05022.

Korobkova, E., T. Emonet, J. M. G. Vilar, T. S. Shimizu, and P. Cluzel, 2004, Nature (London) **428**, 574.

Kotulski, M., 1995, J. Stat. Phys. **81**, 777.

Kozma, B., M. B. Hastings, and G. Korniss, 2005, Phys. Rev. Lett. **95**, 018701.

Kutner, R., and P. Maass, 1997, Phys. Rev. E **55**, 71.

Kutner, R., and P. Maass, 1998, J. Phys. A **31**, 2603.

Lamperti, J., 1958, Trans. Amer. Math. Soc. **88**, 380.

Lauga, E., and R. E. Goldstein, 2012, Phys. Today **65**, 30.

Lee, K., Y. Kim, S. Chong, I. Rhee, and Y. Yi, 2013, IEEE/ACM Transactions on Networking **21**, 1621.

Lemons, D. S., and A. Gythiel, 1997, Am. J. Phys. **65**, 1079.

Lenagh, W., and P. Dasgupta, 2010, in *Proceedings of 19th Conference on Behavior Representation in Modeling and Simulation*, Charleston, SC (Curran Associates, New York), pp. 103–109.

Lenz, F., A. V. Chechkin, and R. Klages, 2013, PLoS ONE **8**, e59036.

Lepri, S., R. Livi, and A. Politi, 2003, Phys. Rep. **377**, 1.

Lepri, S., R. Livi, and A. Politi, 2008, in *Anomalous Transport: Foundations and Applications*, edited by R. Klages, G. Raddons, and I.M. Sokolov (Wiley-VCH, Weinheim), chapter Anomalous Heat Conduction, pp. 293–321.

Lepri, S., and A. Politi, 2011, Phys. Rev. E **83**, 030107.

Levandowsky, M., J. Klafter, and B. S. White, 1988, J. Protozool. **35**, 65.

Levandowsky, M., B. White, and F. L. Schuster, 1997, Acta Protozool. **36**, 237.

Levitz, P., 1997, Europhys. Lett. **39**, 593.

Lévy, P., 1937, *Theorie De L'addition Des Variables Aleatoires* (Gauthier-Villars, Paris).

Li, L., S. F. Norrelykke, and E. C. Cox, 2008, PLoS ONE **3**, e2093.

Liu, S., P. Hänggi, N. Li, J. Ren, and B. Li, 2014, Phys. Rev. Lett. **112**, 040601.

Liu, S., X. Xu, R. Xie, G. Zhang, and B. Li, 2012, Eur. Phys. J. B **85**, 337.

Lomholt, M., K. Tal, R. Metzler, and J. Klafter, 2008, Proc. Nat. Acad. Sci. USA **105**, 11055.

López-López, P., J. Benavent-Corai, C. García-Ripollés, and V. Urios, 2013, PLoS ONE **8**, e54352.

Lovely, P. S., and F. Dahlquist, 1975, J. Theor. Biol. **50**, 477.

Lubashevsky, I., R. Friedrich, and A. Heuer, 2009a, Phys. Rev. E **80**, 031148.

Lubashevsky, I., R. Friedrich, and A. Heuer, 2009b, Phys. Rev. E **79**, 011110.

Lubelski, A., I. M. Sokolov, and J. Klafter, 2008, Phys. Rev. Lett. **100**, 250602.

Lutz, E., 2003, Phys. Rev. A **67**, 051402.

Lutz, E., and F. Renzoni, 2013, Nat. Phys. **9**, 615.

MacKay, R. S., J. D. Meiss, and I. C. Percival, 1984a, Phys. Rev. Lett. **52**, 697.

MacKay, R. S., J. D. Meiss, and I. C. Percival, 1984b, Physica D **13**, 55.

Magdziarz, M., W. Szczotka, and P. Żebrowski, 2012, J. Stat. Phys. **147**, 74.

Magdziarz, M., A. Weron, K. Burnecki, and J. Klafter, 2009, Phys. Rev. Lett. **103**, 180602.

Mandelbrot, B. B., 1982, *The Fractal Geometry of Nature* (W. H. Freeman and Company, New York).

Mandelbrot, B. B., and J. W. V. Ness, 1968, SIAM Rev. **10**, 422.

Mantegna, R. N., and H. E. Stanley, 1994, Phys. Rev. Lett. **73**, 2946.

Marathe, R., C. Meel, N. C. Schmidt, L. Dewenter, R. Kurre, L. Greune, S. A.M., M. Müller, R. Lipowsky, B. Maier, and S. Klumpp, 2014, Nat. Commun. **5**, 3759.

Marchioro, C., A. Pellegrinotti, M. Pulvirenti, and L. Triolo, 1978, J. Stat. Phys. **19**, 499.

Margolin, G, and E. Barkai, 2005, Phys. Rev. Lett. **94**, 080601.

Margolin, G., V. Protasenko, M. Kuno, and E. Barkai, 2005, in *Fractals, Diffusion, and Relaxation in Disordered Complex Systems: Advances in Chemical Physics*, edited by W. T. Coffey and Y. P. Kalmykov (John Wiley & Sons, New York), pp. 327–356.

Margolin, G., V. Protasenko, M. Kuno, and E. Barkai, 2006, J. Phys. Chem. B **110**, 19053.

Marksteiner, S., K. Ellinger, and P. Zoller, 1996, Phys. Rev.

A **53**, 3409.

Matthäus, F., M. Mommer, T. Curk, and J. Dobnikar, 2011, PLoS ONE **6**, e18623.

Meerschaert, M. M., and E. Scalas, 2006, Physica A **370**, 114.

Meiss, J. D., 1992, Rev. Mod. Phys **64**, 795.

Meiss, J. D., and E. Ott, 1986, Physica D **20**, 387.

Méndez, V., D. Campos, and F. Bartumeus, 2014, *Stochastic Foundations in Movement Ecology* (Springer, Berlin/Heidelberg).

Mendl, C. B., and H. Spohn, 2014, Phys. Rev. E **90**, 012147.

Meng, Z., R. M. Thorne, and D. Summers, 1992, J. Plasma Phys. **47**, 445.

Mercadier, N., W. Guerin, M. Chevrollier, and M. Kaiser, 2009, Nat. Phys. **5**, 602.

Meroz, Y., I. M. Sokolov, and J. Klafter, 2013, Phys. Rev. Lett. **110**, 090601.

Metzler, R., E. Barkai, and J. Klafter, 1999, Phys. Rev. Lett. **82**, 3563.

Metzler, R., J.-H. Jeon, A. G. Cherstvy, and E. Barkai, 2014, Phys. Chem. Chem. Phys. **16**, 24128.

Metzler, R., and J. Klafter, 2000, Phys. Rep. **339**, 1.

Metzler, R., and J. Klafter, 2004, J. Phys. A **37**, R161.

Metzler, R., and I. M. Sokolov, 2002, Europhys. Lett. **58**, 482.

Min, I. A., I. Mezić, and A. Leonard, 1996, Phys. Fluids **8**, 1169.

Marell, A., J. P. Ball, and A. Hofgaard, 2002, Can. J. Zool. **80**, 854.

Molisch, A. F., and B. P. Oehry, 1998, *Radiation Trapping in Atomic Vapours* (Oxford University Press, Oxford).

Monin, A., A. Yaglom, and J. Lumley, 2007, *Statistical Fluid Mechanics: Mechanics of Turbulence* (Dover, New York).

Montroll, E. W., and M. F. Shlesinger, 1984, in *Nonequilibrium Phenomena II: from Stochastics to Hydrodynamics*, edited by J. Leibowitz and E.W. Montroll (North-Holland, Amsterdam), pp. 1–121.

Montroll, E. W., and G. H. Weiss, 1965, J. Math. Phys. **6**, 167.

Mörters, P., and Y. Peres, 2010, *Brownian motion* (Cambridge University Press, New York).

Nachtergaele, B., H. Raz, B. Schlein, and R. Sims, 2009, Commun. Math. Phys. **286**, 1073–1098.

Nelson, E., 1967, *Dynamical Theories of Brownian motion* (Princeton University Press, Princeton, NJ).

Nirmal, M., B. O. Dabbousi, M. G. Bawendi, J. J. Macklin, J. K. Trautman, T. D. Harris, and L. E. Brus, 1996, Nature (London) **383**, 802.

Nurzaman, S. G., Y. Matsumoto, Y. Nakamura, S. Koizumi, and H. Ishiguro, 2009, in *Proceeding of the 2008 IEEE International Conference on Robotics and Biomimetics*, IEEE (IEEE), pp. 806–811.

Palyulin, V. V., A. V. Chechkin, and R. Metzler, 2014, Proc. Nat. Acad. Sci. USA **111**, 2931.

Pasternak, Z., F. Bartumeus, and F. W. Grasso, 2009, J. Phys. A **42**, 434010.

Pearson, K., 1905, Nature (London) **72**, 294.

Pease, K., 2014, Legal Criminol. Psych. **19**, 221.

Pereira, E., J. M. G. Martinho, and M. N. Berberan-Santos, 2004, Phys. Rev. Lett. **93**, 120201.

Petrovskii, S., A. Mashanova, and V. A. A. Jansen, 2011, Proc. Nat. Acad. Sci. USA **108**, 8704.

Pfeilsticker, K., 1999, J. Geophys. Res. **104**, 4101.

Plank, M. J., and E. A. Codling, 2009, Ecology **90**, 3546.

Podlubny, I., 1999, *Fractional differential equations: an introduction to fractional derivatives, fractional differential equations, to methods of their solution and some of their applications* (Academic, San Diego).

Primo, C., I. G. Szendro, M. A. Rodriguez, and J. M. Gutiérrez, 2007, Phys. Rev. Lett. **98**, 108501.

Prudnikov, A., Y. A. Brychkov, and O. Marichev, 1986, *Integral and Series*, Vol. 1 (Gordon and Breach, New York).

Purcell, E. M., 1977, Am. J. Phys. **45**, 3.

Raichlen, D. A., B. Wood, A. D. Gordon, A. Z. P. Mabulla, F. W. Marlowe, and H. Pontzer, 2014, Proc. Nat. Acad. Sci. USA **111**, 728.

Ramos-Fernández, G., J. L. Mateos, O. Miramontes, G. Cocho, H. Larralde, and B. Ayala-Orozco, 2004, Behav. Ecol. and Sociobiol. **55**, 223.

Rayleigh, L. F., 1880, Philosophical Magazine Series 5 **10**, 73.

Rebenshtok, A., and E. Barkai, 2007, Phys. Rev. Lett. **99**, 210601.

Rebenshtok, A., and E. Barkai, 2008, J. Stat. Phys. **133**, 565.

Rebenshtok, A., S. Denisov, P. Hänggi, and E. Barkai, 2014a, Phys. Rev. E **90**, 062135.

Rebenshtok, A., S. Denisov, P. Hänggi, and E. Barkai, 2014b, Phys. Rev. Lett. **112**, 110601.

Redner, S., 2001, *A Guide to First-Passage Processes* (Cambridge University Press, New York).

Reichel, J., F. Bardou, M. B. Dahan, E. Peik, S. Rand, C. Salomon, and C. Cohen-Tannoudji, 1995, Phys. Rev. Lett. **75**, 4575.

Reynolds, A., A. D. Smith, R. Menzel, U. Greggers, D. R. Reynolds, and J. R. Riley, 2007, Ecology **88**, 1955.

Reynolds, A. M., and M. A. Frye, 2007, PLoS ONE **2**, e354.

Reynolds, A. M., L. Leprêtre, and D. A. Bohan, 2013, Sci. Rep. **3**, 3158.

Reynolds, A. M., P. Schultheiss, and K. Cheng, 2014, J. Theor. Biol. **340**, 17.

Rhee, I., M. Shin, S. Hong, K. Lee, S. J. Kim, and S. Chong, 2011, IEEE/ACM Trans. Netw. **19**, 630.

Richardson, L., 1926a, Proc. R. Soc. London, Ser. A **110**, 709.

Richardson, L. F., 1926b, Proc. R. Soc. London, Ser. A **110**, 709.

Risken, H., 1996, *The Fokker-Planck Equation: Methods of Solution and Applications* (Springer, Berlin/Heidelberg/New York).

Ross, R., 1905, Br. Med. J. **13**, 1025.

Sagdeev, R. Z., D. A. Usikov, and G. M. Zaslavsky, 1992, *Nonlinear Physics: from the Pendulum to Turbulence and Chaos* (Harwood Academic, Chur, Switzerland).

Sagi, Y., M. Brook, I. Almog, and N. Davidson, 2012, Phys. Rev. Lett. **108**, 093002.

Saichev, A. I., and G. M. Zaslavsky, 1997, Chaos **7**, 753.

Samko, S., A. A. Kilbas, and O. Marichev, 1993, *Fractional Integrals and Derivatives: Theory and Applications* (Taylor & Francis, London).

Sanders, D. P., and H. Larralde, 2006, Phys. Rev. E **73**, 026205.

Savo, R., M. Burresi, T. Svensson, K. Vynck, and D. S. Wiersma, 2014, Phys. Rev. A **90**, 023839.

Schanz, H., T. Dittrich, and R. Ketzmerick, 2005, Phys. Rev. E **71**, 026228.

Schanz, H., M.-F. Otto, R. Ketzmerick, and T. Dittrich, 2001, Phys. Rev. Lett. **87**, 070601.

Scher, H., and E. W. Montroll, 1975, Phys. Rev. B **12**, 2455.

Schmiedeberg, M., M. Miri, and H. Stark, 2005, Eur. Phys. J. E **18**, 123.

Schmiedeberg, M., and H. Stark, 2006, Phys. Rev. E **73**, 031113.

Schmiedeberg, M., V. Yu. Zaburdaev, and H. Stark, 2009, J. Stat. Mech-Theory E **2009**, P12020.

Schreier, A. L., and M. Grove, 2014, Am. J. Primatol. **76**, 421.

Schultheiss, P., and K. Cheng, 2013, Behav. Ecol. **24**, 128.

Schulz, J. H. P., E. Barkai, and R. Metzler, 2014, Phys. Rev. X **4**, 011028.

Segall, J. E., S. M. Block, and H. C. Berg, 1986, Proc. Nat. Acad. Sci. USA **83**, 8987.

Selmeczi, D., L. Li, L. I. Pedersen, S. F. Norrelykke, P. H. Hagedorn, S. Mosler, N. B. Larsen, E. C. Cox, and H. Fly-vbjerg, 2008, Eur. Phys. J. Special Topics **157**, 1.

Seuront, L., and H. E. Stanley, 2014, Proc. Nat. Acad. Sci. USA **111**, 2206.

Shaffer, C. A., 2014, Am. J. Primatol. **76**, 472.

Shepelyansky, D. L., 2010, Phys. Rev. E **82**, 055202.

Shlesinger, M., J. Klafter, and B. J. West, 1986, Physica A **140**, 212.

Shlesinger, M., B. West, and J. Klafter, 1987, Phys. Rev. Lett. **58**, 1100.

Shlesinger, M. F., 2009, J. Phys. A **42**, 434001.

Shlesinger, M. F., and J. Klafter, 1985, Phys. Rev. Lett. **54**, 2551.

Shlesinger, M. F., and J. Klafter, 1986, in *On Growth and Form*, edited by H. E. Stanley and N. Ostrowsky (Martinus Nijhoff, Dordrecht), pp. 279–283.

Shlesinger, M. F., J. Klafter, and Y. Wong, 1982, J. Stat. Phys. **27**, 499.

Shlesinger, M. F., J. Klafter, and G. Zumofen, 1999, Am. J. Phys. **67**, 1253.

Shlesinger, M. F., G. M. Zaslavsky, and J. Klafter, 1993, Nature (London) **363**, 31.

Sims, D. W., A. M. Reynolds, N. E. Humphries, E. J. Southall, V. J. Wearmouth, B. Metcalfe, and R. J. Twitch-ett, 2014, Proc. Nat. Acad. Sci. USA **111**, 11073.

Sims, D. W., E. J. Southall, N. E. Humphries, G. C. Hays, C. J. A. Bradshaw, J. W. Pitchford, A. James, M. Ahmed, A. S. Brierley, M. A. Hindell, D. Morritt, M. K. Musyl, *et al.*, 2008, Nature (London) **451**, 1098.

von Smoluchowski, M., 1906, Ann. Phys. **326**, 756.

Sokolov, I., A. Blumen, and J. Klafter, 2001, Physica A **302**, 268.

Sokolov, I., J. Mai, and A. Blumen, 1997, Phys. Rev. Lett. **79**, 857.

Sokolov, I. M., and R. Metzler, 2003, Phys. Rev. E **67**, 010101.

Solomon, T., E. R. Weeks, and H. L. Swinney, 1994, Physica D **76**, 70.

Solomon, T. H., E. R. Weeks, and H. L. Swinney, 1993, Phys. Rev. Lett. **71**, 3975.

Spohn, H., 2014, J. Stat. Phys. **154**, 1191.

Stefani, F. D., J. P. Hoogenboom, and E. Barkai, 2009, Phys. Today **62**, 34.

Straka, P., and B. Henry, 2011, Stoch. Proc. Appl. **121**, 324.

Su, T.-W., L. Xue, and A. Ozcan, 2012, Proc. Nat. Acad. Sci. USA **109**, 16018.

Sutantyo, D. K., S. Kernbach, P. Levi, and V. A. Nepom-nyashchikh, 2010, in *2010 IEEE International Workshop on Safety Security and Rescue Robotics (SSRR)* (IEEE), pp. 1–6.

Sutantyo, D. K., C. Moslinger, and M. Read, 2013, in *2013 IEEE International Conference on Mechatronics and Au-tomation (ICMA)* (IEEE), pp. 456–462.

Takagi, H., M. J. Sato, T. Yanagida, and M. Ueda, 2008, PLoS ONE **3**, e2648.

Taktikos, J., H. Stark, and V. Zaburdaev, 2013, PLoS ONE **8**, e81936.

Taylor, G. I., 1922, Proceedings of the London Mathematical Society **s2-20**, 196.

Tejedor, V., R. Voituriez, and O. Bénichou, 2012, Phys. Rev. Lett. **108**, 088103.

Thaler, M., and R. Zweimüller, 2006, Probab. Theor. Rel. **135**, 15.

Theves, M., J. Taktikos, V. Zaburdaev, H. Stark, and C. Beta, 2013, Biophys. J. **105**, 1915.

Thiel, F., L. Schimansky-Geier, and I. M. Sokolov, 2012, Phys. Rev. E **86**, 021117.

Tong, P., and W. Goldburg, 1988, Phys. Lett. A **127**, 147.

Torcini, A., P. Grassberger, and A. Politi, 1995, J. Phys. A **28**, 4533.

Torcini, A., and S. Lepri, 1997, Phys. Rev. E **55**, R3805.

Travis, J., 2007, Science **318**, 742.

Trizac, E., A. Barrat, and M. H. Ernst, 2007, Phys. Rev. E **76**, 031305.

Tsallis, C., 1988, J. Stat. Phys. **52**, 479.

Tsallis, C., 1999, Braz. J. Phys. **29**, 1.

Tsujii, K., 2008, Polym. J. **40**, 785.

Tunaley, J. K. E., 1974, Phys. Rev. Lett. **33**, 1037.

Turchin, P., 1998, *Quantitative Analysis of Movement: Mea-suring and Modeling Population Redistribution in Animals and Plants* (Sinauer Associates, Sunderland, MA).

Turgeman, S., L., and E. Barkai, 2009, Phys. Rev. Lett. **103**, 190201.

Uchaikin, V., and V. Zolotarev, 1999, *Chance and Stability: Stable Distributions and their Applications*, Modern Prob-ability and Statistics (De Gruyter, Berlin/New York).

Uchaikin, V. V., 2003, Physics-Uspekhi **46**, 821.

Van Kampen, N., 2011, *Stochastic Processes in Physics and Chemistry*, North-Holland Personal Library (Elsevier, Am-sterdam).

Vandercone, R., K. Premachandra, G. P. Wijethunga, C. Di-nadh, K. Ranawana, and S. Bahar, 2013, Am. J. Primatol. **75**, 1209.

Venegeroles, R., 2009, Phys. Rev. Lett. **102**, 064101.

Vermeersch, B., A. M. S. Mohammed, G. Pernot, Y. R. Koh, and A. Shakouri, 2014, Phys. Rev. B **90**, 014306.

Vezzani, A., R. Burioni, L. Caniparoli, and S. Lepri, 2011, Philos. Mag. **91**, 1987.

Viswanathan, G., M. da Luz, E. Raposo, and H. Stanley, 2011, *The Physics of Foraging: An Introduction to Random Searches and Biological Encounters* (Cambridge University Press, Cambridge).

Viswanathan, G. M., V. Afanasyev, S. V. Buldyrev, E. J. Murphy, P. A. Prince, and H. E. Stanley, 1996, Nature (London) **381**, 413.

Viswanathan, G. M., S. V. Buldyrev, S. Havlin, M. G. E. da Luz, E. P. Raposo, and H. E. Stanley, 1999, Nature (London) **401**, 911.

Wearmouth, V. J., M. J. McHugh, N. E. Humphries, A. Naegelen, M. Z. Ahmed, E. J. Southall, A. M. Reynolds, and D. W. Sims, 2014, P. Roy. Soc. B-Biol. Sci. **281**, 20132997.

Weeks, E. R., 1997, *Experimental studies of anomalous diffu-sion, blocking phenomena, and two-dimensional turbulence*, Ph.D. thesis, The University of Texas at Austin.

Weeks, E. R., and H. L. Swinney, 1998, Phys. Rev. E **57**, 4915.

Weigel, A. V., B. Simon, M. M. Tamkun, and D. Krapf, 2011, Proc. Nat. Acad. Sci. USA **108**, 6438.

Weiss, G., 1994, *Aspects and Applications of the Random Walk* (North Holland, Amsterdam).

Weiss, M., L. Hufnagel, and R. Ketzmerick, 2002, Phys. Rev. Lett. **89**, 239401.

West, B. J., 2014, Rev. Mod. Phys. **86**, 1169.

Xie, L., T. Altindal, S. Chattopadhyay, and X.-L. Wu, 2011, Proc. Nat. Acad. Sci. USA **108**, 2246.

Zaburdaev, V., N. Biais, M. Schmiedeberg, J. Eriksson, A.-B. Jonsson, M. P. Sheetz, and D. A. Weitz, 2014, Biophys. J. **107**, 1523.

Zaburdaev, V. Yu., and K. Chukbar, 2002, JETP **94**, 252.

Zaburdaev, V. Yu., and K. Chukbar, 2003, JETP Lett. **77**, 551.

Zaburdaev, V., S. Denisov, and P. Hänggi, 2011a, Phys. Rev. Lett. **106**, 180601.

Zaburdaev, V, S. Denisov, and P. Hänggi, 2012, Phys. Rev. Lett. **109**, 069903.

Zaburdaev, V., S. Denisov, and P. Hänggi, 2013, Phys. Rev. Lett. **110**, 170604.

Zaburdaev, V., M. Schmiedeberg, and H. Stark, 2008, Phys. Rev. E **78**, 011119.

Zaburdaev, V., and I. M. Sokolov, 2009, Appl. Nonlin. Dyn. **4**, 79.

Zaburdaev, V., S. Uppaluri, T. Pfohl, M. Engstler, R. Friedrich, and H. Stark, 2011b, Phys. Rev. Lett. **106**, 208103.

Zaburdaev, V. Yu., 2006, J. Stat. Phys. **123**, 871.

Zaburdaev, V. Yu., 2008, J. Stat. Phys. **133**, 159.

Zaslavsky, G. M., 2002, Phys. Rep. **371**, 461.

Zhao, H., 2006, Phys. Rev. Lett. **96**, 140602.

Zimbardo, G., A. Greco, and P. Veltri, 2000, Phys. Plasmas **7**, 1071.

Zumofen, G., and J. Klafter, 1993, Phys. Rev. E **47**, 851.

Zumofen, G., and J. Klafter, 1994a, Europhys. Lett. **25**, 565.

Zumofen, G., and J. Klafter, 1994b, Chem. Phys. Lett. **219**, 303.

Zwanzig, R., 2001, *Nonequilibrium Statistical Mechanics* (Oxford University Press, New York).